Self-organizational Behaviour of Chiral Nematic Liquid Crystals doped with Nanoparticles

A Thesis Submitted

For the

Award of the Degree of

DOCTOR OF PHILOSOPHY

By

Manju Middha

(Roll no. 951112006)

To

School of Physics and Material Science

Thapar University, Patiala 147001

October 2016

CERTIFICATE

This is to certify that the thesis entitled "Self-organizational Behaviour of Chiral Nematic Liquid Crystals doped with Nanoparticles" being submitted by **"Ms. Manju Middha"** in partial fulfilment of the requirements for the award of degree of Doctor of Philosophy to **Thapar University**, Patiala is a record of bonafide research work carried out by her under my supervision and guidance. In my opinion, the work fulfils the requirements for which it is being submitted.

To the best of my knowledge, the work included in this thesis has not been submitted elsewhere earlier, in part or in full, for the award of any other degree in this or any other institution or university.

Supervisor

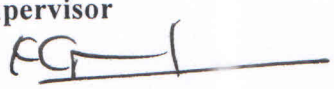

Dr. K.K. Raina
Distinguished Professor
School of Physics and Material Science
Thapar University
Patiala- 147004

Om Shri Ganeshaya Namah

A FEW WORDS OF GRATITUDE

Hey, Krishna! with the completion of this thesis my journey with liquid crystals comes to a halt. All through my sojourn it was you whose colours I enjoyed. As you have said in the 'Holy Geeta' that you are 'The Beginning' and everything ends in you; every time the liquid crystal was nearing its isotropic temperature its textures reflected multiple hues which always reminded me of 'The Morpankh' that you adorn. Ultimately, it used to become dark as you O Sanwle Krishna! And the darkness seemed to envelope all the colours, as at the end of worldly journey everything coalesces in you. While doing research I always admired your spectacular manifestation in everything. I found you as endless. No one could claim complete knowledge of yours. You are simple yet complex. O God, you are beautiful! Thanks for holding my hand all through my endeavour to understand 'Nature' which I found nothing but

'YOU'.

DEDICATED TO MY PARENTS AND

LATE PARENTS IN LAW

ACKNOWLEDGEMENTS

This presentation is towards the partial fulfillment of the requirement for the course work for the degree of Doctor of Philosophy (Physics). With this comes the end of a memorable period, which I shall keep as an asset in my memory. Initially, becoming a regular student after 26 years seemed quite taxing, but with the help of my affectionate lab mates, especially Rishi, Ramneek, Gurpreet, and Supreet the time passed like a sweet memory.

I am indebted to **Dr. K K Raina**, Distinguished Professor and Vice Chancellor, DIT, Dehradun, who reposed faith in me and accepted me as a student. His words of wisdom have always encouraged me to work till perfection. Despite his awfully busy schedule, he, with his encyclopedic knowledge was always available for discussion. It was very enriching experience to work under his guidance. Without his constant support, this work would have never been completed.

My sincere thanks are due to **Prof. Parkash Gopalan**, Director, Thapar University, Patiala, for providing the necessary infrastructure and basic facilities to carry out the experimental work related to this thesis and allowing me to attend the various conferences, symposiums, and seminars during the term of my Ph.D.

I place on record my sincere thanks to the **University Grants Commission**, New Delhi, India for giving me the teacher fellowship under the FIP to pursue the research work.

I am grateful to **The Govt. Of Punjab** for giving me permission to avail the fellowship.

I am thankful to **Dr. O P Pandey**, Dean, Research and Sponsored Projects, TU for his constructive guidance and encouragement. I have learnt a lot from him.

I express my sincere gratitude for **Dr. Manoj Kumar Sharma**, HOD, SPMS. He always made the official procedures very easy with his welcome smile. I can also never forget the gentle and prompt response of **Dr. Puneet Sharma** for taking care of all lab related problems.

I have found teachers in Thapar University as workaholics, hardworking and considerate. I express my gratitude to **Dr. Kulveer Singh, Dr. B N Chudasamma, Dr. S P Tiwari, Dr.**

D P Singh and Dr. Rajeev Mehta for always helping and guiding me. I also want to take this opportunity to thank **Ms. Lovleen Kaur Brar** for keeping me always motivated by healthy discussions.

I am indebted to **Dr. Parveen Malik** of NIT, Jalandhar, for ensuring me all kinds of help from his department.

I shall be failing in my duties if I don't convey my sincere thanks and blessings to my lab mate **Dr. Rishi Kumar** for helping me learn the language of the liquid crystal lab. Without his sincere guidance and perspicacious discussions, a thorough knowledge of the subject would have been difficult to gain. I shall always remember the days spent in the company of **Dr. Supreet, Dr. Ramneek Kaur Dhaliwal, Dr. Gurpreet Kaur and Ms. Shivani** as a cherished memory. I thank them for their unconditional help rendered to me. I feel immense pleasure in thanking the office and the lab staff of the SPMS department for always being kind enough to help me.

On this auspicious day, I am getting emotional as I remember my father-in-law, **Late Sh. Satya Pal Arora**, who would have been the happiest person to see me accomplish my dream. I thankfully acknowledge the blessings of my mother-in-law, **Late Smt. Raj Karni Arora**, who always inspired me to have those two words 'Dr.' in front of my name. I hope both send their blessings from heaven. I owe my family, especially, my mother **Smt. Jaimala Middha**, my father **Sh. Nanak Chand Middha** and my husband **Dr. Janak Arora** for unconditionally supporting me. A special thanks to my sister **Mrs. Bindiya Kalra** and my nephew **Bharat Middha** for being there, whenever I needed them. Last but not the least I thank my children **Dr. Aditi Arora Bansal, Dr. Ankur Bansal, Dr. Kanika Arora and Dr. Sohrab Arora** for inspiring me to realize my cherished dream. In the end, I most lovingly thank my granddaughter, **Saanvi** for rejuvenating me with her purest smile.

Manju Middha (Arora)

ABSTRACT

In the recent past, an increasing interest has been noticed in the nanoparticles doped liquid crystal (LC) composites with a focus on their broader applicability and scientific understanding. The self-assembly of nanomaterials in the soft superstructure of LCs comes naturally due to its anisotropic nature. The use of carbon nanotubes (CNTs) and various other nanoparticles in the nematic and ferroelectric liquid crystals has been shown to improve electro-optic switching behavior, nonvolatile memory effects, diffractive properties and the threshold voltage. Their use is also found in protein biosensors, biocatalysts, bio separators and for drug storage and delivery.

Although a lot has been done in this field, the understanding of the manipulation of nanotubes and spherical nanoparticles in the helical superstructures of chiral liquid crystals remains unexplored. In the present study, we have tried to study the effects of nanoparticles and nanotubes doping on the optical, morphological and electro-optic switching behaviour of induced chiral nematic LCs. These investigations are expected to open new avenues in the field of optical memory research in soft materials.

Cholesteric liquid crystals (CLC) being chiral, have a helical structure. The pitch of the helix can be compressed or extended by external perturbations. The dispersion and self-assembly of nanomaterials into soft and well-defined functional superstructures is facilitated due to the flexibility and anisotropic nature of liquid crystals.

We have induced chirality in a nematic liquid crystal by adding an optimized amount of chiral dopant into it. Functionalized nanomaterials (SWCNTs, MWCNTs, Silver nanoparticles, Aluminum-doped ZnO nanoparticles) were homogeneously dispersed in this medium. The effect of nanoparticle doping on the helical supramolecular structure of induced chiral medium for different concentrations of nanoparticles was investigated in the presence of surface anchoring, electric field, incident radiation and thermal perturbations.

Morphological and optical studies of doped materials have shown that nanotubes and nanoparticles produce defects in the CLC phase and break its continuous rotational symmetry. As the performance of the display applications depends on the faster electrically induced Freedericksz transition, the collective reorientation of the liquid crystal director with

applied electric field was investigated during the experiment until it gets aligned parallel to the electric field. A significant change in the onset voltage of Freedericksz transition of doped samples as a function of dopant concentration was observed. Multifold enhancement in the PL intensity because of silver and AZO nanoparticle doping highlighted the aggrandized anisotropic behavior of the doped samples. Improved electro-optic response in terms of conductivity and dielectric constant of the carbon nanotubes doped materials was evident from the dielectric investigations of the doped samples. Transmission and photoluminescence behavior of the doped samples were studied to confirm the emergence of the nonvolatile memory in the doped samples.

OBJECTIVES

The following objectives were proposed to be achieved for the fulfillment of requirements for the award of the degree.

1. Preparation of chiral nematic liquid crystal films by optimization of chiral dopant concentration.
2. To study the self-organization of different nanoparticles into chiral nematic liquid crystal matrix.
3. To investigate the switching behaviour and optical properties of different nanoparticles doped chiral nematic versus undoped chiral nematic liquid crystals.

To fulfill the objectives of the proposed work, the following series of the liquid crystals were prepared and characterized:

Series I: CLC I, CLC II, CLC III, CLC IV, and CLCV (ZLI 4151, doped with different concentrations of CB15)

Series II: CLC+0.1wt% SWCNTs, CLC+0.3wt% SWCNTs, CLC+0.4wt% SWCNTs

Series III: CLC+0.01wt% MWCNTs, CLC+0.10wt% MWCNTs, CLC+0.50wt% MWCNTs, CLC+1.00wt% MWCNTs.

Series IV: CLC+0.005wt% Ag NPs, CLC+0.01wt% Ag NPs, CLC+0.015wt% Ag NPs and CLC+0.020wt% Ag NPs.

Series V: CLC+0.010wt% AZO, CLC+0.015wt% AZO, CLC+0.020wt% AZONPs

SUMMARY OF CHAPTERS

The thesis has been divided into six chapters. A summary of the chapters is as follows:

Chapter 1: Introduction

In this chapter, liquid crystals (with a special focus on chiral phase) have been introduced. A brief discussion about the liquid crystalline nanoparticles and their technical applications has been summarized. A review of the research work in this field has been presented.

Chapter II: Experimental Methods and Characterization Techniques

The physical characteristics and phase sequence of the liquid crystals and nanoparticles used in the present study have been added in this chapter. The methodology used for the sample preparation and the characterization techniques used for investigating the optical and dielectric properties of the material have been discussed. A detailed review of the experimental techniques and brief information about the equipment used for characterization has been also been given.

Chapter III: Preparation of Chiral Nematic Liquid Crystal Materials

This chapter deals with the induction of chirality into the nematic liquid crystal. Our purpose was to prepare a suitable matrix for nanoparticle doping which exhibits good contrast, and an optimum flavor of chirality to serve as a common base material for all the nanoparticles. With this goal in mind we optimized the chiral dopant concentration. The criteria and procedure followed for the optimization have been discussed.

Chapter IV: Effects of CNT Doping in Chiral Nematic Medium

Octadecylamine functionalized Single-Walled Carbon Nanotubes (SWCNT) dispersion in induced CLC influenced the collective orientation of nematic liquid crystal molecules in helical layers. The properties of the doped matrix were manipulated by varying dopant

concentration. As confirmed by polarized fluorescence spectroscopy, highly anisotropic nature of single wall CNTs enhanced the anisotropy of the liquid crystal. The π–π interaction of SWCNTs present in the planar alignment layers and chiral nematic liquid crystal molecules affects the molecular relaxation process. We also observed and quantified an electro-optical hysteresis of permanent nature.

We investigated the physical, optical and electro-optical behavior of the samples confined in similar boundary conditions and doped with different concentrations of COOH functionalized MWCNTs. The doping of MWCNTs altered the morphological and electro-optic switching behaviour of the host material. The functional group restricted the CNTs from the aggregate formation. MWCNT doping could significantly reduce the threshold electric field for Freedericksz transition and potentially improve the ac conductivity, optical anisotropy and dielectric properties of the material. Polarized fluorescence spectroscopy established the anisotropic changes brought in by CNT doping with a significant increase in absorbance of the doped samples. The early onset of Freedericksz transition also endorses the change in switching behavior of the CLC after doping. The reorientation of the liquid crystal director and CNTs with applied electric field was observed until the homeotropic state was achieved. We also noted the emanation of memory in the doped samples after the withdrawal of the electric field

Chapter V: Effects of Nanoparticles Doping in Chiral Nematic Liquid Crystals

Electrically induced Optical hysteresis and enhanced photoluminescence were observed in the samples doped with Dodecanethiol functionalized silver nanoparticles, which virtually vamooses at 0.020wt% dopant concentration. We have recorded an uptrend of enhancement in emission peak intensity till 0.015wt% dopant concentration above which, we noticed a fall in the peak intensity. We also detected a significant shift in the peak position with dopant concentration.

Another study about the Impact of chirality on nematic liquid crystal matrix doped with Dodecanethiol-capped silver nanoparticles (AgNPs) was also conducted. The temperature dependent morphological behaviour was investigated by polarized optical microscopy. We recorded a lowering of the threshold of Freedericksz transition and about a tenfold rise in

dielectric constant with rising temperature. We also observed a pronounced surge in photoluminescence in addition to an irreversible memory in the chiral medium.

The second part of the chapter deals with the emergence of optical hysteresis and enhanced photoluminescence in chiral medium dispersed with functionalized Aluminum-doped ZnO nanoparticles. We recorded a lowering of the threshold of Freedericksz transition and a nearly tenfold rise in dielectric constant with temperature. We also observed a pronounced surge in photoluminescence in addition to an irreversible memory in the doped chiral medium. Optical hysteresis was recorded in the doped samples and measured with transmission studies.

Chapter VI: Summary and Future Scope

The results of my experiments and their analysis have been summarized and inferences drawn. The scope of further work in this field has also been suggested.

LIST OF PUBLICATIONS

I. Research Papers Published/Accepted/Communicated in International Journals

1. **Manju Middha**, Rishi Kumar, KK Raina. Memory effects in chiral nematic liquid crystals doped with functionalized single-walled carbon nanotubes. **Liquid Crystals**. 2015;**42**:1028-1035.
2. **M Middha**, R Kumar, KK Raina. Improved Electro-Optical Response of Induced Chiral Nematic Liquid Crystal Doped with Multi-Walled Carbon Nanotubes. **Ferroelectrics**. 2016;**495**:75-86.
3. **Manju Middha**, Rishi Kumar, KK Raina. Photoluminescence Tuning and Electro-optical Memory in Chiral Nematic Liquid Crystals Doped with Silver Nanoparticles. **Liquid Crystals.** 2016;**43**:1002-1008.
4. **Manju Middha**, Rishi Kumar, KK Raina. Effects of chirality on optical and electro-optic behavior of nematic liquid crystals doped with functionalized silver nanoparticles. **Journal of Molecular Liquids**. 2016;**219**:631–636.
5. Rishi Kumar, Pooja Goyal, **Manju Middha**, KK Raina. Morphological and Dielectric Relaxation Responses of Polymer-Stabilized Ferroelectric Liquid Crystal Composite

Films. **Journal of Thin Films Coating: Science Technology, and Application**. 2015;**2:**8-12.

6. **M Middha**, R Kumar, KK Raina: Dielectric Investigations of Induced Memory in Chiral Doped Nematic Liquid Crystal. **AIP Conference Proceedings.** 2015**;1675:**030006.
7. **M Middha**, R Kumar and KK Raina: Electrically tuned photoluminescence in large pitch cholesteric liquid crystal. **AIP Conference Proceedings.** 2014;**1591**:200.

II. Papers Presented and Published in National/ International Conference Proceedings

1. **Manju Middha**, Rishi Kumar, KK Raina. Dielectric and morphological investigations of induced memory in chiral doped nematic liquid crystals as a function of frustration ratio. **International Conference on Latest Developments in Materials, Manufacturing and Quality Control**, GZSCCET (Maharaja Ranjit Singh State Technical University), 12th -13th February 2016.
2. **Manju Middha**, KK Raina. Polarizing Optical Microscopy in Liquid Crystals: An Indispensable Investigating Tool. 2nd conference on microscopy in material science **(AMST)**, TU, Patiala. 25-27th February 2016.
3. **M Middha**, R Kumar, KK Raina. Improved Electro-Optical Response of Induced Chiral Nematic Liquid Crystal Doped with Multi-Walled Carbon Nanotubes International Conference on Challenges in Polar self-assembling systems (***FLC–15***). Prague, Czech Republic. June 28 – July 3, 2015.
4. **M Middha,** R Kumar, and KK Raina. Dielectric and optical investigations of induced memory in chiral doped nematic liquid crystals as a function of frustration ratio, **RAINSAT**-15, Sathyabhama University, Chennai. July 8th - 10th, 2015.
5. **Manju Middha**, Rishi Kumar, and KK. Raina. Effect of chirality on the dielectric and electro-optic behaviour of nematic liquid crystals doped with functionalized silver nanoparticles. 22nd National Conference on Liquid Crystals, **NCLC**, DIT University, Dehradun, India. December 21-23, 2015
6. Rishi Kumar, **Manju Middha,** and KK. Raina. Improved Morphological and Electrical Responses of Polyvinyl Dene fluoride Composite Films Doped with Multi-Walled Carbon Nanotubes. Indo-UK workshop On Sustainable Polymer Applications, **IUWSPA**, Thapar University, Patiala, India. December 8-9, 2015.

7. **M Middha,** R Kumar, and KK Raina. Estimation of optical hysteresis of induced memory in chiral doped nematic liquid crystals. **NAEM**, Dehradun. March 20-21, 2015.
8. **M Middha**, R Kumar, KK Raina: Dielectric Investigations of Induced Memory in Chiral Doped Nematic Liquid Crystal. 4th National Conference on Advanced Materials and Radiation Physics **(AMRP-2015)**, SLIET Longowal. March 13-14, 2015.
9. **M Middha,** R Kumar and KK Raina. Polarizing microscopy as a tool to study liquid crystal materials. **NCMAMS**, Jammu University, Jammu, March 2-4, 2015.
10. **M Middha,** R Kumar, and KK Raina. Electro-optic responses of chiral nematic liquid crystals doped with Multiwall carbon nanotubes. **Punjab science congress**, Desh Bhagat University, Mandi Gobindgarh, India, February 7-9, 2015.
11. **M Middha,** R Kumar, and KK Raina. Electroconvection in the chiral doped nematic liquid crystal. DAVIET, Jalandhar, November 7-8, 2014.
12. **M Middha**, R Kumar and KK Raina: Electrically tuned photoluminescence in large pitch cholesteric liquid crystal, 58th **DAE** Solid State Physics Symposium, Thapar University, Patiala. December 17-21, 2013.
13. **M Middha,** R Kumar, and KK Raina. Investigation of optical contrast of cholesteric liquid crystal film with a fluorescence spectrophotometer. **(DAV-NCST 2013)**, Jalandhar May 30-31, 2013.
14. **M Middha,** R Kumar, and KK Raina. Kerr constant as a measure of molecular anisotropy: An Overview. **NCLC**, TU 2012.

III. Awards/Prize/Achievements

1. **Best poster** prize at 4th National Conference on Advanced Materials and Radiation Physics (AMRP-2015), SLIET, Longowal.

TABLE OF CONTENTS

1. Certificate
2. Acknowledgements
3. Abstract
4. Objectives
5. Plan of the thesis and summary of the chapters
6. List of Publications

Chapter 1	**Introduction**	
	Overview	1
1.1	Liquid Crystals	2
1.2	Liquid Crystalline Phases	4
1.2.1	The Nematic Phase	6
1.2.2	The Smectic Phase	7
1.3	Chirality in liquid crystals	7
1.4	New phases after the induction of chirality	8
1.4.1	Chiral Nematic Phase	8
1.4.2	Chiral Smectic Phase	10
1.4.3	Blue Phase and TGB Phase	11
1.5	Response of liquid crystals to external stimuli	12
1.5.1	Effect of temperature	12
1.5.2	Effect of Electric and Magnetic Fields	13
1.5.3	Effect of wavelength and intensity of incident light	14
1.6	Defects in liquid crystals	14

1.7	Classification and Applications of Nanomaterials	15
1.8	Functionalised Nanoparticles	18
1.9	Doping of nanoparticles in Liquid crystals	19
	References	20-27
Chapter 2	**Experimental Methods and Characterization Techniques**	
	Overview	28
2.1	Selection of Materials	29
2.2	Cell Fabrication and Sample Preparation	32
2.3	Sample Characterization Techniques	33
2.3.1	Polarizing Optical Microscopy in liquid crystals	33
2.3.2	Fluorescence Spectroscopy	35
2.3.3	FTIR Spectroscopy	38
2.3.4	Measurement of Refractive Index	39
2.3.5	Dielectric Relaxation Spectroscopy	41
2.3.6	Electro-Optic Switching	45
2.3.7	Transmission Studies and Measurement of Hysteresis	46
	References	48-51
Chapter 3	**Preparation of Chiral Nematic Liquid Crystal Materials**	
	Overview	52
3.1	Chiral Phase	53
3.2	Sample Characterization	55

3.2.1	Morphological Analysis by POM	56
3.2.2	Electro-Optical Switching and Threshold Voltage	58
3.2.3	Optical investigations of induced memory	61
3.2.4	Electro-Optical Investigation of Memory	65
3.2.5	Electrically Tuned Photoluminescence in Chiral nematic Liquid Crystals	66
	References	70-73
Chapter 4	**Effects of CNT doping in chiral nematic medium**	
	Overview	74
	Memory Effects in Chiral Nematic Liquid Crystals Doped with Functionalized Single-Walled Carbon Nanotubes	75
4.1	Sample Preparation and Characterization	76
4.1.1	Functionalization of SWCNTs and their homogeneous mixing in CLC matrix	76
4.1.2	Fourier transform Analysis	76
4.1.3	Morphological Analysis	77
4.1.4	Electro-Optic Switching	78
4.1.5	Optical Investigations of Induced Memory	81
4.1.6	Effect of Doping on the Refractive Index	83
4.1.7	Fluorescence Anisotropy Measurements	83
	Improved Electro-Optical Response of Induced Chiral Nematic Liquid Crystal Doped with Multi-Walled Carbon Nanotubes	84
4.2	Sample Preparation and Analysis	86

4.2.1	Functionalization of MWCNTs	86
4.2.2	Fourier Transform Analysis	86
4.2.3	Morphological Analysis	87
4.2.4	Photoluminescence Studies	89
4.2.5	The Electro-Optical Switching Behaviour	91
4.2.6	Electrical Conductivity and Dielectric Response	93
4.2.7	Measurement of Optical Hysteresis through Transmission Studies	93
	References	94-100
Chapter 5	**Effects of Nanoparticles Doping in Chiral Nematic Liquid Crystals**	
	Overview	101
	Photoluminescence Tuning and Electro-Optical Memory in Chiral Nematic Liquid Crystals Doped with Silver Nanoparticles	102
5.1	Sample Characterization	103
5.1.1	Morphological Analysis	103
5.1.2	Photoluminescence Studies	105
5.1.3	Electro-Optic Switching and Conductivity Analysis	107
5.1.4	Electro-Optical Hysteresis	108
	Effect of Chirality on Optical and Electro-optic Behaviour of Nematic Liquid Crystals Doped with Functionalized Silver Nanoparticles.	111
5.2	Sample preparation and characterization	113
5.2.1	Thermo-optical Studies through POM	115

5.2.2	Electro-Optical Switching	113
5.2.3	Dielectric investigations	114
5.2.4	Conductivity Measurements	116
5.2.5	Photoluminescence Studies	117
	***Effect of Aluminum Doped Zinc Oxide Nanoparticles Doping on the Electro-optical and Photoluminescence Behaviour of a Chiral Matrix*.**	119
5.3	Sample Preparation and Characterization	120
5.3.1	Functionalization of AZO Nanoparticles	120
5.3.2	Fourier Transform Infrared Spectroscopy	121
5.3.3	Transmission Electron Microscopy	121
5.3.4	Morphological Studies	122
5.3.5	Electro-Optical Studies	123
5.3.6	Dielectric Response of the Doped samples	124
5.3.7	Electrical Conductivity Measurements	126
5.3.8	Investigations for Electro-Optical Hysteresis	128
5.3.9	Photoluminescence Studies	129
	References	131-138
Chapter 6	**Summary and Future Scope**	139-142

LIST OF FIGURES

Chapter I	**Introduction**	**Page no.**

1.1	Types of liquid crystal molecules.	3
1.2	Thermally induced phase transitions of matter	3
1.3	Classification of liquid crystals	5
1.4	Order Parameter	5
1.5	(a) Arrangement of molecules in nematic phase (b) Schlieren Texture	6
1.6	Molecular Order in Smectic Liquid Crystals	7
1.7	Molecular Arrangement in a Chiral Supramolecule	9
1.8	Schematic of the molecular arrangement in chiral nematic liquid crystals	10
1.9	Molecular arrangement in SmC* phase and corresponding microtexture	11
1.10	(a) Formation of a blue phase (b) The structure of BPI (c) BPII.	11
1.11	(a) Schematic of SWCNTs and MWCNTs [53] (b) Different types of arrangement of carbon atoms in CNTs [54].	17
1.12	Functionalized silver nanoparticles	19
Chapter II	**Experimental Methods and Characterization Techniques**	
2.1	Schematic of a Liquid Crystal Sample Cell	30
2.2	Methodology Followed for the Experimental Work	30
2.3	(a) Schematic of optical polarizing microscope (b) Carl Zeiss Scope A1	32
2.4	(a) Scheme of Spectrophotometer (b) View of Fluorescence Spectrophotometer	35
2.5	(a) Scheme of FTIR Spectrophotometer (b) View of FTIR	36
2.6	(a) Schematic of refractometer (b) Dark and bright regions at the crosswires (c) View of Abbe's refractometer	39

2.7	View of the LCR Bridge used for dielectric analysis.	41
2.8	Frequency response of dipolar mechanisms.	42
2.9	Experimental set-up used for transmission studies.	45
Chapter III	**Preparation of Chiral Nematic Liquid Crystal Materials**	
3.1	Microscopic Textures representing freshly prepared doped and undoped sample cells.	55
3.2	Optical micro textures of the nucleation process.	56
3.3	Electro-optic switching in Chiral doped samples at the threshold.	57
3.4	Memory effects in CLCIII (a,b), CLCIV (c,d), CLCV (e,f) after the removal of external electric field	61
3.5	(a) Transmitted intensity as a function of relaxation delay. (b) Optical hysteresis in chiral doped samples.	62
3.6	Dipole relaxation of planar aligned CLC samples with time, after switch OFF bias.	63
3.7	(a) Excitation and Emission spectra of CLCIII (b) PL emission spectra of NLC doped with different concentrations of chiral dopant	65
3.8	Electrically controlled photoluminescence in chiral samples.	66
3.9	Morphology of chiral samples confined in unaligned cells.	67
Chapter IV	**Effects of CNT Doping in Chiral Nematic Medium**	
4.1	(a) Molecular structure (b) FTIR spectra of ODA functionalized SWCNTs	74
4.2	Optical micro textures of ODA functionalized SWCNT-doped CLC for different concentrations of dopant.	75
4.3	Microtextures of doped CLCs depicting Freedericksz transition.	76

4.4	(a, b) Hypothetical model showing the field induced alignment (c) Homotropic state of undoped CLC(d) Spatial distribution of CNTs in the homotropic state of doped CLC	77
4.5	ac conductivity as a function of SWCNT concentration	78
4.6	Electro-optic response of SWCNT-doped CLC samples,	79
4.7	Illustration of memory effects in the SWCNT-doped samples.	80
4.8	(a) Excitation (b) Emission fluorescence spectra of doped samples	82
4.9	FTIR spectra of (a) COOH functionalized MWCNTs (b) Untreated MWCNTs	84
4.10	Optical micro textures of doped CLC as a function of MWCNT concentration.	85
4.11	Optical micro textures depicting the nucleation process in MWCNT-doped samples	87
4.12	Emission spectra of MWCNT-doped samples	88
4.13	Variation of (a) Refractive Index (b) Pitch of the doped samples with MWCNT concentration.	88
4.14	ac conductivity of MWCNT-doped CLC samples as a function of (a) field frequency (b) Doping Concentration	90
4.15	Effect of (a, b) Temperature (c, d) Dopant concentration on dielectric permittivity of MWCNT-doped samples	91
4.16	Illustration of memory effects in the doped samples.	92
Chapter V	***Effects of Nanoparticles Doping in Chiral Nematic Liquid Crystals***	
5.1	Optical micrographs of the scattering state of freshly doped CLC samples with increasing concentration of silver NPs	102
5.2	Optical textures of electrically induced memory effects in the doped CLC samples with increasing dopant concentration.	103

5.3	Photoluminescence spectra of (a) functionalized silver nanoparticles (b) AgNP-doped CLC samples.	104
5.4	(a) ac conductivity versus frequency (b) threshold voltage (at 50 Hz), for various concentrations of silver nanoparticles	106
5.5	(a) PL response of silver nanoparticle-doped CLC with the application and withdrawal of ac electric field (b) Memory parameter as a function of dopant concentration.	107
5.6	Phase transition of silver nanoparticles-doped nematic and Chiral LCs with temperature.	110
5.7	Comparison of Freedericksz Transition in silver nanoparticles-doped NLC and CLC samples.	111
5.8	Variation of dielectric constant of the undoped and silver nanoparticles-doped samples with applied electric field frequency	112
5.9	Variation of dielectric constant of silver nanoparticles-doped (a) NLC (b) CLC samples with applied electric field frequency at different temperatures	113
5.10	Variation of the electrical conductivity of undoped and AgNP-doped NLC and CLC samples.	114
5.11	PL emission spectrum of the undoped and AgNP-doped NLC and CLC samples.	115
5.12	FTIR spectroscopy profile of ODA functionalized AZO nanoparticles.	118
5.13	TEM micrograph of AZO NPs dispersed in ethanol solution	119
5.14	Optical micrographs of the scattering state of freshly doped CLC samples with increasing concentration of AZO NPs.	120
5.15	Ion transport mechanism in (a) AZO NP-doped CLC cell before the application of electric field (b) undoped and (c) AZO-NPs doped CLC cell undergoing Freedericksz transition	121
5.16	Variation of the real part of dielectric permittivity with frequency for doped samples.	122

5.17	Temperature dependence of dielectric permittivity of the AZO-doped chiral nematic composite systems.	124
5.18	ac conductivity of the doped CLC samples as a function of (a) Frequency (b) Doping concentration.	125
5.19	Illustration of Electro-optical memory effects in the AZO-doped samples through optical microtextures.	126
5.20	Normalized transmission as a function of applied voltage for AZO doped samples.	127
5.21	PL spectra of undoped and AZO nanoparticles doped CLCs.	128

LIST OF TABLES

Chapter 2	**Experimental Methods and Characterization Techniques**	
2.1	Data sheet of Nematic Liquid Crystal Mixture ZLI 4151.	27
2.2	Phase Sequence and Molecular Structure of Chiral Liquid Crystal.	27
2.3	Physical properties and Molecular Structure of ODA functionalized SWCNTs	28
2.4	Physical parameters and structure of COOH functionalized MWCNTs.	29
2.5	Physical parameters of DDT functionalized AgNPs.	29
2.6	Physical parameters of ODA functionalized AZO NPs.	29
Chapter III	**Preparation of Chiral Nematic Liquid Crystal Materials**	
3.1	Composition and Nomenclature of the Investigated Samples.	53
3.2	Pitch and switching parameters of various concentrations of chiral doped nematic liquid crystals.	58
Chapter IV	**Effects of CNT doping in chiral Nematic medium**	

4.1	Optical characteristics of Undoped and SWCNT-doped CLC samples.	81
4.2	Phase transition temperatures for undoped and MWCNT-doped samples.	86
4.3	Optical characteristics of Undoped and MWCNTs-doped CLC samples.	89
Chapter V	**Nanoparticles Doped Chiral Liquid Crystals**	
5.1	Photoluminescence Response of the Undoped and AgNP-Doped CLC samples with different dopant concentration.	104
5.2	Summary of Thermo-optic, Electro-optic, and PL response of the undoped and AgNP-doped NLC and CLC samples	115
5.3	Electro-optical and optical properties of AZONP-doped CLC samples	125

ABBREVIATIONS AND SYMBOLS

AC/ac	Alternating current
AFM	Atomic Force Microscopy
AgNP	Silver doped nanoparticles
AZO	Aluminum doped zinc oxide nanoparticles
CNTs	Carbon nanotubes
CR	Contrast Ratio
CLC	Chiral liquid crystal
DC	Direct Current
DDT	Dodecanethiol
E-O	Electro-Optical

E_{gap}	Energy Gap
FLC	Ferroelectric liquid crystal
FM	Frequency modulation
FTIR	Fourier Transform Infra-Red
ITO	Indium tin oxide
I_o	Incident light intensity
LC	Liquid Crystal
LCD	Liquid Crystal Display
MWCNTs	Multi-wall Carbon Nanotubes
NLC	Nematic Liquid Crystal
NOA	Norland optical adhesive
ODA	Octadecylamine
PL	Photoluminescence
POM	Polarizing optical microscopy
SWNTs	Single wall nanotubes
TEM	Transmission electron microscope
TN	Twisted nematic
UV-Vis	Ultra Violet-Visible
V	Voltage
Vth	Threshold Voltage
E	Electric field
P	Polarization vector

$\Delta\varepsilon$	Dielectric Anisotropy
5CB	(4-Cyano-4'-pentylbiphenyl (5CB) molecule)
$\varepsilon_{\parallel}$	The dielectric permittivity along the molecular axis
$\varepsilon_{\perp}$	The dielectric permittivity perpendicular to the molecular axis
ε''	Dielectric loss
ε'	Real part of dielectric permittivity
ε_0	Vacuum Permittivity

CHAPTER- 1

INTRODUCTION

Overview

A general overview of the liquid crystals and their phases with a special emphasis on chiral phase has been given in this chapter. The influence of external stimuli on the pitch related properties of chiral phase has been discussed. A brief introduction of nanoparticles used as dopants in present study and their role in changing the properties of liquid crystals has been summarized. A brief review of their applications and the research work being done in this field has been added.

1.1 Liquid Crystals

Based upon the physical state of existence, matter can broadly be divided into three categories: solid, liquid and gaseous state. But there also exist a large number of intermediate phases having distinctly different properties known as liquid crystals [1]. Due to weak intermolecular interactions, molecules or mesogens present in such a phase, possess either positional or orientational order, but to quite a lower degree of organization than in a crystalline solid and of course, to a much higher degree than in an isotropic liquid [2]. Liquid crystalline materials are much more viscous, (often turbid) as compared to ordinary liquids [3]. Equipped with properties like viscoelasticity, high refractive index and anisotropic dielectric constant etc., they have a great scope for their use as functional electro-optical materials [4].

As a truly special gift from nature, liquid crystals possess smallest elastic constants and are most birefringent among all known materials with their broadband birefringence spanning the entire visible-infrared spectrum and beyond [5,6]. Being organic in nature, they can be chemically synthesized and their large scale processing is possible [7]. Owing to their ability to self-assemble into various crystalline phases and to conform to various flexible forms and shapes in both isotropic and ordered phases, they are well- suited for almost all optoelectronic devices [8]. They possess extraordinarily large optical nonlinearities with a wide range of nonlinear optical phenomena been observed throughout the spectrum. Liquid crystal elastomers are being extensively used as smart materials, such as artificial muscles, light scattering electro-optical switches and display materials, electro-or photo-controllable micro- or nano-machinery, electrically switchable color-tunable reflectors (mirrors) and full-color reflective display, fine-tunable and low-threshold mirrorless lasing, etc. [9]. Moreover, easy manipulation of the orientation of liquid crystals by external perturbations such as temperature, electric and magnetic fields, surface anchoring, light, and acoustic waves, makes them excellent candidates for development of active devices [10]. The inherent helicity of chiral liquid crystals has been extensively exploited in lasers. The use of liquid crystals in lasing allows selection of emission wavelength and provides wide spectrum tunability of the range of several nanometers. While maintaining the size of diode lasers, liquid lasers are easy to manufacture. Due to remarkable flexibility in their structure,

the liquid crystals have turned out to be ideal media for nanoparticle doping [11,12]. The nanodoped liquid crystals exhibit a plethora of unique and attractive properties that offer tremendous potential for research as well as device manufacturing well beyond the realm of displays. There exist a large number of molecules in nature which, depending upon their orientation type and degree of organizational behaviour, tend to form liquid crystalline phases [13]. Liquid crystal molecules are generally moderate size organic molecules, which are either elongated rod-like (calamitic), disc-like (discotic) or bent-core type [Fig 1.1]. Anisotropicity of shape is the key feature in all such molecules. This attribute of theirs strongly transpires in their assembly at the macroscopic level with thus formed materials exhibiting peculiar physical behavior.

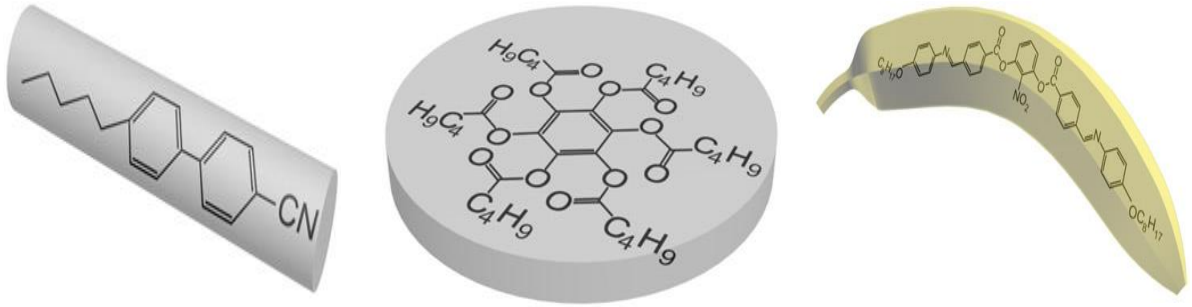

(a) (b) (c)

Fig. 1.1: Types of liquid crystal molecules (a) Calamitic (b) Discotic (c) Bent-core [14]

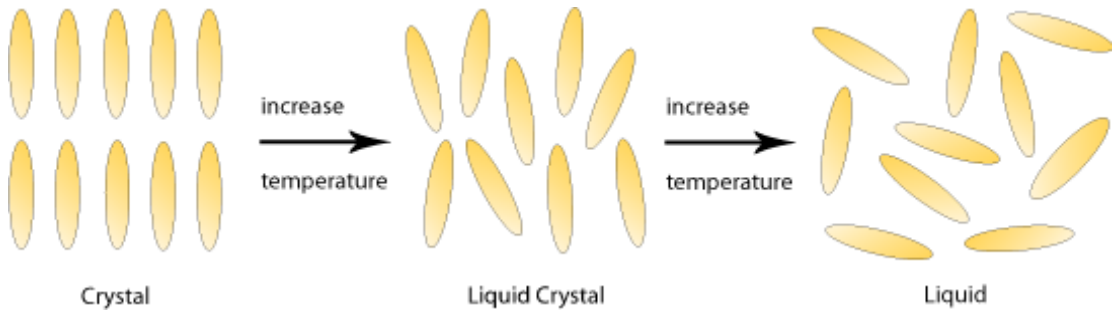

Fig. 1.2: Thermally induced phase transitions of matter [15].

Some of the liquid crystals are thermotropic in nature, with their degree of orientational and positional order depending on the temperature and so their liquid crystalline phase occurs

within a limited temperature range between the solid and liquid phase [Fig.1. 2]. These are solvent free and remain liquid crystalline only in a limited temperature range (Thermotropic), however in other systems, which are solvent-solute type, the concentration of solute decides the fate (Lyotropic).

1.2 Liquid Crystalline Phases

Liquid crystalline systems are composed of molecules having rigid and flexible parts. Hence in addition to mobility, they possess an inherent order as well [16]. The rigidness facilitates structural alignment while the flexibility helps mobility, thus avoiding crystallization. As there are a large variety of mesogens available with varying order of rigidity and mobility, many liquid crystalline phases are possible. Most liquid crystal compounds exhibit polymorphism as more than one phase is observed in liquid crystalline state. Mesophases are basically the sub-phases having a different amount of order in the sample. The order can be varied by permitting the molecules to have one, two or three degrees of freedom thus imposing order on either of the three dimensions. The nematic, smectic and, columnar phase types possess 3, 2 and 1 translational degrees of freedom respectively.

Liquid crystals can be classified in many ways. The distinction can be made on the basis of molecular shape (calamitic, discotic and bent-core), molecular weight, amphiphilic or non-amphiphilic, metallic or non-metallic liquid crystals [17]. Fig.1.1 shows classification of liquid crystals based on molecular shape and structure.

We shall limit our discussion to calamitic mesogens with thermotropic behaviour. These can be divided into several sub-phases. The most important sub-phases are nematic (N) and smectic (Sm). A unit vector called the ‘director’ represented as “n or –n” (both being equivalent vectors) is used to identify the orientation of molecules in these phases. The degree of order in a sample is quantitatively measured by the scalar order parameter (S). The value of S lies between 0 for an isotropic and 1 for a crystalline phase. For a typical liquid crystal, S lies in the range 0.4-0.7. The value of the order parameter decreases with increasing temperature [Fig.1.4] as a consequence of the increased mobility and disorder [18].

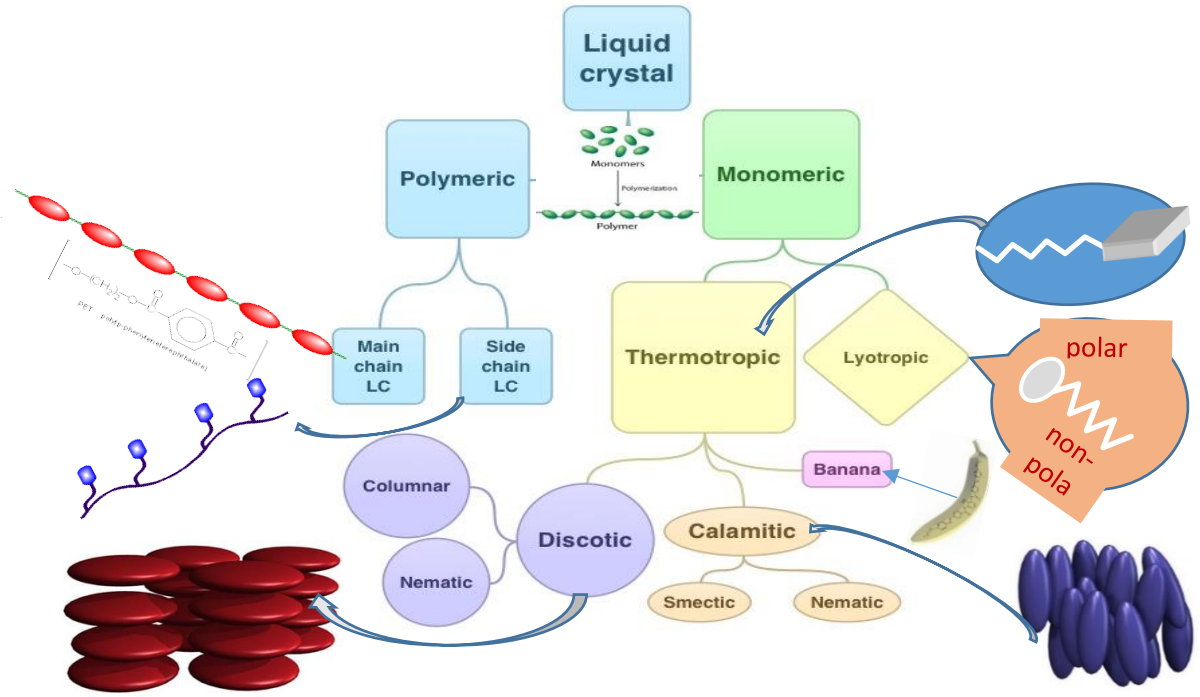

Fig. 1.3: Classification of liquid crystals

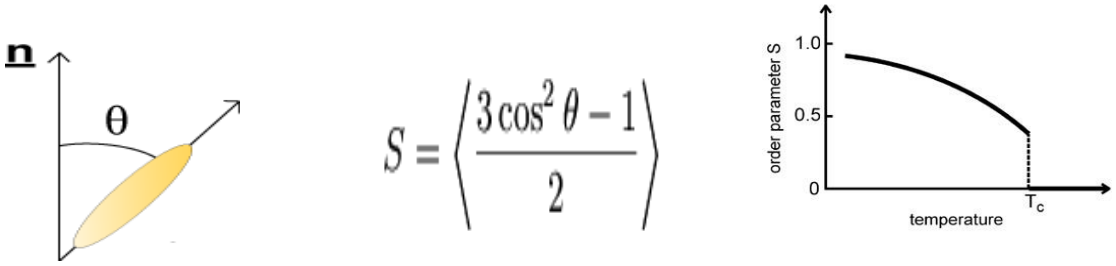

(a) (b) (c)

Fig. 1.4: (a) 'n' represents the director and 'θ' is the angle that the long axis of a mesogen makes with the director (b) Order parameter (c) Effect of temperature on order parameter [14]

Both the nematic and smectic phases are briefly described as below.

1.2.1 The Nematic Phase (N): Nematic phase is the simplest possible liquid crystalline mesophase which is least ordered among all the liquid crystal (LC) phases. When observed through a microscope, it often appears to have minuscule threads, thus named nematic or

thread like. The molecules in this phase can move about freely and can rotate about their long axis, which may not be possible in other phases.

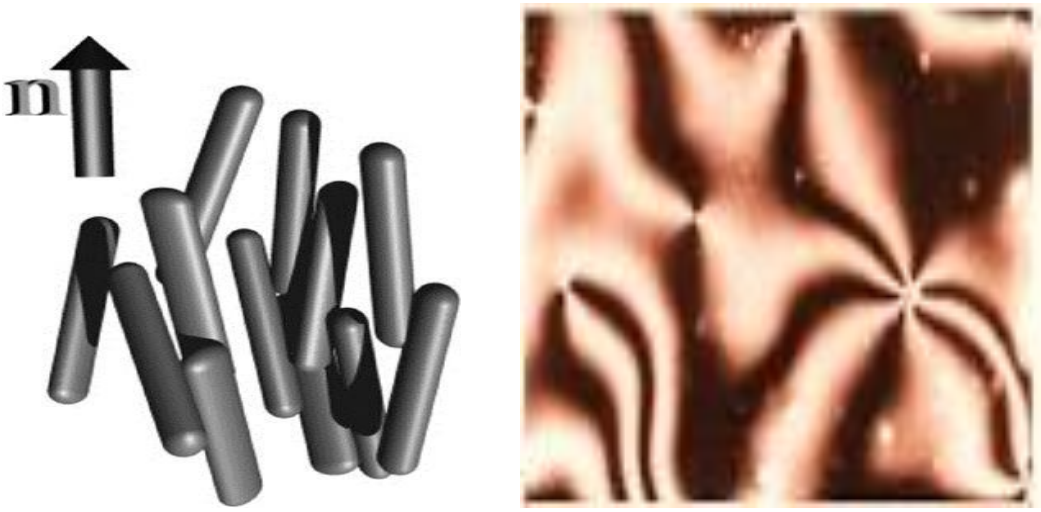

Fig. 1.5: (a) Arrangement of molecules in nematic phase [7] ***(b) Schlieren Texture at room temperature and 10X magnification.***

In the nematic phase, the centers of mass of the molecules remain isotropically distributed, leading to a long-range orientational order and a very short range positional order. There exists a preferred direction defined by a unit vector n called the 'director', along which long axis of most of the liquid crystal molecules point [4][Fig. 1.5a]. The molecules, exhibiting the nematic phase, can rotate around both, their short and long molecular axes. In general, nematic liquid crystals made of rod like molecules constitute a uniaxial medium with non-polar symmetry. If the breadth of molecules is increased, the rotation about their long molecular axis restricts and the phase is termed as biaxial nematic. This phase is characterized by complete rotational and inversion symmetry about the director [19]. Owing to their low viscosity, even weak external forces can deform them. These deformations can be either splay or twist, or bend with K1, K2, and K3 as the elastic constants respectively. The free energy density of distortions can be written as

$$F_d = \frac{1}{2}[K_1(\nabla.n)^2 + \frac{1}{2}\,K_2(\mathrm{n}.\nabla \times \mathrm{n})^2 + \frac{1}{2}\,K_2(\mathrm{n}.\nabla \times \mathrm{n})^2] \ldots\ldots\ldots (1.1)$$

This is the basic equation for the theoretical treatment of defects and optical textures of nematic LCs. The solution of the above equation must yield relative minima in the free energy for a stable distortion. The micro-level organizational properties of liquid crystals exhibiting this phase are expressed at the macro level as optical anisotropy and birefringence. Anisotropy in dielectric permittivity turns them sensitive to low-frequency electric fields and they show switching behavior. Due to all these properties, this phase finds its widespread use in optical and functional materials.

1.2.2 Smectic Phase (Sm): With molecules laid stratified in layers having positional order along with a long-range orientational order, smectic phase is more ordered than nematic phase. It is also differently as one needs two independent order parameters to describe a smectic. These layers can slide past each other, thus exhibiting highly viscous behavior. Based on the orientation and position of constituent molecules within the layer and correlation among the layers, different smectic phases exist: denoted as SmA, SmB, SmC etc. [Fig 1.6] When the director is perpendicular to the smectic layer, it leads to the formation of **SmA** phase. In this phase the director is parallel to the layer normal but there is no positional order within the layer. In **smB** mesophase, director orients perpendicular to the smectic plane but within a layer, molecules are arranged in a network of hexagons. Upon further cooling, the **SmC** phase is achieved, where molecules are tilted with respect to the layers. The tilt angle, defined as the angle between layer normal and the director generally increases with decreasing temperature.

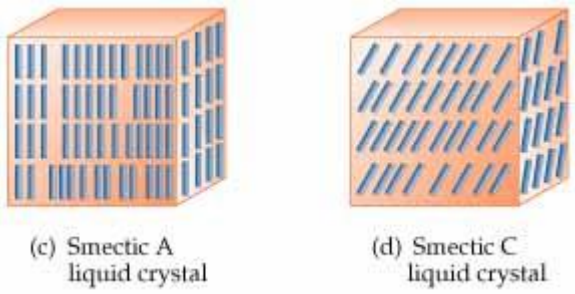

Fig. 1.6: Molecular Order in Smectic Phase of Liquid Crystals [20]**.**

1.3 Chirality in Liquid Crystals: Chirality has always been an important topic in the field of liquid crystals research. This is a property which gives rise to a variety of new phases

like Cholesteric, SmC*, Blue, and TGB [21]. These phases have found extensive use in optics, materials science, memory devices and laser manufacturing [22–24]. Naturally occurring liquid crystals with cholesteric properties are generally cholesteric esters and are chemically non-stable. Nematic liquid crystals, twisted by adding chiral materials or by adding asymmetric side chain, also exhibit cholesteric phase and are relatively more stable. The cholesteric phase is not strictly a different phase, but simply a nematic phase composed of chiral molecules. Thermodynamically, nematic and cholesteric phase are equivalent. Chirality affects the macroscopic arrangement of liquid crystal molecules and this, in turn has major consequences on optical behavior of the substance. The pitch of helix is characteristic of this phase and it depends on several factors.

1.4 New Phases After the Introduction of Chirality

1.4.1 Chiral Nematic Phase (N*): A chiral nematic liquid crystal can either be inherently chiral or chirality can be induced in a nematic via adding some chiral dopant to it, which by inducing helicity, enforce molecules to align at a slight angle to one another in a helical symmetry. The molecules in each layer get twisted perpendicular to the director with their molecular axis parallel to the director as shown in Figure 1.7. The revolution of director results in the formation of a superhelical structure with its axis lying perpendicular to the local director. Directional periodicity is realized along helical axis because of the uniform magnitude of twist throughout the sample. Equipped with all such properties, the phase is known as C**hiral Nematic or Cholesteric.** This phase is characterized by the pitch 'p', which is defined as the distance over which the director undergoes a full 360° twist. For a given chiral nematic mixture, the magnitude of pitch of the helix depends on various factors, like temperature, structure and concentration of chiral medium added etc. The cholesteric LCs are prepared by mixing the nematic LC and a chiral dopant. The concentration 'c' of the chiral dopant is related to the helical twisting power 'HTP' and pitch 'p' as

$$c = (pHTP)^{-1} \text{.....(1.2)}$$

Where, HTP is of the chiral dopant and p is the necessary pitch.

The cholesteric phase appears through nucleation as isotropic – cholesteric phase transition is of the first order. The cholesteric LC with the pitch much smaller than the size of deformations have a quasi-layered structure, like smectic phase.

If pitch of the helix is of the order of wavelength of visible light, many useful properties like Bragg reflection, laser emission at a lower threshold are displayed [25]. The handedness of helical structure depends on the chiral configuration of the dopant. The isotropic – cholesteric phase transition is of the first order, i.e., the cholesteric

If we shine circularly polarized light of wavelength comparable to pitch, along the helical axes, it is totally reflected leaving the substance showing iridescent colour depending on the handedness of helical superstructure and the handedness of circularly polarized light. The reflected wavelength that is given by $\lambda_0 = n\ p$ where n is the average refractive index and p is the pitch of liquid crystal medium. The width of reflection band is $\Delta\lambda = \Delta np$, where Δn is optical anisotropy. If we shine light with a wavelength greater than the helical pitch, chiral medium can be treated as optically homogeneous at macroscopic level. Polarizing microscopy is done to identify the mesophases. The type of texture seen in the microscope depends on the phase, structure and alignment of molecules

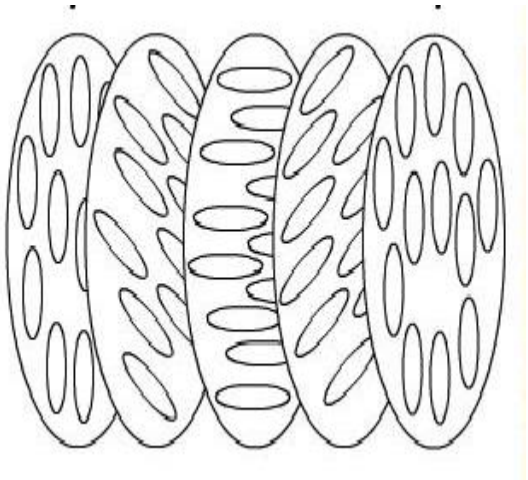

Fig. 1.7 Molecular arrangement in a cholesteric liquid crystal and texture.

in the sample. [Fig. 1.8] The sample can either be in homogeneous (planar) alignment presenting itself as Grandjean Texture or in homotropic alignment, where, long axes of molecules is aligned perpendicular to the substrate and we see complete darkness if helical super structure is completely unwound. Although, for tilted smectic and bi-axial phases, complete extinction does not happen. Sometimes due to anchoring conditions, a random

distribution of helical axes takes place, which represents itself as focal conic texture. In this case, incident light is weakly scattered in all directions.

Electro-optic Switching in Cholesteric Phase: When a square wave ac electric field is applied normal to a chiral liquid crystal confined in the planar boundary conditions of conducting substrates, director of chiral liquid crystal tends to align along the electric field depending on the sign of dielectric anisotropy. A small field will switch the material from planar to fingerprint texture, where helical axis remains parallel to the substrates [Fig. 1.8 (e)].

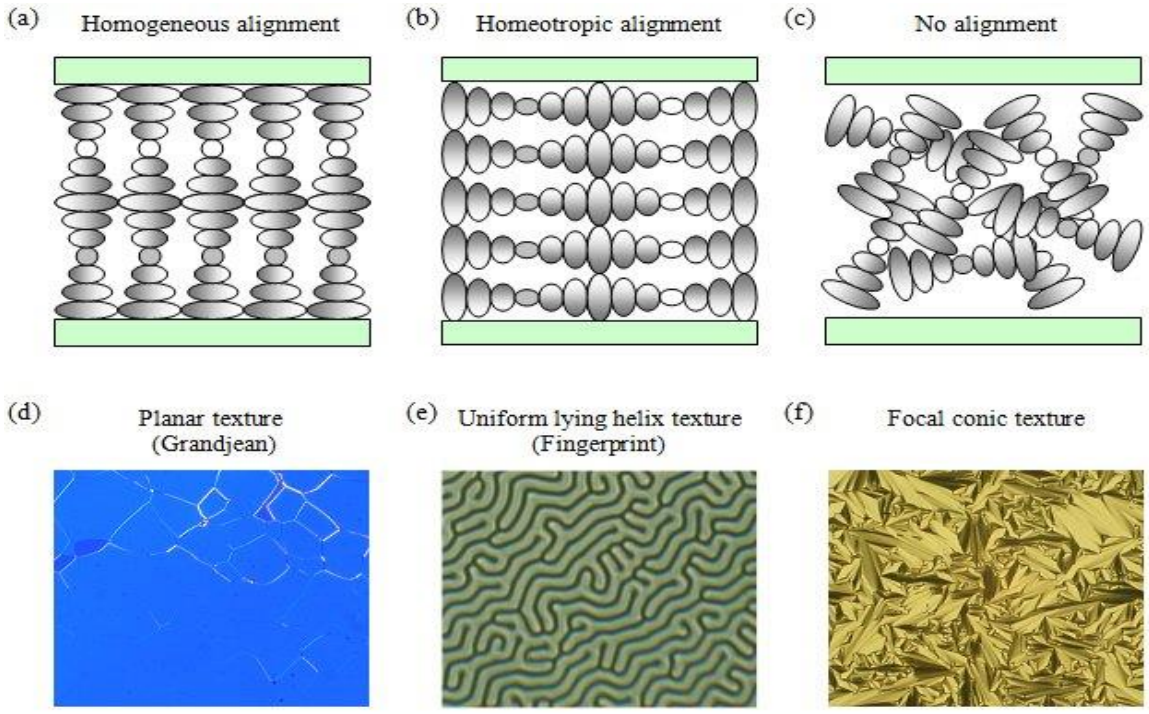

Fig. 1.8: (a,b,c) Schematic of the molecular arrangement in chiral nematic liquid crystals, (d,e,f) The micro textures representing various alignments [26]**.**

A competition between anchoring forces due to the pre-aligned cell surfaces and the elastic forces of the medium in the presence of electric field can result in the formation of focal conic texture [Fig. 1.8 (c,f)]. Here, helical axes corresponding to individual domains being unevenly oriented, there is an abrupt change of refractive indices at the domain boundaries and scattering can be seen throughout the cell [27]. Depending upon the boundary

conditions and director orientation / helix axis orientation a further increase in applied electric field leads to homeotropic state.

1.4.2 Chiral Smectic Phase (Sm*)*:* As in nematics, smectic mesophases also have a chiral state designated as Sm*. Here, director makes a tilt angle with respect to the smectic layer normal and rotates from layer to layer forming a helix resulting in a structure that lacks mirror symmetry. [Fig. 1.9]

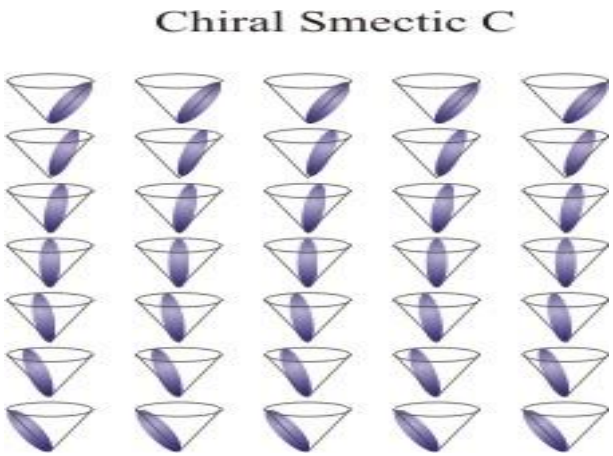

Fig. 1.9: Molecular arrangement in SmC* phase [26]**.**

Since the molecules are lying in a layered structure, they can not be twisted within the layer. In this case, chirality is brought in via a spontaneous twist and bend of the director field. Bending imposes a shearing force on the molecules, due to which their electric polarization takes place and they exhibit ferroelectric qualities while in this phase.

1.4.3 Blue Phase and TGB Phase:

The blue phases are a set of thermodynamically distinct phases that occur between the helical phase and isotropic phase of highly chiral liquid crystals *i.e.*, for materials with cholesteric pitches below about one micrometer. They disappear on decreasing enantiomeric excess. These mixtures may exhibit one or more blue phases (BP) as they are heated from the helical phase to isotropic phase. In order of increasing temperature, blue phases are called BPI, BPII and BPIII (leaving smectic blue phases, which are still inexplicable). These are formed by a regular three-dimensional lattice of defects within a chiral liquid crystal. At the highest temperature BPIII is observed, which is an amorphous phase with a local cubic

defect structure of short correlation length. As it is normally difficult to detect via optical microscopy, it was named as Fog phase or Blue fog.[28] It reflects circular polarized light, which indicates a photonic structure with a helical superstructure where the reflection band is relatively broad when compared to other Blue Phases or cholesteric phase. BPI and BPII comprise of double twist cylinders with the director spiraling around any radius of the cylinder. On a macroscopic scale three of the double twist cylinders arrange mutually perpendicular to each other. Such a structure cannot fill three-dimensional space without the introduction of defects. [Figure 1.10].

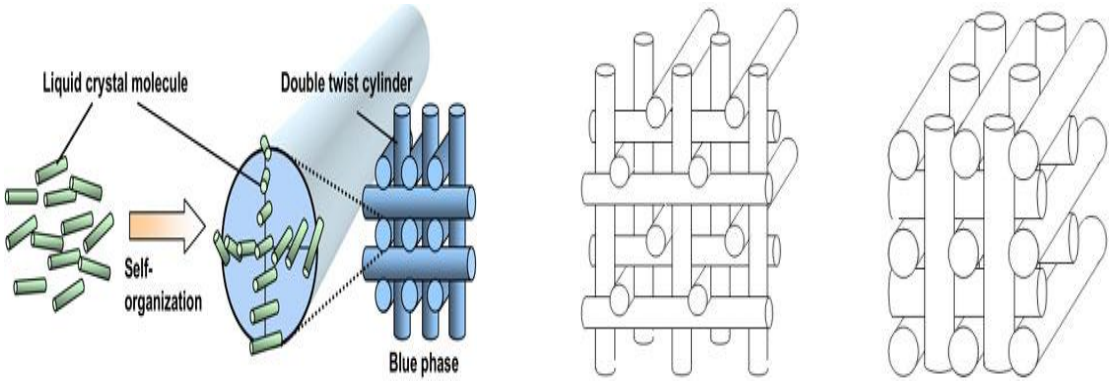

Fig. 1.10: (a) Formation of a Blue phase (b) The structure of BPI (c) BPII [26]**.**

Being of cubic symmetry, the Blue Phases are optically isotropic, while the colors observed in polarizing microscopy are due to the orientations of the systems of double twist cylinders and the different defect lattice planes observed. This phase holds vast utility for a spectrum of applications in 3D lasers, light filters, and displays [29]. Recently, a new display mode has been proposed, which utilizes the Kerr effect appearing in a polymer stabilized BP. These displays have higher switching speeds and improved vision quality.

The major hindrance in their utility is narrow temperature range of existence (~1K) of BP phase during transition from clear isotropic to liquid crystalline helical phase. Research is being done to widen the temperature range of their existence [30–33]. These are observed only for highly chiral materials (pitches below one micrometer) [28].

Twist Grain Boundary (TGB) phases are formed between cholesteric and fluid smectic phases. They occur when chirality is added to a layered phase [34]. They are a type of frustrated phases where, blocks with smectic ordering are slightly twisted with respect to one another, resulting in the formation of dislocations at the places between the layers in adjoining blocks [35]. As twist distortions are not allowed in layered phases, a competition between chirality and layered symmetry starts in such media. The existence of smectic blue phase where, the smectic layers are not perfect planes, but appear to be rotated about a hypothetical axis has also been reported [36,37]. The TGB phases also exist in a very narrow temperature range only.

1.5 Response of liquid crystals to external stimuli

As discussed earlier, liquid crystalline phases belong to a state of matter, which exists only for a limited temperature range and type of mesogens used. These phases are highly dependent on the degree of organization and dynamic behavior of the samples. Hence, they strongly respond to various external stimuli, such as temperature, incident radiation, electric and magnetic fields and nature and concentration of non-mesogenic dopants added to them. This property of liquid crystals makes them interesting as a topic of research, and potentially useful as a functional material.

1.5.1 Effect of temperature: Most of the liquid crystals are thermotropic where the degree of anisotropicity depends on the degree of organization of mesogens, which in turn depends on the temperature. So, physical properties like colour, texture, transparency, birefringence, dielectric constant, and, thermal conductivity etc., depend on temperature. Similarly, anisotropy in thermal conductivity affects the final shape as it approbates growth in specific directions. Optical birefringence is a vital parameter for liquid crystal devices. Liquid crystals, being doubly refracting have two indices of refraction (extraordinary n_e and ordinary n_o) and they show birefringence $\Delta n = n_e - n_o$. As refractive index is linearly dependent on absolute temperature, optical birefringence is also greatly affected by changes in temperature [38].

The order parameter, defined as the measure of the degree of orientational order in nematic liquid crystals also depends on temperature as shown in figure 1.3 (c). This leads to the

formation of different temperature-dependent phases. In chiral phases, the pitch plays the lead role in deciding the optical behavior of the material. Being temperature dependent, a variety of optical and electro-optical properties have been reported following the thermal variation in pitch [39].

1.5.2 Effect of Electric and Magnetic Fields: Liquid crystals may possess permanent or electrically induced dipole moment depending upon whether they consist of polar or non-polar molecules. Because of the uniaxial anisotropy of liquid crystal molecules, value of the dielectric constant experienced by an applied electric field depends on its direction with respect to the director of liquid crystal medium. The difference in the values of dielectric constants in a direction parallel and perpendicular to the director is called the dielectric anisotropy. The dielectric anisotropy is positive ($\Delta \varepsilon > 0$) and the molecules tend to align parallel to the applied electric field direction if the molecular dipole moments are parallel to the long molecular axis. The molecular alignment is perpendicular to an electric field in case of negative anisotropy. The dielectric anisotropy leads to the anisotropy in the susceptibility of electric field, due to which liquid crystal molecules experience a torque. Final structure of the medium is decided by the outcome of the competition between electric (or magnetic) field force and the elastic torques. The vulnerability of the director to electric or magnetic field allows manipulation of optical anisotropy or birefringence, externally [18,40].

The application of electric field, to a chiral nematic liquid crystal, with due care of its direction of application with respect to the helical axis, can be helpful in manipulating the pitch of the helix. This method of tuning the pitch has been used for controlling the position of photonic band gap [41–43].

1.5.3 Effect of wavelength and intensity of incident light: When irradiated by laser light, some special liquid crystals like dye doped, align themselves perpendicular to the direction of polarization and remain oriented even in the absence of laser radiation. Subsequent illumination reorients them. This property of liquid crystals finds application in optical memories, binary and adaptive optics and molecular micro-assembly for large area displays.

High-intensity laser beams directed onto liquid crystals produce a reorientation of the director molecules within the liquid crystal at a microscopic level [44]. They themselves remain undiffracted and confined in a narrow beam, thus producing a waveguide. Use of a liquid crystal medium prompts active control or tenability to the waveguide device [45].

1.6 Defects in Liquid Crystals: Defects are defined as local discontinuities in the symmetry of an ordered medium. Dislocations are basic defects of media with continuous symmetries like liquid crystals which break translational and rotational symmetries. When all the molecules are perfectly aligned to point along a single director, then the liquid crystals are most stable. The alignment of their anisotropic molecules gives nematics a local orientational degree of freedom. Smectic phase, as mentioned earlier, is formed of equally spaced fluid layers of molecules stacked one over the other forming an ordered array along one axis with liquid crystal molecules arranged in a symmetrical pattern within the layers [46]. Defect structures are normally formed due to the external perturbations. The direction of the liquid crystal director can abruptly change at any place within the sample. At such places, the director is said to be undefined, and a disclination is formed. Liquid crystals allow topological defects as do all the materials with broken symmetry. These are regions where discontinuity is forced by the topological behavior of the configuration outside of them. As these defects, cannot be removed by an entirely local perturbation within the sample so they are considered stable. They must be either moved out to the boundary of the sample or merged into other such defects within the sample. Frank free energy of the liquid crystal (section 1.2.1) must be calculated to know the stability of a disclination.

1.7 Classification and Applications of Nanomaterials

The materials where at least one dimension is less than approximately 100 nanometers are defined as nanoscale substances. As per Siegel [47], nanomaterials are classified as zero-dimensional (spheres and clusters), one-dimensional (wires, and rods) two-dimensional (thin films, plates, and networks) and three-dimensional nanomaterials.

They have structural features and properties different from bulk materials. Owing to their nanometer size they have (i) a larger fraction of surface atoms and hence high surface energy; (ii) spatial confinement and reduced imperfections, which are absent in the corresponding bulk materials. (iii) Higher chemical reactivity due to large surface area to

volume ratio (iv) Quantum effects, which play a decisive role in determining material's properties and characteristics, are also prominent at nanoscale. Nanomaterials show gross changes in electro-optical, optical and magnetic behavior which lead to several useful properties from the application point of view. For example, metallic nanoparticles are very active catalysts. Chemical sensors using nanomaterials have enhanced sensitivity and selectivity. Lasers and light emitting diodes (LED) from both: quantum dots and quantum wires are very promising indeed. High-density information storage using quantum dot devices is also an upcoming field. A lesser number of imperfections give enhanced chemical stability and better mechanical properties of nanomaterials e.g., in carbon nanotubes [48].

The optical properties of nanomaterials strongly depend on their size, shape, anisotropy and surface conditions. Factors like doping and presence of other particles in the surrounding environment also affect their properties. Applications based on optical properties of nanomaterials include optical detectors, lasers, sensors, display devices and solar cells [49]. They are also finding their use in the fields of photoelectrochemistry and biomedicine [50]. Nanomaterials are already in commercial use with a wide range of available products which include cosmetics, sunscreens, electronics, paints and, stain-resistant and wrinkle-free textiles. Nano-coatings and nanocomposites are being used in windows, sports equipment, bicycles and, automobiles. To protect beverages from damage by sunlight, the glass bottles are now available with UV-block coatings. Butyl rubber/nano-clay composites are used to make tougher tennis balls. Nanoscale titanium dioxide, for instance, is used in cosmetics, sunblock creams, and self-cleaning windows. Nanoscale silica is commercially used as a filler in cosmetics and dental fillings.

We, in the present study, have used single walled carbon nanotubes (SWCNTs) and multiwalled carbon nanotubes (MWCNTs) as dopants in CLC matrix. Carbon nanotubes (CNTs) are hollow cylinders of carbon atoms with hexagonal carbon rings forming the walls. They are usually formed in large bundles. While SWCNTs have only one single layer of graphene cylinders; the MWCNTs are multilayered (approximately 50 layers) [Figure 1.11] [51,52]. They can be further classified as an armchair, zigzag, and chiral depending upon the shape of their unit cell as shown in [Figure 1.12]

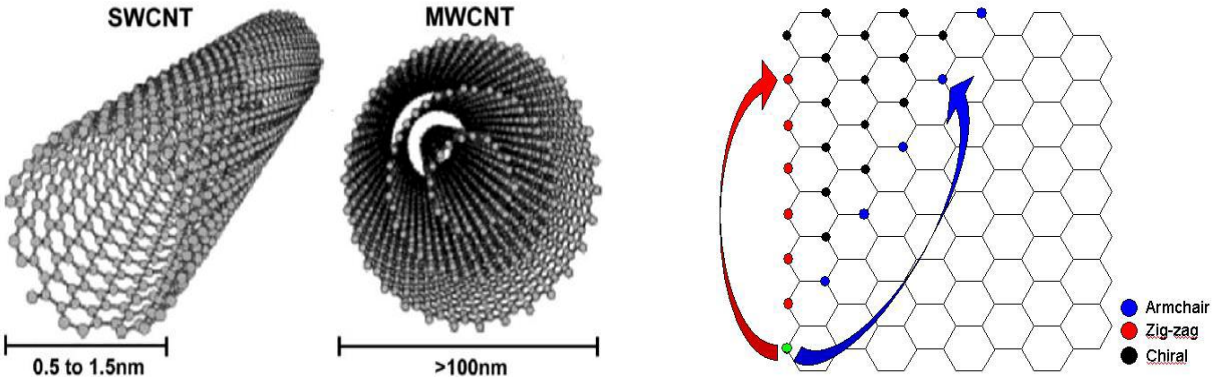

Fig. 1.11: (a) Schematic of SWCNTs and MWCNTs [53] ***(b) Different types of arrangement of carbon atoms in CNTs*** [54]**.**

CNTs can behave either as a metal or a semiconductor depending upon the symmetry and the way they "wind up." Carbon Nanotubes have exceptional mechanical and electrical properties. Despite having a diameter as small as 50,000 times thinner than a human hair, they are stronger than steel per unit weight. Although they have high aspect ratio yet they possess high tensile strength of the order of 200 Giga pascals.

Various methods have been used by researchers for the growth of CNTs e.g., arc discharge, laser ablation, and chemical vapor deposition (CVD) [55]. The best technique is expected to deliver uniformity in length and width of the CNTs. CVD is considered as the best technique to synthesize CNTs as with this technique CNTs can be produced at relatively low temperatures and their size can be controlled by varying the size of catalyst particles. Owing to their small size, high aspect ratio and, smooth surface, nanotubes find their use for energy storage. MWCNTs are nowadays considered as a superior replacement of electrically conductive carbon blacks in electrically conductive ink for printable circuits, wind power generators, aircraft, automotive and electronic industries. Due to their low density and high mechanical strength, CNT-reinforced thermoplastics are used in almost every sports item and automotive industry, where a low weight material is required to save energy as a replacement to metals [56].

We have also used silver nanoparticles and 6% aluminum doped Zinc oxide nanoparticles (AZO) as dopants in CLC. Silver nanoparticles (AgNPs) have been a subject of great interest among scientists due to their remarkable electrical and chemical properties such as

good conductivity, catalytic and anti- bacterial effect [57]. Moreover, a successful use of AgNPs in modification and preparation of materials with improved properties for application in fields like clothing and semiconductors has also been reported [58,59]. The silver nanoparticles show an efficient uptake into macrophages as compared to gold nanoparticles [60]. Moreover, they are much cheaper than gold nanoparticles.

Zinc oxide is an intrinsic n-type semiconductor having several remarkable properties like good transparency [61], high electron mobility 2000 $cm^2/(Vs)$ at 80 K [62] and strong room-temperature luminescence [63,64]. The most important characteristic is its wide band gap ~3.37 eV in the ultraviolet (UV) region and Zn and O stacked in alternate layers which make ZnO a suitable candidate for UV light lasers and detectors functioning in the range of 368–390 nm [62]. Due to a large number of extrinsic and intrinsic deep-level impurities and clusters, ZnO emits all constituents of white light [65]. The ZnO doped liquid crystals are nowadays being used in transparent electrodes for liquid crystal displays, energy saving and heat protecting windows, thin film transistors and, light emitting diodes (LED). Elements like Al, In, Ga, etc. act as donors in ZnO lattice and further widen band gap thus improving electrical and optical properties of ZnO [66]. Al-doped ZnO has been reported to be useful in the fabrication of optoelectronics devices and detectors [67,68].

1.8 Functionalized Nanoparticles

Owing to the unique properties and easy organization of nanoparticles into more complex systems, they need to be incorporated into some organized systems to make an optimum use of their potential. Among all the active mediums, liquid crystals stand out from the rest because of their large birefringence on refractive index, low threshold on transition among different states, and versatile driven methods to cause transitions [69]. The intrinsic order, mobility and sensitivity of liquid crystals to external stimuli make them most suitable candidates for nanoparticle organization and their subsequent use as advanced functional materials [70].

To reduce interparticle interactions and make them adapt the liquid crystalline phase, we need to either cap the nanoparticles with some suitable capping agent or make a dilution by adding some solvent. The method of choice is to attach a suitable group to the nanoparticle so that the self-assembling and phase forming properties of the attached group may be passed on to the final product. While in the case of nanoparticles with high aspect ratio,

formation of liquid crystal phases is facilitated by their inherent shape [71], we need to enhance the anisotropy of [72] quasi-spherical NPs by attaching ligands which force them to self-assemble in an ordered structure. The attached functional groups should be able to provide enough flexibility and mobility to the NPs to get themselves well-adjusted into the ordered phase and still maintain a fluid state.

Functionalized nanoparticles e.g., silver nanoparticles capped with dodecanethiol [73], ZnO capped with octadecylamine (ODA) are the materials made for a variety of potential applications.

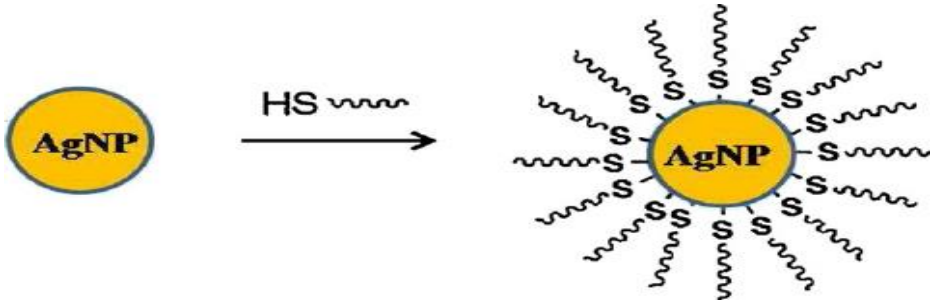

Fig.1.2: Functionalized silver nanoparticles

Combined with the supramolecular ordering and defect tolerance of LC phases and the pronounced, size related properties of NPs, functionalized nanoparticles promise a bright future for their use in the production of novel materials with structural and functional versatility [74]. With the unfolding of new physical properties, they have strongly emerged as a promising medium for the fabrication of high-density recording media [75,76], charge-transport devices [77] nanoscale Plasmon waveguides [35] and metamaterials or negative refractive index materials with unusual optical properties [78].

1.9 Doping of nanoparticles in Liquid crystals

The characteristics of doped LCs are determined by the type of nanoparticles used as guest dopants. Generally, four main kinds of nanoparticles are doped in LC materials, such as conductive, inorganic, ferroelectric nanoparticles and carbon nanotubes (CNTs). The Nano-doped LCs display many special features such as induced vertical alignment, faster electro-optical switching, frequency modulation and, enhancement of dielectric anisotropy and birefringence. Different composite media with functionalized metallic or semiconductor nanoparticles doped in liquid crystals have been studied by researchers for their optical and

electro-optic properties [79][80]. Depending on the type of functionalization and concentration of nanoparticles, anchoring conditions and, external stimulants, significant differences in the observed parameters have been recorded. The inherent flexibility of liquid crystals, combined with size and shape-dependent properties of nanoscale particles brings in the much-needed versatility in fabrication of functional materials.

The integration of liquid crystals with functionalized nanoparticles has paved way for the development of new active materials and devices with enhanced performance. Surface plasmonics combined with advanced nanofabrication techniques have found their vast application in the fields of super-resolution imaging [81–85] optical cloaking [86–88] and energy harvesting [89–93]. Being organic in nature, chemical synthesis and large scale processing of liquid crystals are possible. Moreover, they show compatibility with most of the technologically important optoelectronic materials. Based on these observations, a lot of research work is being done. Their sensitivity towards external stimuli like temperature, electric and magnetic fields, light, and acoustic waves makes them suitable for the development of active Nanophotonics.

References

1. Singh S. Liquid Crystals: Fundamentals. Liq. Cryst. Phys. Prop. Nonlinear. 2002.

2. Paleos CM. Thermotropic Liquid Crystals Formed by intermolecular hydrogen bonding interactions. Angew. Chem. Int. Ed., 1995;34:1696–711.

3. Stephen MJ, Straley JP. Physics of liquid crystals Liquid crystals in general. Rev. Mod. Phys. 1974.

4. Andrienko D. Introduction to liquid crystals. Int. Max Planck Res. Sch. Model. Soft Matter. 2006;1–32.

5. Khoo IC. Nonlinear optics of liquid crystalline materials. Phys. Rep. 2009. p. 221–67.

6. Wu ST, Efron U, Hess LD. Birefringence measurements of liquid crystals. Appl. Opt. 1984;23:3911–5.

7. Lagerwall JPF, Scalia G. A new era for liquid crystal research: Applications of liquid

crystals in soft matter nano, bio and microtechnology. Curr. Appl. Phys. 2012. p. 1387–412.

8. Hanna J. Towards a new horizon of optoelectronic devices with liquid crystals. Opto-Electronics Rev. 2005;13:259–67.

9. Xie P, Zhang R. Liquid crystal elastomers, networks and gels: advanced smart materials. J. Mater. Chem. 2005;15:2529.

10. O'Neill M, Kelly SM. Liquid crystals for charge transport, luminescence, and photonics. Adv. Mater. 2003;15:1135–46.

11. Yadav N, Dabrowski RS, Dhar R. Effect of alumina nanoparticles on dielectric permittivity, electrical conductivity, director relaxation frequency, threshold and switching voltages of a nematic liquid crystalline material. Liq. Cryst. 2014;41:1803–10.

12. Paul SN, Dhar R, Verma R, Sharma S, Dabrowski R. Change in dielectric and electro-optical properties of a nematic material (6CHBT) due to the dispersion of BaTiO3 nanoparticles. Mol. Cryst. Liq. Cryst. 2011;545:105–11.

13. Paleos CM, Tsiourvas D. Supramolecular hydrogen-bonded liquid crystals. Liq. Cryst. 2001;28:1127–61.

14. Senyuk B. Liquid Crystals: a Simple View on a Complex Matter. 2014.

15. TLP Library Liquid Crystals - Introduction.

16. Kato T, Mizoshita N, Kishimoto K. Functional liquid-crystalline assemblies: Self-organized soft materials. Angew. Chemie - Int. Ed. 2005. p. 38–68.

17. Kouwer PHJ, Mehl GH. Hierarchical organisation in shape-amphiphilic liquid crystals. J. Mater. Chem. 2009;19:1564–75.

18. Collings PJ. Introduction to Liquid Crystals: Chemistry and Physics. Am. J. Phys. 1998. p. 551.

19. Popa-Nita V, Gerlič I, Kralj S. The influence of disorder on thermotropic nematic liquid crystals phase behavior. Int. J. Mol. Sci. 2009. p. 3971–4008.

20. Chemistry: The Central Science, Chapter 12, Section 2.

21. Goodby JW. Chirality in liquid crystals. J. Mater. Chem. 1991;1:307.

22. Kim KH, Song DH, Shen ZG, Park BW, Park KH, Lee JH. Fast switching of long-pitch cholesteric liquid crystal device. Opt. Express. 2011;19:10174–9.

23. Tamaoki N. Cholesteric liquid crystals for color information technology. Adv. Mater. 2001. p. 1135–47.

24. Petriashvili G, Japaridze K. Paper like cholesteric interferential mirror. Opt. 2013;21:20821–30.

25. Furumi S. Recent progress in chiral photonic band gap liquid crystals for laser applications. Chem. Rec. 2010;10:394–408.

26. CMMPE - University of Cambridge. 2015.

27. Tarasov OS, Krekhov AP, Kramer L. Dynamics of cholesteric structures in an electric field. Phys. Rev. E. Stat. Nonlin. Soft Matter Phys. 2003;68:031708.

28. Dierking I. Chiral liquid crystals: structures, phases, effects. Symmetry (Basel). 2014;6:444–72.

29. Cao W, Muñoz A, Palffy-Muhoray P, Taheri B. Lasing in a three-dimensional photonic crystal of the liquid crystal blue phase II. Nat. Mater. 2002;1:111–3.

30. Coles HJ, Pivnenko MN. Liquid crystal “blue phases” with a wide temperature range. Nature. 2005;436:997–1000.

31. Castles F, Morris SM, Terentjev EM, Coles HJ. Thermodynamically stable blue phases. Phys. Rev. Lett. 2010;104.

32. Yoshida H, Tanaka Y, Kawamoto K, Kubo H, Tsuda T, Fujii A. Nanoparticle-stabilized cholesteric blue phases. Appl. Phys. Express. 2009;2.

33. Kikuchi H, Yokota M, Hisakado Y, Yang H, Kajiyama T. Polymer-stabilized liquid crystal blue phases. Nat. Mater. 2002;1:64–8.

34. Lubensky TC, Harris AB, Kamien RD, Yan G. Chirality in Liquid Crystals: from Microscopic Origins to Macroscopic Structure. Ferroelectrics. 1998;212:1–20.

35. Si G, Zhao Y, Leong ESP, Liu YJ. Liquid crystal enabled active plasmonics: A review. Materials (Basel). 2014. p. 1296–317.

36. Sebastiao PJ, Gradišek A, Pinto LF V, Apih T, Godinho MH, Vilfan M. Fast field-cycling NMR relaxometry study of chiral and nonchiral nematic liquid crystals. J. Phys. Chem. B. 2011;115:14348–58.

37. Dierking I. A review of textures of the TGBA* phase under different anchoring geometries. Liq. Cryst. 1999;26:83–95.

38. Kelly SM, O'Neill M. Liquid crystals for electro-optic applications. Handb. Adv. Electron. Photonic Mater. Devices, Vol. 7 Liq. Crystals, Disp. Laser Mater. 2000.

39. Stephen MJ, Straley JP. Physics of liquid crystals. Rev. Mod. Phys. 1974;46:617–704.

40. Renn SR, Lubensky TC. Abrikosov dislocation lattice in a model of the cholesteric to smectic-A transition. Phys. Rev. A. 1988;38:2132–47.

41. Yamamoto J, Nishiyama I, Inoue M, Yokoyama H. Optical isotropy and iridescence in a smectic “blue phase”. Nature. 2005;437:525–8.

42. Huang Y, Zhou Y, Doyle C, Wu ST. Tuning the photonic band gap in cholesteric liquid crystals by temperature-dependent dopant solubility. Opt. Express. 2006;14:1236–42.

43. Kimura H, Hosino M, Nakano H. Temperature dependent pitch in the cholesteric phase. Le J. Phys. 1979;174–7.

44. For B, Crystals L. The physics of liquid crystals (International Series of Monographs on Physics) by J . Prost. Liq. Cryst. 1974;

45. Whinnery J, Hu C, Kwon Y. Liquid-crystal waveguides for integrated optics. Quantum Electron. IEEE. 1977;262–7.

46. Chen BG. Topological defects in nematic and smectic liquid crystals. ProQuest. 2012;1–

132.

47. Sanjay SS, Pandey AC. A brief manifestation of nanotechnology. Adv. Struct. Mater. 2017. p. 47–63.

48. Alagarasi A. Chapter - Introduction to nanomaterials. 2016;

49. Suresh S. Semiconductor Nanomaterials, Methods and Applications: A Review. Nanosci. Nanotechnol. 2013;3:62–74.

50. Salata OV. J. Nanobiotechnology. 2004;6:1–6.

51. Sinha N, Yeow JTW. Carbon nanotubes for biomedical applications. IEEE Trans. Nanobioscience. 2005;4:180–95.

52. Iijima S. Helical microtubules of graphitic carbon. Nature. 1991;354:56–8.

53. Malhotra BD, Srivastava S, Augustine S. Biosensors for food toxin detection: Carbon nanotubes and graphene. Mater. Res. Soc. Symp. Proc. 2015;1725.

54. https://web.stanford.edu/group/cpima/education/nanotube_lesson.pdf

55. Purohit R, Purohit K, Rana S, Rana RS, Patel V. Carbon nanotubes and their growth methods. Procedia Mater. Sci. Elsevier B.V.; 2014;6:716–28.

56. Kingston C, Zepp R, Andrady A, Boverhof D, Fehir R, Hawkins D. Release characteristics of selected carbon nanotube polymer composites. Carbon N. Y. Elsevier Ltd; 2014;68:33–57.

57. Jiang ZJ, Liu CY, Sun LW. Catalytic properties of silver nanoparticles supported on silica spheres. J. Phys. Chem. B. 2005;109:1730–5.

58. Armelao L, Bottaro G, Campostrini R, Gialanella S, Ischia M, Poli F. Synthesis and structural evolution of mesoporous silica–silver nanocomposites. Nanotechnology. 2007;18:155606.

59. Thomas S, Nair SK, Jamal EMA, Al-Harthi SH, Varma MR, Anantharaman MR. Size-dependent surface plasmon resonance in silver silica nanocomposites. Nanotechnology.

2008;19:075710.

60. Haase A, Mantion A, Graf P, Plendl J, Thuenemann AF, Meier W. A novel type of silver nanoparticles and their advantages in toxicity testing in cell culture systems. Arch. Toxicol. 2012;86:1089–98.

61. Liu X, Pan K, Li W, Hu D, Liu S, Wang Y. Optical and gas sensing properties of Al-doped ZnO transparent conducting films prepared by sol-gel method under different heat treatments. Ceram. Int. 2014;40:9931–9.

62. Thandavan TMK, Gani SMA, Wong CS, Nor RM. Enhanced photoluminescence and Raman properties of Al-doped ZnO nanostructures prepared using thermal chemical vapor deposition of methanol assisted with heated brass. PLoS One. 2015;10.

63. Arya SK, Saha S, Ramirez-Vick JE, Gupta V, Bhansali S, Singh SP. Recent advances in ZnO nanostructures and thin films for biosensor applications: Review. Anal. Chim. Acta. 2012;1–21.

64. Özgür Ü, Alivov YI, Liu C, Teke A, Reshchikov MA, Doğan S. A comprehensive review of ZnO materials and devices. J. Appl. Phys. 2005;1–103.

65. Look DC. Recent advances in ZnO materials and devices. Mater. Sci. Eng. B Solid-State Mater. Adv. Technol. 2001;80:383–7.

66. Sernelius BE, Berggren KF, Jin ZC, Hamberg I, Granqvist CG. Band-gap tailoring of ZnO by means of heavy Al doping. Phys. Rev. B. 1988;37:10244–8.

67. Kumar R, Al-Dossary O, Kumar G, Umar A. Zinc oxide nanostructures for no2 gas–sensor applications: A review. Nano-Micro Lett. 2014;1–24.

68. Ozgür M, Hofstetter D, Morkoç H. ZnO Devices and Applications: A Review of Current Status and Future Prospects. Proc. IEEE. 2010;98:1255–68.

69. Wu ST. Birefringnece dispersions of liquid crystals. Development. 1986;33:1270–4.

70. Busseron E, Ruff Y, Moulin E, Giuseppone N. Supramolecular self-assemblies as functional nanomaterials. Nanoscale. 2013;5:7098–140.

71. Li Shi-L, Walda J, Manna L, Alivisatos AP. Semiconductor Nanorod Liquid Crystals. Nano Lett. 2002;2:557–60.

72. Lane JMD, Grest GS. Spontaneous asymmetry of coated spherical nanoparticles in solution and at liquid-vapor interfaces. Phys. Rev. Lett. 2010;104.

73. Ravindran A, Chandran P, Khan SS. Biofunctionalized silver nanoparticles: Advances and prospects. Colloids Surfaces B Biointerfaces. Elsevier B.V.; 2013;105:342–52.

74. Bedanta S, Kleemann W. Supermagnetism. J. Phys. D Appl. Phys. 2009;42:13001.

75. Shi J, Gider S, Babcock K, Awschalom DD. Magnetic clusters in molecular beams, metals, and semiconductors. Science. 1996;271:937–41.

76. Sun, Murray, Weller, Folks, Moser. Monodisperse FePt nanoparticles and ferromagnetic FePt nanocrystal superlattices. Science. 2000;287:1989–92.

77. Garbovskiy Y, Glushchenko I. Nano-Objects and Ions in Liquid Crystals: Ion trapping effect and related phenomena. Crystals. 2015;5:501–33.

78. Bisoyi HK, Kumar S. Liquid crystal nanoscience: an emerging avenue of soft self-assembly. Chem. Soc. Rev. 2011;40:306–19.

79. Bisoyi HK, Kumar S. Carbon nanotubes in discotic liquid crystals. J. Indian Inst. Sci. 2009;89:101–12.

80. Rahman M, Lee W. Scientific duo of carbon nanotubes and nematic liquid crystals. J. Phys. D. Appl. Phys. 2009;42:063001.

81. Pendry JB. Negative refraction makes a perfect lens. Phys. Rev. Lett. 2000;85:3966–9.

82. Fang N, Lee H, Sun C, Zhang X. Sub-Diffraction Limited Optical Imaging with a Silver Superlens. Science. 2005;308, 5721:534–7.

83. Pendry JB, Smith DR. The quest for the superlens. Sci. Am. 2006;295:60–7.

84. Xiong Y, Liu Z, Durant S, Lee H, Sun C, Zhang X. Tuning the far-field superlens: from UV to visible. Opt. Express. 2007;15:7095–102.

85. Liu Z, Durant S, Lee H, Pikus Y, Xiong Y, Sun C. Experimental studies of far-field superlens for sub-diffractional optical imaging. Opt. Express. 2007;15:6947–54.

86. Schurig D, Mock JJ, Justice BJ, Cummer SA, Pendry JB, Starr AF. Metamaterial electromagnetic cloak at microwave frequencies. Science. 2006;314:977–80.

87. Pendry JB, Schurig D, Smith DR. Controlling electromagnetic fields. Science. 2006;312:1780–2.

88. Jacob Z, Narimanov EE. Semiclassical description of non magnetic cloaking. Opt. Express. 2008;16:4597.

89. Zhu G, Lin ZH, Jing Q, Bai P, Pan C, Yang Y. Toward large-scale energy harvesting by a nanoparticle-enhanced triboelectric nanogenerator. Nano Lett. 2013;13:847–53.

90. Walter MJ, Borys NJ, Van Schooten KJ, Lupton JM. Light-Harvesting action spectroscopy of single conjugated polymer nanowires. Nano Lett. 2008;8:3330–5.

91. Andreussi O, Biancardi A, Corni S, Mennucci B. Plasmon-controlled light-harvesting: Design rules for biohybrid devices via multiscale modeling. Nano Lett. 2013;13:4475–84.

92. Dang X, Qi J, Klug MT, Chen PY, Yun DS, Fang NX. Tunable localized surface plasmon-enabled broadband light-harvesting enhancement for high-efficiency panchromatic dye-sensitized solar cells. Nano Lett. 2013;13:637–42.

93. Si G, Zhao Y, Lv J, Lu M, Wang F, Liu H. Reflective plasmonic color filters based on lithographically patterned silver nanorod arrays. Nanoscale. 2013;5:6243–8.

CHAPTER -II

EXPERIMENTAL METHODS AND CHARACTERIZATION TECHNIQUES

Overview

The selection of liquid crystals and nanoparticles (used as dopants), their properties, preparation of doped samples with desired concentration of dopant and the procedure followed to ensure a homogeneous mixing of nanoparticles into liquid crystals have been included in this chapter. The experimental setup and methodology used for fabricating liquid crystal cells and filling of doped liquid crystal samples in them have been thoroughly explained. Details of the procedure adopted for functionalization of nanoparticles have also been given. An appraisal of the role of polarizing optical microscope in deciphering the phase changes after induction of nanoparticles has also been appended. Other characterization techniques employed for the analysis of nanoparticles and doped samples, like Transmission electron microscopy (TEM), Fourier transform infrared (FTIR) Spectroscopy, Fluorescence Spectrophotometry (PL), *dielectric spectroscopy, and Abbe's refractometer have also been reviewed.*

2.1 Selection of Materials

Nowadays, synthesis of new liquid crystal materials, exploration of suitable dopants and capping materials for them has become essential for their enhanced applicability in electro-optical and display devices like light modulators, optical switches, detectors, sensors and large area displays having high contrast [1–10]. Keeping this fact in mind we found it pertinent to dope nanoparticles in a nematic liquid crystal in which chirality had been pre-induced by adding known percentage of chiral molecules. With this conation, we selected ZLI 4151 (commercial name), a nematic mixture, provided by M/s E. Merck, UK, with a positive dielectric anisotropy. Its phase sequence and other properties are enlisted in the table below.

Table 2.1 Data sheet of Nematic Liquid Crystal Mixture ZLI 4151 [11].

1.	Commercial name	ZLI 4151 000, Merck Ltd. UK.
2.	N⇒I Transition temp.	99^{o}C
3.	Dielectric anisotropy	$\Delta\epsilon$ = +10.6 ($\epsilon_{\parallel}$ = 15.0, $\epsilon_{\perp}$ = 4.4)
4.	Elastic constants	k_1 = 1.15 x 10^{-11}N, k_3/k_1= 1.62, $k3/k2$ = 2.90
5.	Optical anisotropy	Δn = + 0.15 (n_o = 1.51 and n_e = 1.66)

Chirality was induced in this nematic mixture by adding an optimum amount of chiral dopant, CB15 (commercial name), also obtained from Merck Co. Ltd. Darmstadt, Germany. The properties of CB15 are tabulated below in Table 2.2.

Table 2.2 Phase Sequence and Molecular Structure of Chiral Liquid Crystal [12].

1.	Commercial name	CB15, Merck Ltd. Darmstadt, Germany
2.	Molecular structure	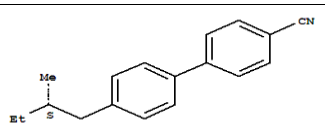
3.	Molecular formula	$C_{18}H_{19}N$
4.	Density	1.02 g/cm^3
5.	Molecular weight	249.35
6.	Refractive Index	1.567
7.	Flash Point	190.1°C
8.	Phase sequence	4^oC -54^oC -30^oC Crystal $\Rightarrow$ SmA $\Rightarrow$ N* $\Rightarrow$ Isotropic

Doping of nematic liquid crystals with small amounts of nanoparticles can significantly alter their electro-optic response [13–16]. To accomplish enhancement in optical and electrooptical properties and to study effects of dopant concentration on the CLC matrix, there was a need to select nanoparticles of various sizes having good optical properties. The following nanoparticles and nanotubes were used as dopants in the CLC.

1. ODA (Octadecylamine) functionalized SWCNTs.

2. COOH (carboxyl group) functionalized MWCNTs.

3. DDT (Dodecanethiol) functionalized silver nanoparticles (AGNPs).

4. ODA functionalized 6% Aluminum-doped Zinc Oxide nanoparticles (AZO).

The properties of dopant nanoparticles are summarized as follows

Table 2.3 Physical properties and Molecular Structure of ODA functionalized SWCNTs [17]**.**

	Dopant name	ODA functionalized SWCNTs (Sigma-Aldrich)
1.	Diameter	2–10 nm
2.	Length	0.5–2μm
3.	Purity	98% (Aldrich)
4.	Structure	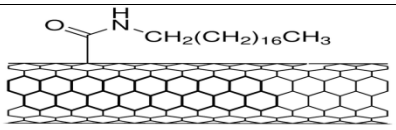

Table 2.4 Physical parameters and structure of COOH functionalized MWCNTs [17]**.**

	Dopant name	COOH functionalized MWCNTs (Sigma-Aldrich)
1.	Diameter	110-170 nm
2.	Length	5-9μm
3.	Purity	97% (Aldrich)
4.	Structure	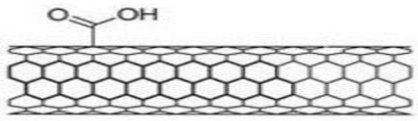

Table 2.5 Physical parameters of DDT functionalized AgNPs [17]**.**

	Dopant name	Dodecanethiol (DDT) functionalized silver nanoparticles [0.1% (w/v) in hexane] (Sigma Aldrich)
1.	Size	5-15nm
2.	Purity	98% (Aldrich)
3.	Density	0.672g/mL at 25°C

Table 2.6 Physical parameters of ODA functionalized AZO NPs [18]**.**

	Dopant name	Octadecylamine functionalised 6% Aluminium doped ZnO (AZO) nanoparticles (Sigma-Aldrich)
1.	Size	≤ 50nm
2.	Purity	97% (Aldrich)

2.2 Cell Fabrication and Sample Preparation

The antiparallel aligned liquid crystal cells of thickness 5 μm were obtained from Linkam Scientific Instruments (UK). The liquid crystal cell is constructed from glass slides coated with indium tin oxide (ITO) on one side of both the slides.

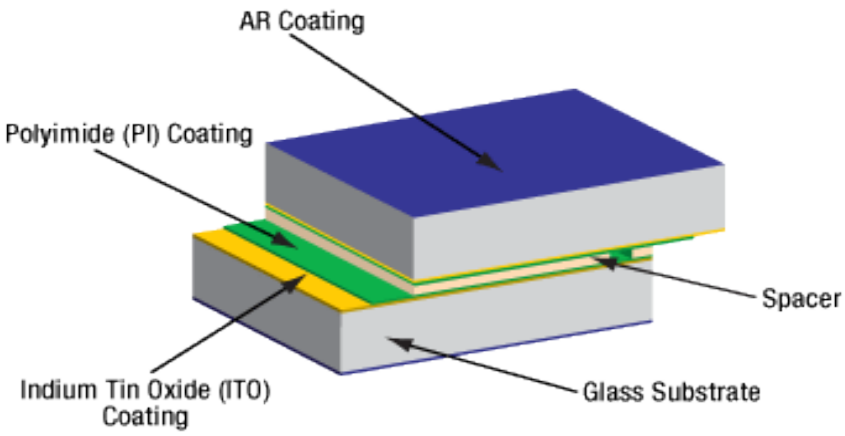

Fig. 2.1 Schematic of a Liquid Crystal Sample Cell [19]**.**

These transparent glass plates having a resistivity of nearly 200 ohm-m are pre-treated with Polyimide and rubbed in anti-parallel direction.

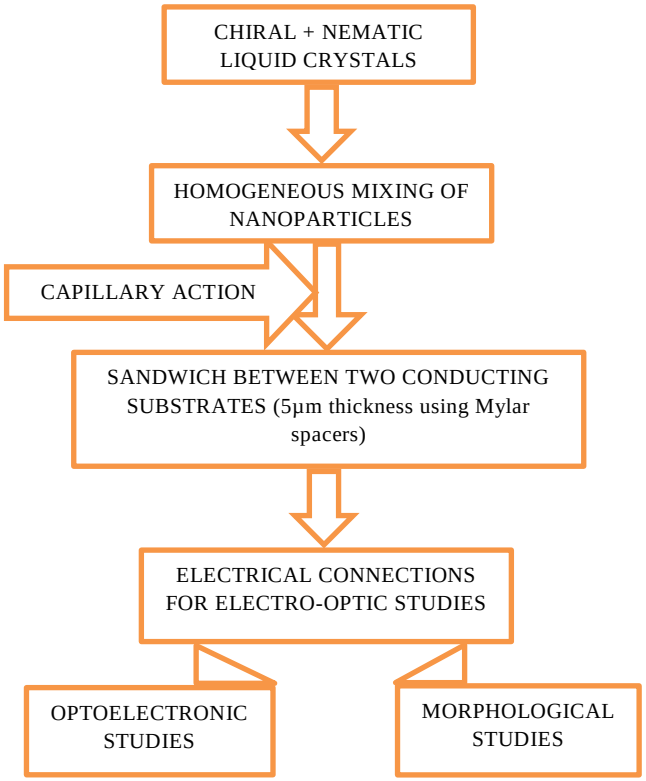

Fig. 2.2 Methodology Followed for the Experimental Work

Thin spacers are used to maintain uniform thickness between the two slides, which are placed one upon the other with their ITO coated sides facing each other. The cell is then

sealed from two sides using optical adhesive and is subsequently filled with liquid crystal composites by capillary action. Electrical connections to the conducting indium tin oxide coated glass substrates were applied using indium solder to comprehend the electro-optic and dielectric responses of the liquid crystal cell.

Carbon nanotubes and nanoparticles were functionalized before dispersing them in CLC to avoid agglomeration and ensure their uniform dispersal. The nanoparticles doped chiral nematic liquid crystal composites were prepared by dispersing appropriate weight percentage of functionalized nanoparticles into the chiral nematic mixture, followed by ultrasonication for about one hour. The methodology has also been depicted in the flow chart above [Fig. 2.2].

2.3. Sample Characterization Techniques

2.3.1. ***Polarizing Optical Microscopy (POM):*** Liquid crystals being birefringent materials strongly interact with polarized light [20]. The inherent anisotropy of their molecules makes them ideal for polarizing microscopy. We have successfully recorded the variations in pitch, phase, color, contrast, isotropic temperature and electro-optic response of the doped CLC samples with the help of transmission optical microscope using polarized light on the liquid crystal sample confined between two indium tin oxide coated plates. We could study all the important parameters and phenomena like the threshold for the Freedericksz transition, electro-convection, defect structures and agglomeration of nanoparticles etc. with varying temperature, electric field, and/or dopant concentration. Typical LC phases like Nematic, Cholesteric and textures like Planar, Grandjean, Fingerprint, Homeotropic, and Focal Conic etc. were also visualized.

The pitch of the cholesteric samples is extremely sensitive to the changes in temperature and other external stimuli [21]. These perturbations can be very minutely observed with the help of POM. In nanoparticles doped CLC samples, where there is a possibility of comportment of many phases, POM helps in identifying them. Liquid crystals being soft crystals, sometimes do not retrieve their original phase after the removal of applied provocations [22]. In such cases, induced memory can be measured by carrying out transmission studies with a photomultiplier tube attached with POM.

Coupled with other investigations like fluorescence spectroscopy (PL) and dielectric spectroscopy, present day POMs equipped with temperature controller and hot stage is indispensable for liquid crystal research. While differential scanning calorimetery (DSC) provides information about phase transition temperatures and the order of transition, polarizing microscopy provides additional information about the phase type from characteristic textures and defect structures. In the field of medicine, birefringence is used as an effective diagnostic tool with the help of polarizing optical microscope [23].

Instrumentation and the Principle of working: As shown in Fig. 2.3, the microscope must be equipped with a polarizer and an analyzer placed in the optical pathway somewhere before the specimen and the objective respectively.

Fig. 2.3 (a) Schematic of optical polarizing microscope [24] ***(b) Carl Zeiss Scope A1.***

To study the morphology of a specimen, light from an incandescent source is made to pass through a polarizer. The polarized light then passes through a prism that splits it into components, having separation equal to the resolution of the objective lens. The beams go to the specimen after passing through a condenser. In a region of the specimen, where adjacent regions differ in refractive index, the two beams get out of phase with respect to each other. The interaction of plane-polarized light with a birefringent specimen produces two wave components, both polarized in mutually perpendicular planes. The speeds of these

components, being a function of the direction of propagation of light through the specimen, are different. After passing through the specimen, the light components become out of phase with each other and interfere constructively or destructively as they pass through the analyzer. The optical path difference between the fast and slow directions is defined as [25]

$$\text{Optical path difference} = \Delta \boldsymbol{n}.t \ldots\ldots\ldots\ldots\ldots\ldots \{2.1\}$$

Where $\Delta \boldsymbol{n}$ is a measure of birefringence and t is the thickness of the sample. The corresponding phase difference is given by

$$\boldsymbol{\delta = 2\pi}\ [(\Delta \boldsymbol{n}.\boldsymbol{t})/\boldsymbol{\lambda}] \ldots\ldots\ldots\ldots\ldots\ldots \quad \{2.2\}$$

Where, λ is the wavelength of light. Differences in brightness be a result of differences in refractive index or thickness of the specimen.

2.3.2 Fluorescence Spectroscopy: Fluorescence Spectroscopy or Spectro fluorometry is the analysis of fluorescence from the sample. When a high-intensity light from a UV-Visible light (200-900 nm) source is used to excite the molecules in a sample, we get fluorescence. Electrons bound in molecules of chemical compounds get excited by absorbing energy from the radiation incident on them. The absorbed energy either appears in the form of an increase in their vibrational energy or they can make a transition between allowed electronic energy states. This value of required energy is discrete and characteristic of the molecules. If conditions permit, the molecules can fall back to any of the vibrational levels of the ground state accompanied by emission of energy. In a normal case, emitted energy is always less than the excitation energy as some of the absorbed energy is lost as heat or vibrational energy. This causes a difference in emitted and the excitation wavelengths known as the Stokes's shift [26].

When the absorption is in infrared, visible or ultraviolet regions, excitation of the outermost electrons of the molecule takes place. Subsequent emission of light in such cases is called photoluminescence. Molecules, which get excited by the absorption of light, dissipate their energy through re-emission, reaction or decomposition. The efficiency of occurrence of these processes to take place is called the quantum efficiency (≤1) and in case of photoluminescence it can be defined as [27]

$$\varphi_E = \frac{No.of\ photons\ emittd}{No.of\ photons\ absorbed} \ldots\ldots\ldots\ldots\ldots \quad \{2.3\}$$

Excited molecules can jump to any of the vibrational sublevels of a higher electronic energy state. Since the absorbed energy is discrete in form, so this should show up as series of distinct absorption bands. But for most of the compounds, the absorption spectra are broad.

After reaching higher vibrational levels of an excited state, excess vibrational energy is rapidly lost by the molecule through collision and it descends to the lowest vibrational level of the excited state. From there, most of the molecules occupying an electronic state higher than the second, undergo internal conversion and pass to a higher vibrational level of a lower excited state having the same energy. The molecules, in the process of returning to any of the vibrational levels of the ground state, again make a transition and lose energy until the lowest vibrational level of the first excited state is reached. From there, they fall back to the vibrational levels of ground state, emitting fluorescence.

For a given excitation wavelength, a plot of the intensity of emission against wavelength is known as the emission spectrum. Emission from the sample plotted against a range of wavelengths of exciting light is known as the excitation spectrum.

The fraction of light (I/I_O) absorbed out of a parallel beam by a sample having a concentration of absorbing molecules 'c', is given by the Beer-Lambert Law. The absorbance or the optical density of the sample is given by

$$log_{10}\frac{I}{I_0} = Ecl \ldots\ldots\ldots\ldots\ldots \quad \{2.4\}$$

Where, E is the molar extinction coefficient, 'c' the concentration in g moles/L^{-1}, and l is the path length of the sample. The intensity of light emitted as photoluminescence of weakly absorbing samples is described by

$$P = \varphi_E I_O(2.303\ Ecl) \ldots\ldots\ldots\ldots \quad \{2.5\}$$

Where, φ_E is the quantum efficiency and Io is the incident radiant power [28].

Instrumentation: The main parts of a fluorescence spectrophotometer are; An excitation source, sample cell, and the detector [Fig. 2.4]. We used Model-Agilent Carry Eclipse G9800A for recording and analysis of fluorescence spectra of the samples. Its main features are discussed below [29].

Excitation Source: A pulsed xenon source was used as the source of exciting light. The pulsed source was preferred over the continuous one as it has been reported earlier [26] that it effectively minimizes the problem of photobleaching. It produces 10-μsec pulses of radiation every 16 msec. Its low voltage (9.9 watts) operation results in minimal heat and ozone dissipation and longer lamp life.

Excitation and Emission slit: The width of the slits is expressed in units of bandpass (wavelength) or millimeters. It needs to be adjusted, as for weakly fluorescing samples, the bandpass must be increased to collect more light and for highly fluorescent samples a narrow band pass is recommended. In our setup, slits can be adjusted bilaterally and continuously from the computer which ensures maximum resolution and instant reproducibility. Depending upon the signal strength, the bandpass width can be varied from 0-30nm.

Fluorescence Detector: The photomultiplier tube detector gated for an 80-msec period in fluorescence mode is in perfect synchronization with the lifetime of the pulse.

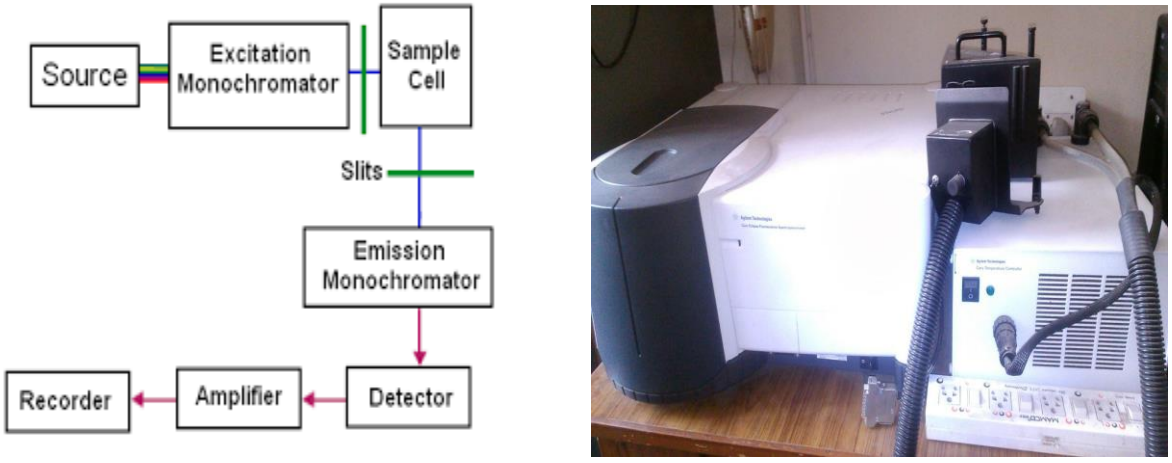

Fig. 2.4 (a) Scheme of Spectrophotometer (b) View of Fluorescence Spectrophotometer (G9800A Carry Eclipse) used for sample analysis.

Gratings: The wavelength drive scans the grating at a very high speed (≈200 nm/s). To ensure maximum light in the UV-visible region, plane and ruled gratings have blazed grooves. The plane gratings are preferred over the concave holographic gratings as they have better polarization performance and adequate imaging during scans.

Excitation Monochromator: The function of the monochromator is to allow only a selected wavelength of light out of a wide spectrum incident on it. The aspheric design of the monochromator ensures that the image diffracted by the grating fits through the slit, even when fluorescence from extremely small sample volumes is to be measured.

The working in room light is possible with this instrument as a phototube dark current is acquired before the onset of each lamp pulse. The excitation and the fluorescence spectrum are plotted by scanning the excitation and the fluorescence monochromators respectively.

2.3.3. FTIR Spectroscopy: To ensure a uniform dispersal and avoid the agglomeration of nanoparticles, we have functionalized the nanoparticles and nanotubes before dispersing them into the CLC matrix. The attachment of desired functional group was confirmed through Fourier transform infrared spectroscopy. The spectra were studied using infrared spectrophotometer [Model-Perkin Elmer BX–II; Waltham, MA, USA]

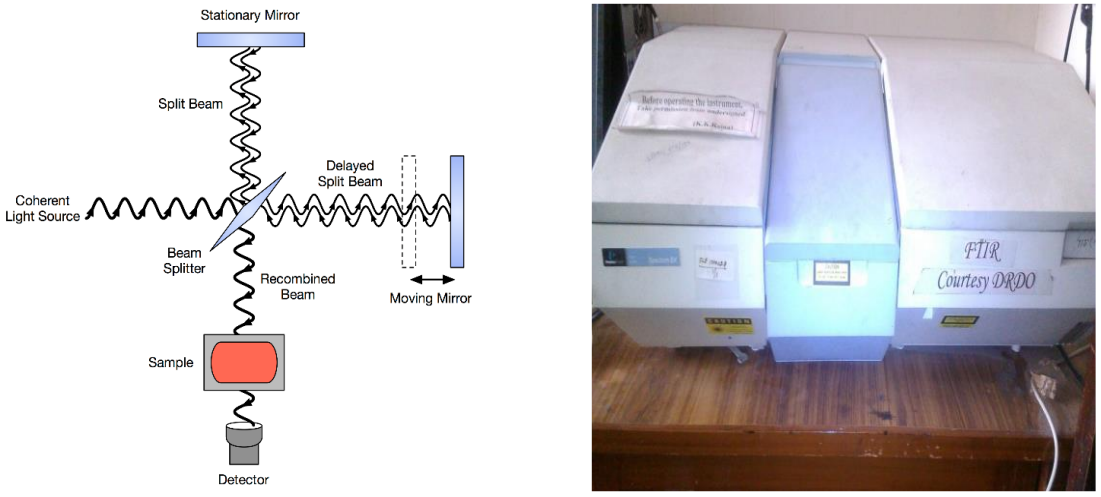

Fig. 2.5 (a) Scheme of FTIR Spectrophotometer [31] ***(b) View of FTIR Spectrophotometer (*Perkin Elmer BX–II*) used for sample analysis.***

I***nstrumentation:*** Following are the essential components of the FTIR Spectroscope [30].

The Source: Infrared radiation from an incandescent blackbody source in the form of a beam passes through an aperture which regulates the amount of energy falling on the specimen.

The Slit: Allows an optimum amount of light to fall on the sample at a given time.

The Interferometer: The light from the sample passes through a beam splitter, one of the beams gets reflected from a fixed flat mirror while the other at right angles to the first, gets reflected from another mirror which can translate through a small distance to and from the beam splitter. The two reflected beams on their way back, interfere at the beamsplitter and due to the difference in the path traversed by them, constructive and destructive interference takes place. The signal which we receive as the outcome is called an interferogram.

Absorption by the sample: The recombined beam passes through the sample. The sample absorbs all the wavelengths characteristic of its spectrum. Thus, specific wavelengths go missing in the interferogram.

The Detector: The specially designed detector reads interferogram by comparing the signals from the sample and the reference. Energy versus time graph is plotted for all the wavelengths simultaneously. The digitized signal is sent to a computer where the Fourier transformation takes place. The final infrared spectrum is then available for interpretation.

2.3.4 Measurement of Refractive Index: The speed of light in vacuum is maximum and constant, but while propagating through other media it is absorbed and subsequently re-emitted by the atoms of the medium and gets slower. The quotient of the speed of light in a vacuum to its speed in a material medium is denoted as the refractive index of the medium.

Uniaxial liquid crystals being *birefringent*, possess two indices of refraction. One corresponding to light polarized along the LC director, and other to the light polarized perpendicular to the director. Let us suppose that the director lies perpendicular to the direction of propagation of the light, and each of the electric and magnetic components is made up of two more components, one parallel and the other perpendicular to the director of the crystal. Due to the property of birefringence, the two components of either the electric or the magnetic field will propagate through the liquid crystal at different speeds and therefore, possibly be out of phase when they exit the liquid crystal medium.

Birefringence presents itself in a different manner in chiral nematic liquid crystals because of the strong twisting of non-polar molecules. Light of different colors gets modified depending on the length of the pitch and the wavelength of light used. Very different behaviour is observed below and above the Maugin limit, away and near the selective reflection band. The modification of light after reflection also depends on helical distortions, boundary conditions and number of pitches in the cell etc. If the helical structure is aligned with the direction of propagation of incident light, circularly polarized light will travel through the crystal at different speeds depending on the sense of rotation of polarization around the axis of propagation. This is called *circular* birefringence.

This depends on one's definition of left and right circular polarized light (looking at the source or looking in direction of light propagation; So, its polarization will rotate faster with respect to the other component's polarization. When the two components emerge out of the helix, their polarizations will again rotate at the same rate and light will again be linearly polarized. But since one of the rotations got ahead of the other, light will now be linearly polarized along a different angle. The value of the new angle depends on the phase difference among two components, which further depends on thickness of the liquid crystal sample. This effect called, '*optical activity',* measures change in polarization angle per unit thickness and thoroughly depends on wavelength of light.

The refractive index is determined in several ways. The commonly used refractometers can either be spectrometric systems or critical angle systems. In case of the spectrometric system, knowledge of the angle of prism and the angle of deviation is vital. For such a system with prism angle A, angle of deviation D (corresponding to a wavelength), refractive index of the prism 'n' w.r.t air is given by

$$n = \frac{sin\frac{1}{2}(A+D)}{sin\frac{1}{2}A} \ldots\ldots\ldots\ldots\ldots\ldots \quad \{2.6\}$$

The other type of systems use the critical angle condition, i.e., the angle at which total internal reflection commences. Refractometers having this system are preferred because of the following advantages.

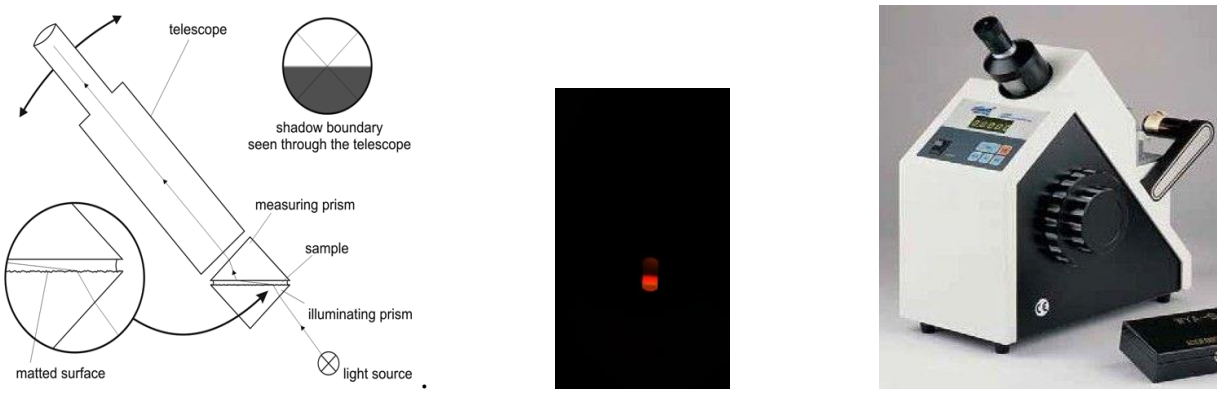

Fig. 2.6 (a) Schematic of refractometer [32] ***(b) Dark and bright regions at the crosswires (c) View of Abbe's refractometer (*****WAY-2S digital*****) used for sample analysis***

.

The problem of measuring the angle of sample prism is avoided.

The recognition of boundary of the critical angle completely specifies the angle of incidence.

Any sample, liquid, solid, colored or opaque can be used as a specimen.

The only disadvantage of critical angle systems is that only skin refractive index is measured with them, which may be different from the refractive index of the bulk.

One of such techniques is the Abbe's refractometer designed by Ernst Abbe in 1869. In this instrument, specimen is sandwiched between two prisms. The top prism is called the measuring (refracting) prism and bottom one, the illuminating prism. Light falling on the sample from the illuminating prism gets refracted through critical angle at the bottom surface of the measuring prism. A telescope is used to detect the refracted light [Fig 2.6(a)]. For measuring the refractive index of a material, angle of incidence is varied by rotating the prisms with a layer of sample sandwiched between them till the total internal reflection takes place at the sample-prism interface and the incident ray is reflected through the sample. Here, the telescope cannot receive the refracted ray and we see a dark spot in the field of view of the telescope. The angle of rotation of the prisms is adjusted to set the angle of incidence equal to the critical angle of the liquid

sample so that the rays graze past the sample without being collected by the telescope. The dividing line between dark and light regions is made sharper by focusing the telescope. We can see two equal portions of dark and bright spots above and below an 'X' shaped cross wire fitted in the eyepiece which serves as a reference for reading the refractive index values [Fig 2.6 (b)]. As the value of critical angle is different for different liquids so we need to rotate the prisms to a different angle for every liquid. To fulfill the condition for measurement of critical angle, refractive index of the sample should be smaller (1.3 to 1.7) than that of the refracting prism. Using the angle of rotation of prism, a calibrated scale which displays the refractive index directly has been provided with the refractometer.

2.3.5. Dielectric Relaxation Spectroscopy: Dielectric relaxation spectroscopy is a useful quantitative investigation for studying molecular structure and dynamics of the thermotropic liquid crystal systems. This technique gives us an insight into the molecular dynamics of various LC cell configurations**.** It is a well-known tool to investigate dipolar ordering and dynamics of collective and non-collective molecular processes in liquid crystals, which exhibit several versatile phases. The use of this technique in the present study for the investigation of chiral media, where many pitch dependent phase variations are possible, seems justified.

The dielectric material increases the storage capacity of the capacitor by neutralizing charges at the electrodes, which ordinarily would contribute to the external field. If a DC voltage source *V* is placed across a dielectric filled parallel plate capacitor, its capacitance C is related to the dielectric constant $\in_r$ as

$$C = C_O \in_r \ldots\ldots\ldots\ldots \qquad \{2.7\}$$

Where, '$c_o = \frac{A}{d}'$ is the capacitance of the parallel plate capacitor of thickness d, area of plates A, with vacuum as a medium between its plates.

If a sinusoidal AC voltage source 'V' is placed across the same capacitor with a dielectric medium between the plates, the resulting current will comprise of a charging current I_c and a loss current I_l, that is related to the dielectric constant. The complex dielectric constant $\in_r^*$ of the medium now consists of a real part $\in_r'$ which represents the storage and an imaginary part $\in_r^{''}$ which represents the loss. $\in_r^{''}$ includes both: the loss due to the dielectric

as well as the loss due to conductivity and is always greater than zero. It is normally much smaller than the real part.

In our experiments, dielectric measurements were taken using Fluke Impedance analyzer [Fig. 2.9] in the frequency range 50 Hz to 1 MHz using COMPVIEW software. The temperature of the sample was varied and maintained by a computer controlled temperature controller (THMS 2028) and Linkam hot stage (T-95 HS). Experiments were carried out in the temperature range 30°C to 120°C. The effect of DC field was also studied by applying DC voltage from an inbuilt source.

Fig. 2.8: View of the LCR Bridge used for dielectric analysis.

In molecular liquids, the structural units causing relaxation are molecular dipoles. Whenever the director reorientation in liquid crystals is caused by the dielectric effect, we speak of the Freedericksz transition [33]. Liquid crystals consist of either polar or non-polar molecules and can possess either permanent or induced dipole moment along or across the long molecular axis. The permanent electric dipoles are much stronger than induced electric dipoles. The applied electric field E (V/m) causes dielectric displacement D (C/m^2) given as

$$E = {}^{D}/_{\in} \quad \ldots\ldots\ldots\ldots\ldots \qquad \{2.8\}$$

Where, $\in$ (F/m) is the dielectric permittivity and is defined as the material's ability to transmit an electric field. The induced polarization, P is related to applied electric field E as

$$P = \in E - \in_0 E = D - \in_0 E = \in_0 \chi E \ldots\ldots\ldots\ldots \quad \{2.9\}$$

Where, the electric susceptibility 'χ' is the constant of proportionality between P and E and, $\varepsilon_o = 1/c_0\ \mu_0 = 8.85 \times 10^{-12}$ (F/m) is the permittivity of free space. The electric Displacement D can be expressed as

$$D = P + \in_0 E = \in_0 \in_r E \ldots\ldots\ldots\ldots\ldots \quad \{2.10\}$$

Where, the relative permittivity $\in_r = \frac{\in}{\in_0} = 1 + \chi$ is constant of proportionality between D and E.

At the microscopic level, several dielectric mechanisms contribute to the dielectric behaviour. The origin of polarization of a composite material can be (a) Electronic, (b) Atomic or, (c) Orientational. For such materials, interfacial polarization can also be present at very low frequencies due to the difference in conductivity of various coexisting phases.

Orientation polarization results from a permanent dipole, e.g., that arising from asymmetric bonds, which retain polarization even in the absence of an external electric field. Dipolar orientation interacts strongly at microwave frequencies and is quite lossy. Atomic and electronic mechanisms are relatively weak, and usually constant over the microwave region. Each dielectric mechanism has a characteristic "cut off frequency." As the frequency increases, the slow mechanisms drop out in turn, leaving the faster ones to contribute to $\in_r'$ [Fig. 2.7]. The loss factor ($\in_r''$) will correspondingly peak at each critical frequency. The magnitude and "cut off frequency" of each mechanism is unique for different materials.

The macroscopic polarization builds up from assembly of these dipoles. If N is the particle density, 'α' the electronic Polarizability, 'E_o' the orientational electric field, 'E_i' the averaged internal field, 'μ' the dipole Moment, then electronic (P_α) and orientational (P_μ) polarizations are defined as

$$P_\alpha = N\ \alpha\ E_i, \quad \text{and} \quad P_\mu = [(N\mu^2)/3KT]\ E_0$$

The induced polarization is the sum of polarizations from above processes and can be defined as

$$P_{ind} = P_\alpha + P_\mu = \varepsilon_o\ \chi\ E \ldots\ldots\ldots\ldots\ldots \quad \{2.11\}$$

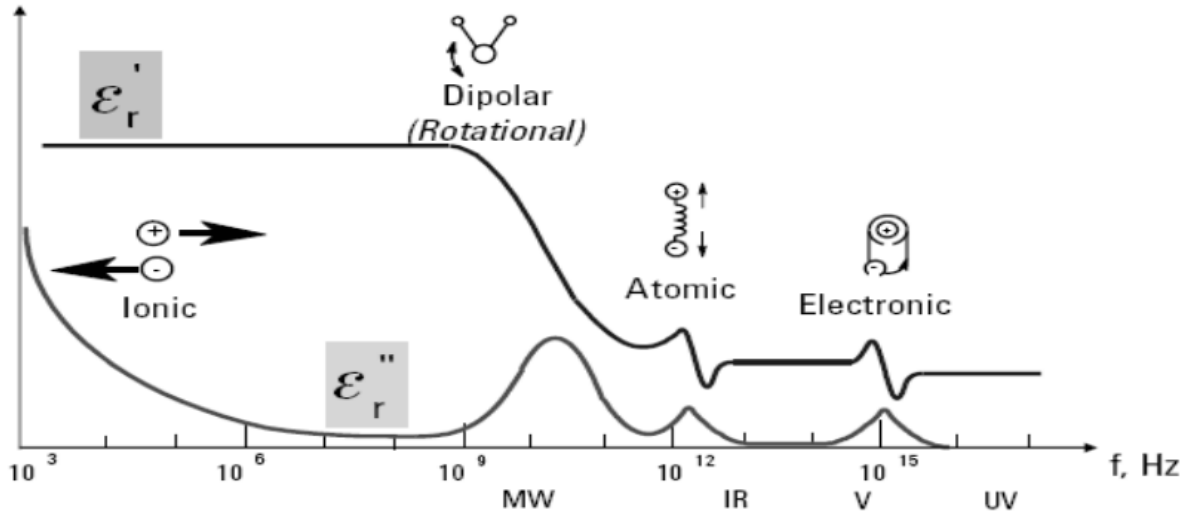

Figure 2.7: Frequency response of dipolar mechanisms [34]**.**

The time required for each type of polarization to reach an equilibrium level varies with the nature and type of polarization of the molecules.

$$P(t) = \epsilon_0 \chi(t) E(t) \ldots\ldots\ldots\ldots \quad \{2.12\}$$

It was observed that orientation polarization requires more time than electronic and atomic polarization to reach its static field value. Therefore, the orientational polarization decreases with increase in frequency while the interfacial polarization generally occurs at much lower frequencies. For anisotropic molecules, Wilhelm Maier and Gerhard Meier calculated two principal dielectric permittivity components $\epsilon_{\parallel}$ and $\epsilon_{\perp}$ (Maier-Meier equation) [35]

$$\Delta\epsilon_s = \epsilon_{\parallel} - \epsilon_{\perp} \ldots\ldots\ldots\ldots \quad \{2.13\}$$

This gives the static **dielectric anisotropy** for rod-like molecules. The value is positive for strong longitudinal dipoles and negative for strong transversal dipoles. Frequency dependence of Polarization leads to the frequency dependence of permittivity [36]

$$P(\omega) = \varepsilon_o \chi(\omega) E(\omega) = \varepsilon(\omega) E(\omega) - \varepsilon_o E(\omega) \ldots\ldots\ldots \quad \{2.14\}$$

Such that static permittivity is the limit of $\varepsilon(\omega)$ as $\omega \rightarrow 0$

$$\epsilon_0 = \epsilon_S = \lim_{\omega \to 0} \epsilon(\omega)$$

$$\epsilon_\infty = \lim_{\omega\to\infty} \epsilon(\omega) \rightarrow n^2 (\text{High frequency limit})$$

The dielectric strength of the medium is defined as $\Delta\epsilon = \epsilon_S - \epsilon_\infty$.

2.3.6 Electro-Optic Switching*:* Electro-optic effect is the influence of slowly varying electric field (w.r.t. the frequency of light) on the optical properties of a material. One such effect is the Fréedericksz transition in which a sufficiently strong magnetic or electric field induces a distortion in uniform director configuration in a liquid crystal matrix [15]. When an electric field is applied to a liquid crystal medium confined in planar boundary conditions of a cell, there is a competition between the dielectric part of the free energy (which promotes an orientation of the director) and the elastic part, which opposes any such change. Thus, reorientation of mesogens takes place along the field direction and at the threshold, when $E/E_0 = 1$, molecules align along the electric field. This results in a distortion in the molecular alignment and energy is stored in the molecules as elastic energy. This transition was first observed by Fréedericksz and Repiewa in 1927 [37]**.** Two mechanisms are mainly responsible for electro-optical effects in liquid crystals.

1) Due to the orientation of molecules prompted by external electric field, absorption and scattering of spectral intensity takes place.
2) The electric field induced shifting of absorption bands changes the gap between energy levels of molecules thus changing the transition intensities.

The energetics of a system under the influence of external electric field has contributions mainly from the following two mechanisms:

The first is the polarization caused by small deformations. For a weak electric field, the elastic forces are dominant and the orientation of molecular director does not show a noticeable change. However, above the critical field, the orientation of director shows switching. If an AC electric field has been applied perpendicular to the director pointing in x- direction, the free energy density F_d becomes

$$F_d = \frac{1}{2} K_2 \left(\frac{d\theta}{dz}\right)^2 \ldots\ldots\ldots\ldots \qquad \{2.15\}$$

The total energy per unit volume stored in the distorted system is given by

$$U = \frac{1}{2} K_2 \left(\left(\frac{d\theta}{dz}\right)^2 - \frac{1}{2} \epsilon_o \ \Delta\chi_e E^2 sin^2\theta\right.$$

Where, '$\Delta\chi_e'$ is the change in susceptibility of the medium. Free energy per unit area is given as [15]

$$F_A = \int_0^d \frac{1}{2} K_2 \left(\left(\frac{d\theta}{dz}\right)^2 - \frac{1}{2} \in_o \Delta\chi_e E^2 sin^2\theta \, dz\right.$$

Minimizing this using calculus of variations

$$K_2 \left(\frac{d^2\theta}{dz^2}\right) + \in_o \Delta\chi_e E^2 sin\theta cos\theta = 0$$

After applying a few mathematical deliberations we get the expression of the threshold field [38].

$$E_{th} = \frac{\pi}{d}\sqrt{\frac{K_2}{\epsilon_0 \Delta\chi_e}} \ldots\ldots\ldots\ldots \quad \{2.16\}$$

Where d is the thickness of the cell. Equation (2.16) shows that the threshold electric field depends on the thickness of the sample and the susceptibility, which in turn depends on the state of polarization of the material.

The second contribution is the response of the dielectric constant to molecular anisotropy ($\in_\perp \neq \in_\parallel$) responsible for birefringence ($n_\perp \neq n_\parallel$) of the liquid crystals. The energy involved in this process is given as [39]

$$W_e = -\frac{1}{8\pi} \in_a (nE)^2 \ldots\ldots\ldots\ldots \quad \{2.17\}$$

Where, n is the LC director, E is the applied electric field and $\in_a = \in_\parallel - \in$, the dielectric anisotropy.

To investigate the unwinding process associated with the helix dynamics, the electric field was applied to doped and undoped CLC in the form of input square wave pulses from 0-30V at 50 Hz across the CLC sample cells through a function generator (SCITECH ST 4060). The Freedericksz transition and the homeotropic states were observed through a polarizing optical microscope and recorded in the computer attached to it.

2.3.7 Transmission Studies and Measurement of Hysteresis: When light passes through a LC sample, the polarization state of transmitted light is changed by its molecular anisotropy.

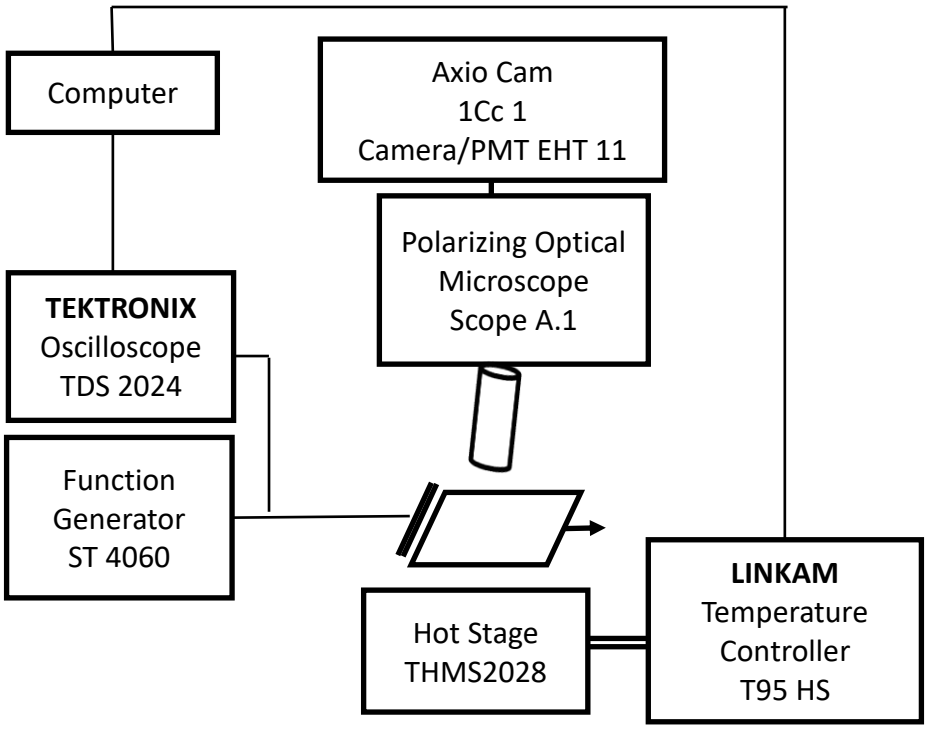

Fig. 2.9: Experimental set-up used for transmission studies.

The propagation of light through anisotropic media like liquid crystals is affected in two ways firstly, due to the anisotropy of the medium light propagates in a different way with respect to the molecular director orientation, secondly light being electromagnetic in nature, can reorient the liquid crystal exhibiting non-linear optical effects [22]. But when LC cell is subjected to an electric field in a direction perpendicular to the substrates, then distortion in molecular alignment due to impinging light can be ignored [40].

We have recorded the output transmission as a function of applied electric field with the help of Tektronix storage dual beam oscilloscope (Model- TDS 2024). As the electric field is switched on, molecular alignment is detected in the form of output wave on the storage oscilloscope. The collective response of the liquid crystal molecules to the applied electric field **E** causes distortions of the director **n**. The optical hysteresis behavior of the samples was investigated using polarizing optical microscope fitted with charge coupling device (CCD) detector interfaced with a computer. Figure 2.8 gives the schematic of the circuit used for investigations. Output electric signal was multiplied by a photomultiplier tube (Model- EHT-11). The memory parameter was calculated by using the relation [41]

$$M = \frac{T_f - T_i}{T_{max} - T_i} \ldots\ldots\ldots\ldots \quad \{2.18\}$$

Where, T_i is the initial value of transmittance while increasing voltage from 0V and T_f is the final value of transmittance at zero applied fields while decreasing the amplitude of voltage. T_{max} is the transmittance corresponding to the peak value.

References

1. Xie P, Zhang R. Liquid crystal elastomers, networks and gels: advanced smart materials. J. Mater. Chem. 2005;15:2529.

2. Beeckman J, Neyts K, Vanbrabant PJM. Liquid-crystal photonic applications. Opt. Eng. 2011;50:081202.

3. Woltman SJ, Jay GD, Crawford GP. Liquid-crystal materials find a new order in biomedical applications. Nat. Mater. 2007;6:929–38.

4. Chua SJ, Li BJ. Introduction to optical switches. Opt. Switch. Mater. Des. 2010;1–4.

5. Lee M, Katz HE, Erben C, Gill DM, Gopalan P, Heber JD. Broadband modulation of light by using an electro-optic polymer. Science. 2002;298:1401–3.

6. Bisoyi HK, Li Q. Light-directing chiral liquid crystal nanostructures: From 1D to 3D. Acc. Chem. Res. 2014;47:3184–95.

7. Caputo R, De Sio L, Cataldi U, Umeton C. Plasmon Resonance Tunability of Gold Nanoparticles Embedded in a Confined Cholesteric Liquid Crystal Host. Mol. Cryst. Liq. Cryst. 2012;559:194–201.

8. Yoshida H, Inoue Y, Shiozaki Y, Takahashi M, Kubo H, Fujii Al. Fast and Continuous Tunable Lasing from a Nano-Pore Embedded Cholesteric Liquid Crystal Film. Mol. Cryst. Liq. Cryst. 2012;560:101–7.

9. Prakash J, Choudhary A, Kumar A, Mehta DS, Biradar AM. Nonvolatile memory effect based on gold nanoparticles doped ferroelectric liquid crystal. Appl. Phys. Lett. 2008;93:112904.

10. Whinnery J, Hu C, Kwon Y. Liquid-crystal waveguides for integrated optics. Quantum Electron. IEEE. 1977;262–7.

11. Na JH, Park SC, Kim SU, Choi Y, Lee SD. Physical mechanism for flat to lenticular lens conversion in homogeneous liquid crystal cell with periodically undulated electrode. Opt. Express. 2012;20:864.

12. Malik P, Chaudhary A, Mehra R, Raina KK. Dielectric Studies and Memory Effect in Nanoparticle Doped Ferroelectric Liquid Crystal Films. Mol. Cryst. Liq. Cryst. 2011;541:243/[481] – 251/[489].

13. Shiraishi Y, Toshima N, Maeda K, Yoshikawa H, Xu J, Kobayashi S. Frequency modulation response of a liquid-crystal electro-optic device doped with nanoparticles. Appl. Phys. Lett. 2002;81:2845–7.

14. Kinkead B, Urbanski M, Qi H, Kitzerow H-S, Hegmann T. Alignment and electrooptic effects in nanoparticle-doped nematic liquid crystals. Proc. SPIE. 2010;7775:77750C/1–77750C/11.

15. Reshetnyak VY, Shelestiuk SM, Sluckin TJ. Fredericksz transition threshold in nematic liquid crystals filled with ferroelectric nano-particles. Mol. Cryst. Liq. Cryst. 2006;454:201/[603] – 206/[608].

16. Sikharulidze D. Nanoparticles: An approach to controlling an electro-optical behavior of nematic liquid crystals. Appl. Phys. Lett. 2005;86:1–3.

17. www.**sigmaaldrich**.com/catalog/product/**aldrich**/652482

18. www.**sigmaaldrich**.com/catalog/product/**aldrich**/793388.

19. https://www.thorlabs.com.

20. Scharf T. Polarized Light in Liquid Crystals and Polymers. Polariz. Light Liq. Cryst. Polym. 2006.

21. Chilaya GS, Elashvili ZM, Lisetski LN, Piliashvili TS, Vinokur KD. Induced cholesteric systems: pitch dependence on temperature and concentration. Mol. Cryst. Liq. Cryst.

1981;74:261–73.

22. Stephen MJ, Straley JP. Physics of liquid crystals. Rev. Mod. Phys. 1974;46:617–704.

23. Hiramoto Y, Hamaguchi Y, Shoji Y, Shimoda S. Quantitative studies on the polarization optical properties of living cells. I. Microphotometric birefringence detection system. J. Cell Biol. 1981;89:115–20.

24. micro.magnet.fsu.edu/**publications**/

25. Milonni PW. Fast light, slow light and left handed light. Mater. Today. 2005;8:60.

26. Royer CA. Fluorescence spectroscopy. Methods Mol. Biol. 1995;40:65–89.

27. Crosby GA, Demas JN. Measurement of photoluminescence quantum yields. Review. J. Phys. Chem. 1971;75:991–1024.

28. Gfroerer TH. Photoluminescence in analysis of surfaces and interfaces. Encycl. Anal. Chem. 2000;9209–31.

29. Agilent technologies. Cary eclipse fluorescence spectrophotometer user's guide. 2012;46.

30. Sawant SD, Baravkar AA, Kale RN. FT-IR spectroscopy: Principle, technique and mathematics. Int. J. Pharma Bio Sci. 2011;2:513–9.

31. Griffths PR. Fourier transform infrared spectrometry: Science. 1983;80; 297–302.

32. http://www.refractometer.pl/Abbe-refractometer.

33. Shiyanovskii SV, Lavrentovich OD. Dielectric relaxation and memory effects in nematic liquid crystals. Liq. Cryst. 2010;37:737–45.

34. http://cp.literature.agilent.com/litweb/pdf/5989-2589EN.pdf

35. Ran Z, Jun H, Zeng-Hui P, Li X. Calculating the dielectric anisotropy of nematic liquid crystals: a reinvestigation of the Maier–Meier theory. Chinese Phys. B. 2009;18:2885–92.

36. Morton JJL. Electrical and optical properties of materials Part 1 . Conductivity : from

insulators to superconductors. 0:1–29.

37. Freedericksz V, Repiewa, A, 1927, Theoretisches und Experimentalles zur Frage nach der Natur der anisotropen Flussigkeiten. Physik. Zeitschr:, 42, 532-546.

38. Collings PJ. Introduction to liquid crystals: chemistry and physics. Am. J. Phys. 1998; 551.

39. Yilmaz S. Optical properties of aligned nematic liquid crystals in electric field. J. Mod. Phys. 2011;02:248–55.

40. Schultze M, Bothschafter EM, Sommer A, Holzner S, Schweinberger W, Fiess M. Controlling dielectrics with the electric field of light. Nature. 2013;493:75–8.

41. Yaroshchuk O, Tomylko S, Gvozdovskyy I, Yamaguchi R. Cholesteric liquid crystal-carbon nanotube composites with photo-settable reversible and memory electro-optic modes. Appl. Opt. 2013;52:E53–9.

CHAPTER - III

PREPARATION OF CHIRAL NEMATIC LIQUID CRYSTAL MATERIALS

Overview

This chapter deals with the induction of chirality in a nematic liquid crystal (NLC) mixture and optimization of chiral dopant concentration into it, to form a suitable matrix for nanoparticle dispersal. Our objective was to look for enhancement of optical and electro-optical properties like morphology, contrast, photoluminescence, the threshold voltage for switching, dielectric constant, and optical hysteresis in the doped samples. We investigated the change brought about in these properties of the NLC after doping with different concentrations of chiral molecules. In this chapter, we have included all the relevant experimental findings and discussed the results to optimize the concentration of chiral dopant.

ELECTRO-OPTICAL AND OPTICAL ANALYSIS OF NEMATIC LIQUID CRYSTALS DOPED WITH DIFFERENT CONCENTRATIONS OF CHIRAL MOLECULES

The Chiral Phase: The history of Cholesteric liquid crystals (CLC) dates back to 1888 with the discovery of first liquid crystal, cholesteryl benzoate by **Reinitzer** [1,2]. **Friedel, in 1922** observed that nematogenic systems have cholesteric structure if their chain contains an asymmetric center [3]. Nematic liquid crystals (NLC) are known to be stable and cholesteryl esters appeared chemically and electrochemically nonstable. Moreover, synthesis and purification of chiral LCs at a large scale with customized properties are also difficult and expensive [4]. More stable nematic liquid crystals twisted by mixing with chiral materials or by adding asymmetric side chain also show cholesteric phases. A cholesteric liquid crystal is described by its supramolecular helical pitch 'p' (distance over which the director rotates through 2π) and the handedness of its intrinsic chirality. The self-assembled helical pitch length is a critical factor which significantly affects the optoelectronic cell properties of a chiral nematic liquid crystal cell. Various approaches for tuning the helical pitch length of CLCs have been proposed, such as mixing different chiral concentrations [5], changing the operating temperature [6], using photo-tunable chiral dopants [7], and applying external electric fields [8]. The dependence of spiral pitch on many factors led to the idea of induction of chirality in nematogenic systems [4]. When no surface alignment is present, the chiral systems can be broadly divided into following categories.

- The first type has an inherent stereogenic center in their molecular structure (e.g. Cholesteryl benzoate) and can form phases with a helical symmetry.
- *The second type, doped or induced CLC consists of chiral guest molecules dissolved in an achiral nematic host, inducing chirality on the achiral mesogens.*
- The third type, called twisted nematic, consist of liquid crystal molecules adopting a 90° helical twist forced on them through two perpendicular alignments layers.

For the present work, we have chosen to induce chirality in the nematic system by adding an optimum amount of chiral guest molecules. In such a case, the sign and magnitude of cholesteric pitch and nature of the induced cholesteric phase highly depend on the properties of chiral dopant. The efficiency of the dopant to induce a helical organization in a liquid

crystalline matrix is expressed as the helical twisting power (β), which is intrinsic to every chiral compound and is different for every guest-host combination. The helical pitch of CLCs and the resultant color reflected from them are directly governed by the concentration of a chiral agent and temperature. The advantages of adding chirality to a nematic system are as follows:

- The optical bistability combined with the reflection selectivity, which is governed by the Bragg's law make CLC displays energy-saving. Reflective CLC displays are easily processable as they do not require a backlight, polarizers, and color filters etc. [9].
- As the pitch of the CLC can be controlled by small temperature and field changes, many useful electro-optic and thermo-optic effects can be achieved.
- The wavelength selective properties of CLCs and the flexible nature of their pitch make them useful to construct frequency tunable lasers [10].
- Depending upon the helical pitch, d/p ratio, optical and dielectric anisotropy of the CLC, frequency of electric field, and the type of surface treatment, a variety of electro-optic effects are observed.
- Typical cholesteric textures like Grandjean, Focal conic, Fingerprint and amorphous, can be seen with the induction of chirality. Several new phases like the TGB phase and Blue phase can also be realized.[11]
- With molecular and structural optical activity and a pitch lying in the visible range of the optical spectrum, CLCs can be of potential use in novel displays, light shutters, polarization modulators, photonic devices, lasers and optical sensors.
- The evidence of electric effects like ferroelectricity, antiferroelectricity, and electroclinic effect have ensured their use as functional materials.
- Since the helix provides a distributed feedback, chiral liquid crystals can show mirrorless lasing [12,13]. These lasers are compact, easy to manufacture and have wide tenability [14].
- The tuning of laser output using temperature [15], pressure, electric fields, [16] and dye doping [17–19] has seen many advances in recent past.

In spite of all these useful features, a typical CLC device suffers from drawbacks like high switching voltage and slow response [20].

To eliminate these drawbacks and enhance the desired properties of CLCs, there is a strong need to explore new composite materials. Nanoparticles Doped CLCs have been reported to show improvements in optical response and driving voltage. There are many reports of realization of distinctive effects, which were not very common in nematics, like stabilization of the blue phase, improved PL response and an emergence of volatile and non-volatile optical hysteresis with doping of nanoparticles in chiral liquid crystals [21–24]. Doping of MWCNTs to a chiral mixture have been reported to modify the physical properties, refractive index, in particular [25]. The combination of pitch dependent properties of chiral molecules and anisotropic properties of nanoparticles were reported to have genuine prospects in the field of active plasmonics, fabrication of functional materials and dielectric spectroscopy [6,10,20,21,26–30].

3.1 Sample Characterization

To optimize a chiral concentration for nanoparticle doping, we used ZLI 4151 (E. Merck, Darmstadt, Germany) as the nematic liquid crystal. Chirality was induced in it with a chiral dopant, CB15 [E. Merck, Darmstadt, Germany].

Table 3.1: Composition and Nomenclature of the Samples Studied

S. NO.	Composition	Sample name	T_{ISO}(K)	T_{N^*}(K)
1	ZLI 4151	NLC	384	372
2	ZLI4151+1.0%CB15	CLC I	385	371
3	ZLI 4151+1.5%CB15	CLC II	387	370
4	ZLI 4151+2.5%CB15	CLC III	390	368
5	ZLI 4151+3.0%CB15	CLC IV	392	367
6	ZLI 4151+5.0%CB15	CLC V	393	363

Five homogeneous mixtures, CLC I, CLC II, CLC III, CLC IV and CLC V [Table 1] were prepared by ultrasonically mixing 1.0, 1.5, 2.5, 3.5 and 5.0 wt% of chiral dopant respectively in nematic liquid crystal.

The mixtures could fill in the antiparallel aligned liquid crystal cells via vacuum induced capillary action in their isotropic phase. These antiparallel aligned cells were made of two conducting substrates rubbed with Polyimide alignment layers with a fixed gap of 5μm maintained between them with the help of spacers. The morphology of these samples was investigated under crossed polarizers, through Carl Zeiss polarizing optical microscope (Model-Scope A.1) fitted with a camera Axiocam 1Cc 1.

The transmission studies for the measurement of optical hysteresis were conducted using a photomultiplier tube (Model- EHT 11; scientific equipment, Roorkee, India) fitted with the microscope. The output transmission signal responses were recorded in Tektronix oscilloscope (Model- TDS 2024). The electro-optic response of the samples was recorded by applying square wave pulse through the pulse generator (Model Scientech-4060; Scientech Technologies Pvt. Ltd., Indore, MP, India). The dielectric studies were conducted by recording cell capacitance in the automatic programmable LCR meter [Fluke PM 6306].

The frequency range for measurement of capacitance was kept from 50 Hz to 1MHz. Before recording the dielectric data, these sample cells were calibrated with a standard solution of acetone. Photoluminescence analysis of chiral doped nematic liquid crystal was done with the help of fluorescence spectrophotometer (Model- Agilent Carry Eclipse).

3.1.1 Morphological Analysis: The microtextures of the doped samples [Fig. 3.1(a-f)] represent planar Grandjean texture. When chirality is induced in a nematic liquid crystal system by adding cholesteric molecules, supramolecular structures in the form of helices are formed. These helical structures, to minimize their energy are confined with their axis perpendicular to the antiparallel surface anchoring of substrates. When such a matrix with director ‘n’ oriented parallel and the helical axis perpendicular to the substrate surfaces, is irradiated with a beam of unpolarized light, the component of the light which has the same handedness as the CLC chirality will be reflected, whereas the oppositely handed component is transmitted. When the sample kept between crossed polarizers is viewed along the helix using a polarizing microscope, a uniform color is

seen which does not change or disappear with a rotation of the sample. This is because the optic axis is parallel to the direction of propagation of light.

Wavelengths originating from helical molecular superstructures are reflected selectively. The reflection bandwidth 'Δλ' depends on upon optical anisotropy (Δn) and pitch (p) of the helix as per the following relation [31]

$$\Delta\lambda = \Delta n\, p \quad \ldots\ldots\ldots\ldots \quad \{3.1\}$$

Where, $\Delta n = n_{\parallel} - n_{\perp}$ ($n_{\parallel}$ and $n_{\perp}$ are the refractive indices of the material in the directions parallel and perpendicular to the director, respectively). The planar cholesteric microtextures in Figure 3.1 show uniform colour. The color of the texture depends on the pitch and/or phase retardation. The irregularities or defects in the cholesteric LC cell present themselves as disclinations, oily streaks and/or different coloured planar regions [Fig. 3.1(f)].

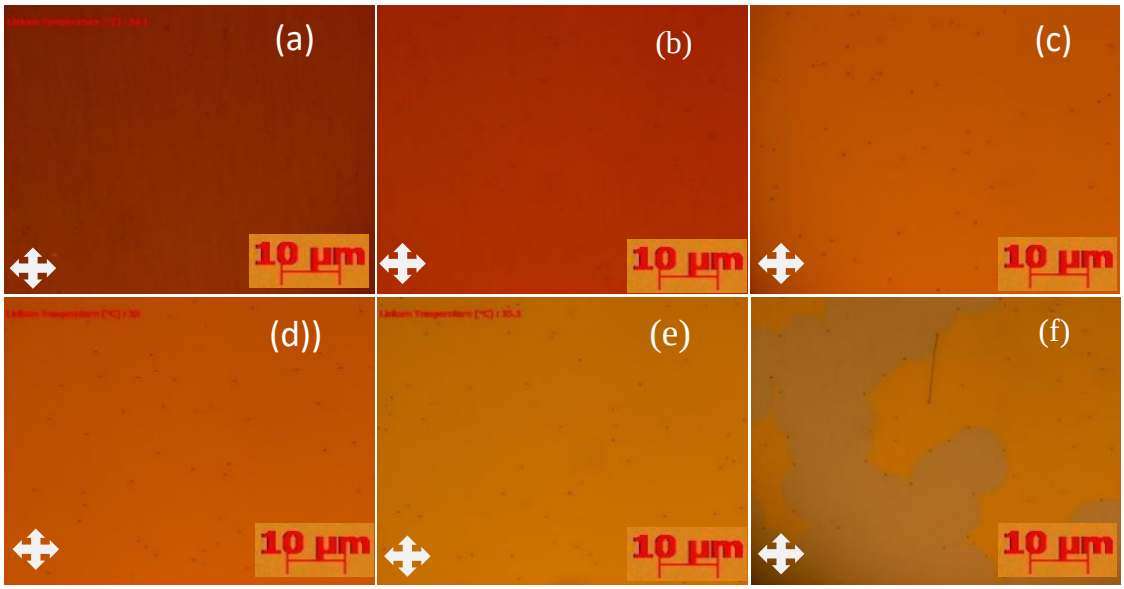

Fig. 3.1: Microscopic Textures representing (a) NLC (b) CLC I (c) CLC II (d) CLC III (e) CLC IV (f) CLC V

The NLCs are insulating organic liquids formed of longitudinally oriented molecules. These structures have molecular orientation like crystals at certain temperature intervals, but the gravity centers of molecules are in random order as in liquids.

In the absence of any external alignment anchoring, the domains are randomly oriented in nematic phase but in case the domain walls are processed, a homogeneous single alignment will

be there [Fig. 3.1a][32]. The isotropic – cholesteric phase transition is a first order transition with cholesteric phase appearing through nucleation and a frequent appearance of two coexisting phases. Fig. 3.2 shows the nucleation process of both; the NLC and CLC samples.

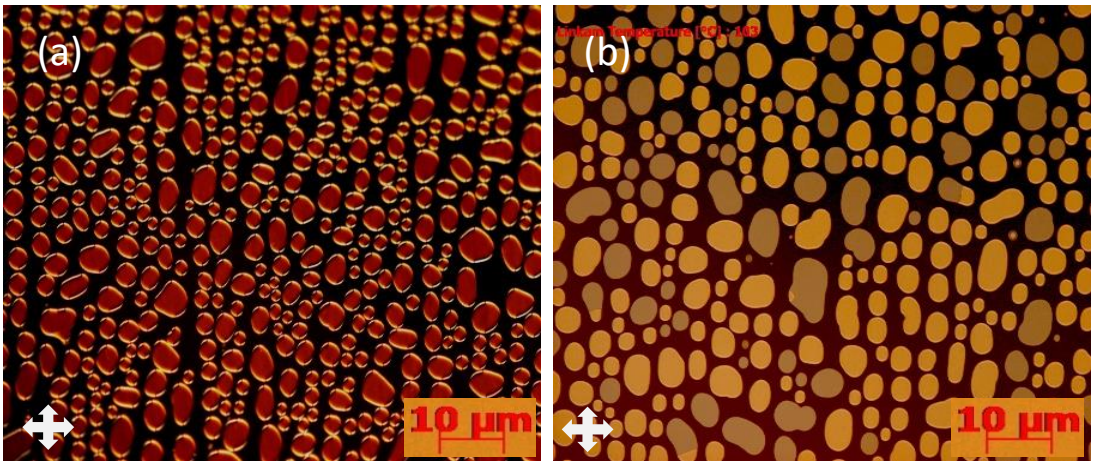

Fig. 3.2: Optical micro textures of the nucleation process in (a) NLC (b) CLC III

In NLC sample [Fig. 3.2 (a)], all the liquid crystal droplets separating from isotropic melt have the same color while addition of chiral molecules leads to two different colored droplets [Fig. 3.2 (b)] revealing the manifestation of two independent twist states in the sample.[11]

3.1.2 Electro-optic Switching and Threshold Voltage: When a weak electric field is applied normal to the cholesteric planar quasi-layers, the dielectric torque tends to reorient them along the electric field. Their free rotation is restricted by the boundary conditions and they undergo periodic sinusoidal deformations called undulations. The nature of resulting texture strongly depends on the thickness/pitch (d/p) ratio. For small values of d/p, cholesterics layers undulate only in one direction. For higher values of d/p, the layers periodically undulate in two directions creating a square pattern of deformations. Length of the period depends on cell thickness and cholesteric pitch ($Lu \propto (pd)^{1/2}$).

Fig. 3.3 shows the electro-optic switching response of induced chiral nematic liquid crystals through optical textures seen under the polarizing optical microscope. Initially, when no field was applied to CLC I, CLC II, CLC III, CLC IV and CLC V, Planar Grandjean texture [Fig.3.1] was seen. The helical axes of chiral supramolecules remain perpendicular to the cell surfaces until the applied external voltage reaches the threshold voltage. On further increasing the voltage, onset of state transition, known as Freedericksz transition is marked

by the appearance of instabilities in various forms [Fig. 3.3]. The orientation of helical axis within the plane of the cell (lying helix) leads to the appearance of characteristic 'fingerprint texture' as the director randomly wanders within the plane of the cell [Fig. 3.3(b, c)]. Random orientation of helical axis in the composite exhibits light scattering due to abrupt change of refractive index at the domain boundaries and the texture thus formed is focal conic [Fig. 3.3(e)].

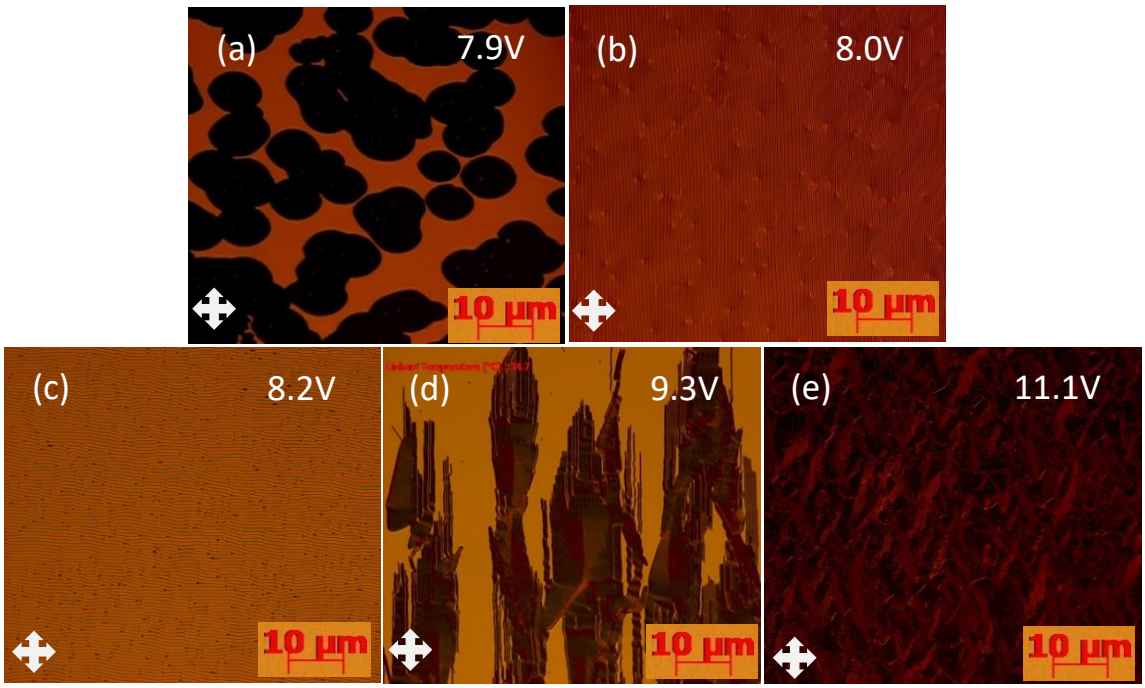

Fig. 3.3: Electro-optic switching in Chiral doped samples (a) CLC I (b) CLC II (c) CLC III (d) CLC IV (e) CLC V at the threshold.

We observed that the threshold voltage increases with increasing chiral concentration. The threshold voltage (V_{th}), of the LC cell, is represented as [33]

$$V_{th} = \frac{d}{p}\sqrt{\frac{k_{22}}{\epsilon_0 . \Delta\epsilon}} \dots\dots\dots\dots\dots \{3.2\}$$

Where k_{22} is the twist elastic constant, d is the thickness of the cell, ε_o is the permittivity of the free space and $\Delta\varepsilon$ is the dielectric anisotropy.

Eq. 3.1 clearly represents the dependence of threshold voltage on frustration ratio, 'd/p'. In order to find d/p for the samples, we first calculated the pitch in all the five cases, from the relation HTP = 1/pc, where p is the pitch and c is the concentration of chiral dopant. As the helical twisting power (HTP) of CB15 is approximately 7.3μm^{-1} [34], pitch as predicted theoretically for various concentrations are as given in the table below.

Table 3.2: Pitch and electrical parameters of chiral doped nematic liquid crystal mixtures.

Sample name	Pitch (μm)	d/p	V_{th} (V)	E_{th} (V/μm)
CLC I	13.6	0.36	7.9	1.54
CLC II	9.1	0.54	8.0	1.60
CLC III	5.5	0.91	8.8	1.76
CLC IV	3.9	1.27	9.3	1.86
CLC V	2.7	1.83	11.1	2.22

Thickness of the sample cell, 'd' has been kept constant (5μm) for all the samples. Considering these values, we observed that an increase in d/p ratio leads to emergence of different kinds of defect structures, accompanied by contraction of the pitch, above the threshold voltage [Fig. 3.3 (d-f)]. The observations clearly indicate that electro-optic and morphological switching response of CLC samples is strongly influenced by the d/p ratio.

The threshold value of electric field needed for the onset of Freedericksz transition can a be calculated using the following relation [30]

$$E_{th} = V_{th}/d \qquad \text{……..\{3.3\}}$$

Where, V_{th} is the threshold voltage needed for onset of the transition and d is the cell gap. We observed that as the frustration ratio (d/p) of the helices becomes nearly equal to, or more than unity, a higher value of electric field is required for the onset of Freedericksz transition.

3.1.3 Optical investigations of induced memory: Memory effects appearing after chiral doping in nematic liquid crystal were successfully investigated. Role of the frustration ratio in bringing about optical and electro-optical hysteresis by slowing down the relaxation process in the OFF state of chiral doped nematics was established. Our observations illustrated that induction of memory as a result of manipulation of the helix director by controlling the boundary/ anchoring conditions of the liquid crystal remains an active field of study [35–37]. It leads to new qualitative effects which can prove useful for the development of memory based bistable low power devices. Further investigations with nanoparticle doping in this matrix are sure to give new results and open new avenues.

The possibility of generating nonlinearity in the output electrical signal is being explored by doping the nematic liquid crystals with carbon nanotubes, nanoparticles, polymers, and dyes. The bistability, thus generated, is long lived and in some cases, even permanent. This property of these optical materials makes them suitable for their use in optical devices such as e–books, optical logic elements, limiters, clippers, shutters and other low power devices [38–43]. Although the sensitivity of nematic liquid crystal molecules to external stimuli leads to their extensive use as a base matrix for all kinds of doping mentioned earlier, the introduction of chirality in such systems can help in retaining the field modified optical state for a longer time and bring variety in the availability of practically useful phases [4][44,45]. Yaroshchuk et al. reported doubling of the efficiency of electro-optical memory as a consequence of doping a nematic mixture with a small amount of chiral agent [46]. Faster bistable switching response and a much longer display time in a three-terminal, In-Plane switching device in unplugged power state, using a cholesteric liquid crystal were reported by Lin et al [47]. Guo et al. achieved longer lasting bistability of several weeks, using a three-electrode twisted nematic liquid crystal cell [11]. Under the effect of applied electric field above the threshold, the appearance of orientational defects was reported to cause bleaching of nematic liquid crystal cells with zero pretilt angle by Kravchuk et al. [12].

In such systems with optical memory, the helical axes of liquid crystal molecules get perturbed due to the field induced orientation and state of partial transmittance are retained by the system even after removal of the field.

The self-assembled helix formation is a unique feature of the chiral phase. Even small variations in pitch of the helix influence optical, electro-optical and morphological properties of the material. Different methods, such as; application of external electric and magnetic fields [13], variation in the composition of chiral mixtures [14-16], changing temperature [17] and, using photosensitive chiral dopants [18] are employed for tuning the helical pitch of the CLCs. The changes in pitch affect the contrast ratio (by changing the amount of transmitted light) and the switching properties of the material [19–22].

We, in the present work, confirmed the formation of supramolecular structures in induced chiral nematic liquid crystal molecules by Grandjean, fingerprint or focal conic textures which provided information about the parallel, perpendicular or random orientations of the helical axis. The molecules in the helix get perturbed due to the application of electric field. Due to interaction of thus created defect lines, surface anchoring and elastic forces of the medium, the system does not completely relax back to the original state for higher concentrations of chiral dopant. Hence, even after the removal of field, optical energy is partially retained by the system as optical hysteresis and the system shows memory effects. Experimental results indicate that chiral dopant concentration combined with boundary/anchoring conditions significantly influence the morphology and electro-optic parameters such as threshold voltage and an optical hysteresis of NLC. We have also attempted to explain the existence of memory in the electro-optic results by dipole relaxation mechanism.

Application of an electric field to a chiral nematic planar cell, induces instabilities in the director field, progenerating an On-state with doubly refracting and transmissive properties. The transition from a low transmission ‘OFF’ state to an electrically induced birefringent ‘ON’ state and vice versa, is normally very fast due to short pitch helical structure of chiral mesogens. This fact is taken into practical use for the fabrication of high contrast devices with faster response. But in the presence of suitable boundary conditions, significant hysteresis in optical and dielectric switching behavior is observed due to defect formation above the threshold for Freedericksz transition. We observed residual defect lines in the optical textures of CLC III, CLC IV and CLC V with their number and duration increasing with increasing chiral concentration while no such defect structures were observed in CLC I and CLC II, where the chiral concentration was low [Fig. 3.4].

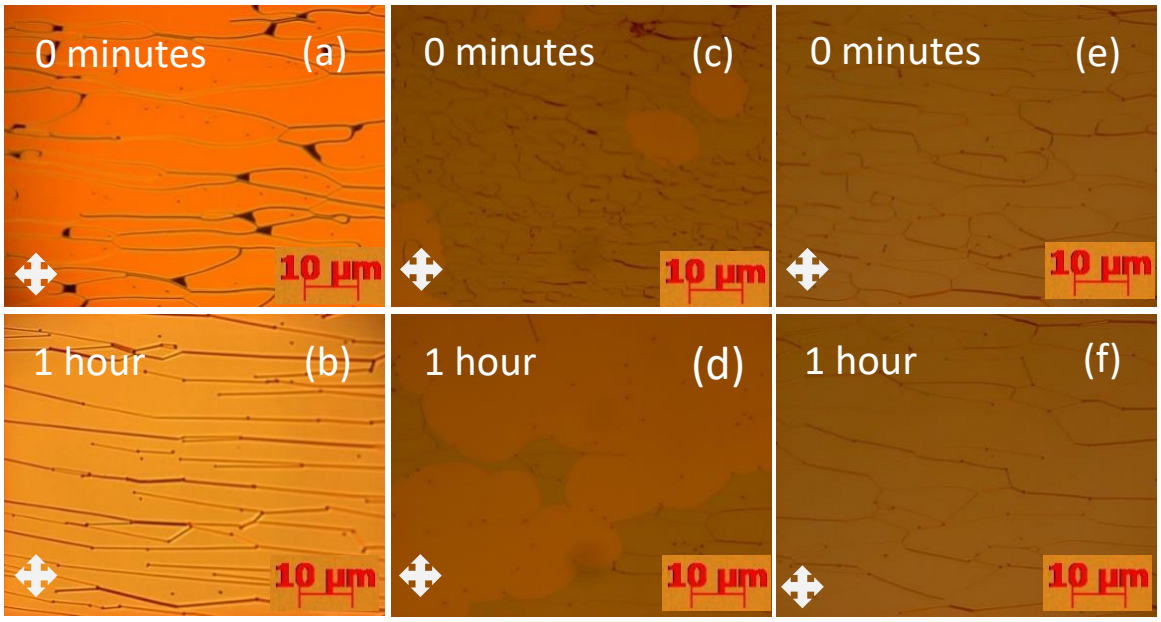

Fig. 3.4: Memory effects in optical textures of CLC III (a,b), CLC IV (c,d), CLC V (e,f) after removal of external electric field.

The probability of a system reverting to original reflecting state after removal of the electric field depends on the outcome of the interaction of various forces like surface anchoring, elasticity, and the topological defects [40]. Microtextures in Fig. 3.4 suggest that partially twisted helical structures were unable to regain their original configuration due to the explicit action of various forces acting on the molecules.

The role of the defect structure formed during transition can be explained on the basis of free energy considerations. The contribution to the free energy of defects (oily streaks) hails from bending elastic energy, defect core energy, and the surface anchoring energy. From the Lubensky-de Gennes coarse-grain theory, we understand that as the frustration ratio, d/p, is maximum for the highest dopant concentration $(d/p)_{clc\ V} = 1.83$ [as compared to the lower ones i.e, $(d/p)_{clc\ III} = 0.91$ and $(d/p)_{clc\ IV} = 1.27$], the free energy of defects is also maximum for this sample. The highest value of E_{th} for this sample also substantiates this observation. The presence of a large number of disclinations [Fig. 3.4f] even after one hour of observation in the OFF state of CLC V indicate that it needs maximum time [Fig. 3.5] to revert back to the planar morphology. We also measured the transmitted intensity as a function of relaxation time for all the samples [Fig. 3.5 (a)]. Decrease in the slope of the

curves with an increase in the concentration of chiral dopant indicates slow relaxation of the samples with higher doping percentage.

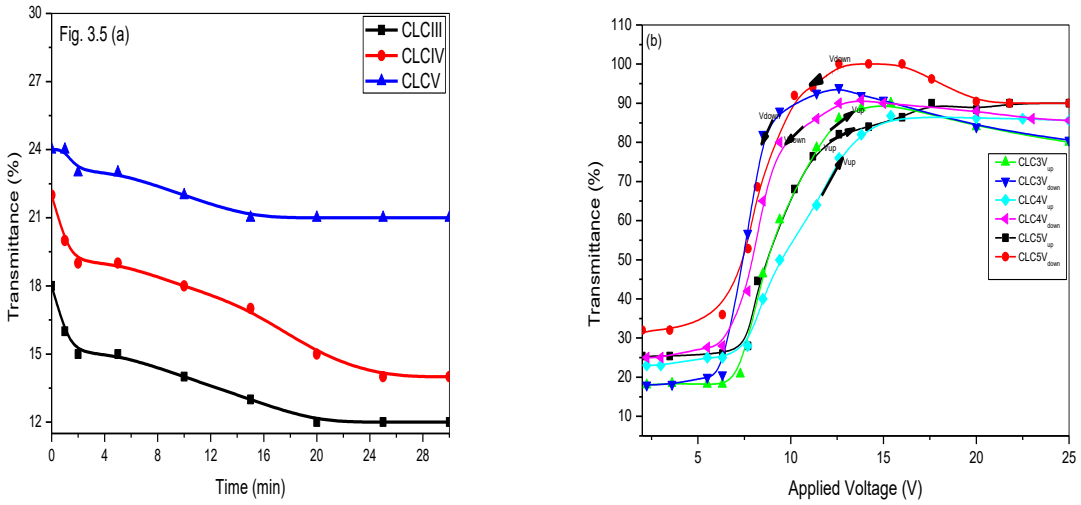

Fig. 3.5: (a) Transmitted intensity as a function of relaxation delay. (b) Optical hysteresis in CLC III, CLC IV, and CLC V. The direction of the arrow represents V_{up} and V_{down}.

To have a quantitative idea of hysteresis, optical transmission was recorded first corresponding to a stepwise increase of applied electric field and then corresponding to its decrease as shown in Figure 3.5 (b). While increasing the applied field above a threshold, chiral molecules start orienting along the field direction and helices start to open. The cell starts becoming more and more translucent, till the transmittance achieves saturation corresponding to the homeotropic state. With a stepwise decrease of applied voltage, transmittance curve does not retrace its earlier path, thus generating a hysteresis loop. The difference in areas enclosed by hysteresis loops for different samples again represents the fact that relaxation of the sample with highest d/p ratio is the slowest [Fig. 3.5 (b)]. The area in CLC V (238 a.u.) is more than that for CLC III (150 a.u.) and CLC IV (175 a.u.)

To further substantiate our observations, we investigated the hysteresis width of curves in [Fig. 3.5 (b)]. We define hysteresis width as the difference between voltage at the midpoint of the V_{up} curve and that at the midpoint of the V_{down} curve, between the maximum and

minimum transmissions [35]. Hysteresis width ΔV for CLC V (1.9V) being more than CLC III (1.3V) and CLC IV (1.6V), slower relaxation of CLC V is evident.

3.1.4 Electro-optical investigations of memory: The manifestation of memory in the electro-optical properties of the chiral doped samples was also established by the dielectric spectroscopy measurements [Fig. 3.6].

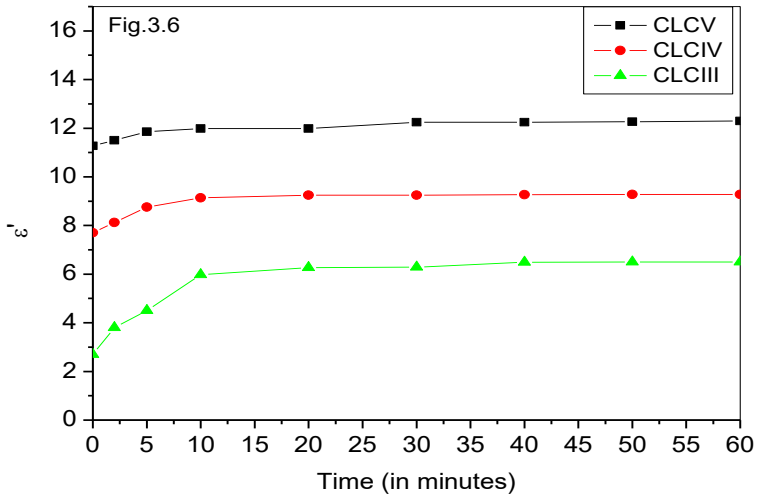

Fig. 3.6: Dipole relaxation of planar aligned CLC cells with different concentrations of chiral dopant with time, after switch OFF bias.

The real part of dielectric permittivity was recorded for one hour of relaxation period, after switching OFF the electric field of 50 Hz frequency. It was observed that relaxation of dipoles in CLC V is much slower than in CLC III and CLC IV [Fig. 3.6], which shows that dielectric relaxation gets delayed with an increase in chiral dopant concentration. We believe that this may be due to induced dipole moment and orientation polarization contribution of the dopant molecules.

Charge transport in a liquid crystal medium is due to the mobility of ions [48]. The dielectric permittivity of liquid crystals medium depends on the induced dipole moment and orientational polarization of its molecules. The applied electric field induces an uneven distribution of ions, which is no more frequency independent [49]. The scenario influences both, the real as well as the imaginary part of dielectric permittivity. When chiral mesogens

are doped into a nematic system, dipole moment of chiral mesogens supports the dipole moment of nematic molecules, indicating that net dipole moment of CLC V should be highest among all the concentrations.

***3.1.5* Electrically Tuned Photoluminescence in Chiral Nematic Liquid Crystals:** Chiral doped nematic fluorophores were excited at 345nm and violet emission was observed corresponding to 385nm wavelength for CLC I [Fig. 3.7(a)].

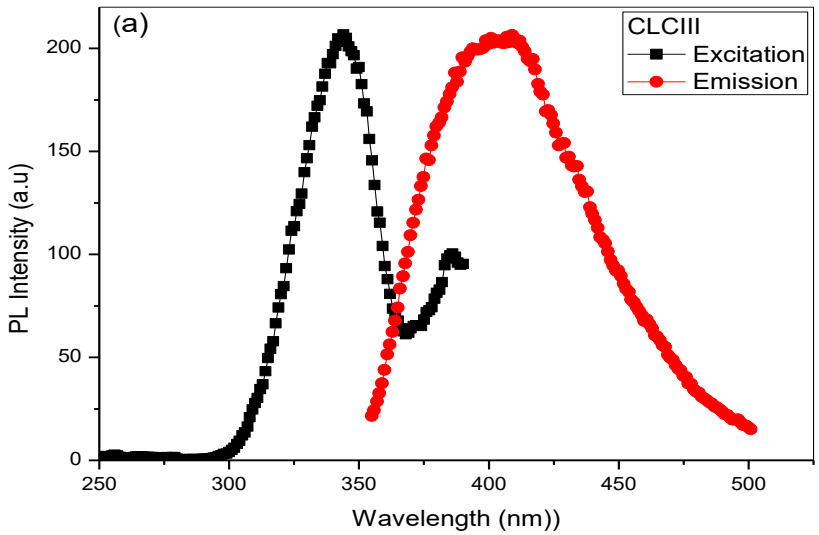

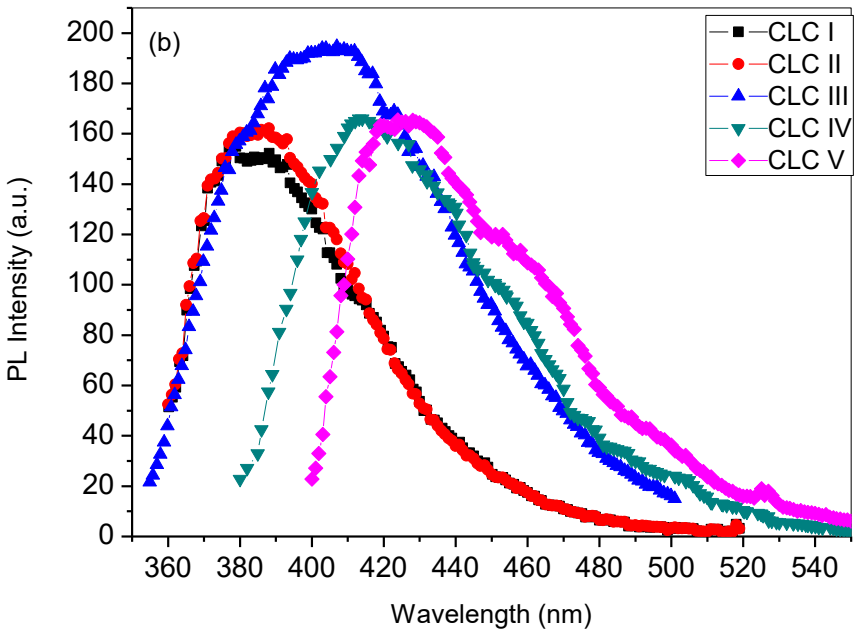

Fig. 3.7: (a) Excitation and Emission spectra of CLC III (b) Photoluminescence spectra of CLC materials at room temperature and zero applied field .

An enhancement in the peak value of PL emission was observed with doping of chiral molecules in NLC mixture. An increase in concentration of chiral dopant (CLC I, CLC II, and CLC III) resulted in an enhancement of photoluminescence peak intensity [Fig. 3.7(b)]. But with further increase in the concentration (CLC IV and CLC V), a decrease in PL intensity was observed.

A square wave ac electric field (0-30V) was also applied to the samples to check their electro-optic response. Samples were scanned for their PL response corresponding to different voltages from 0-30V. A change in PL intensity with applied electric field was observed for CLC I, CLC II, CLC III, and CLC IV, however, CLC V showed only an insignificant response to the applied electric field [Fig. 3.8 (a-e)]. The enhancement of PL intensity can be due to the unwinding of helical pitch and change in molecular anisotropy of the sample [50]. The reasons behind poor response of CLC IV and CLC V towards applied electric field can be due to change in phase of the samples from Planar Grandjean to Focal conic at this concentration (as observed in textures with unaligned cells) [Fig.3.9] and the optical hysteresis present in them. The sample with 2.5 wt% of chiral dopant (CLC III) showed maximum response to the electric field.

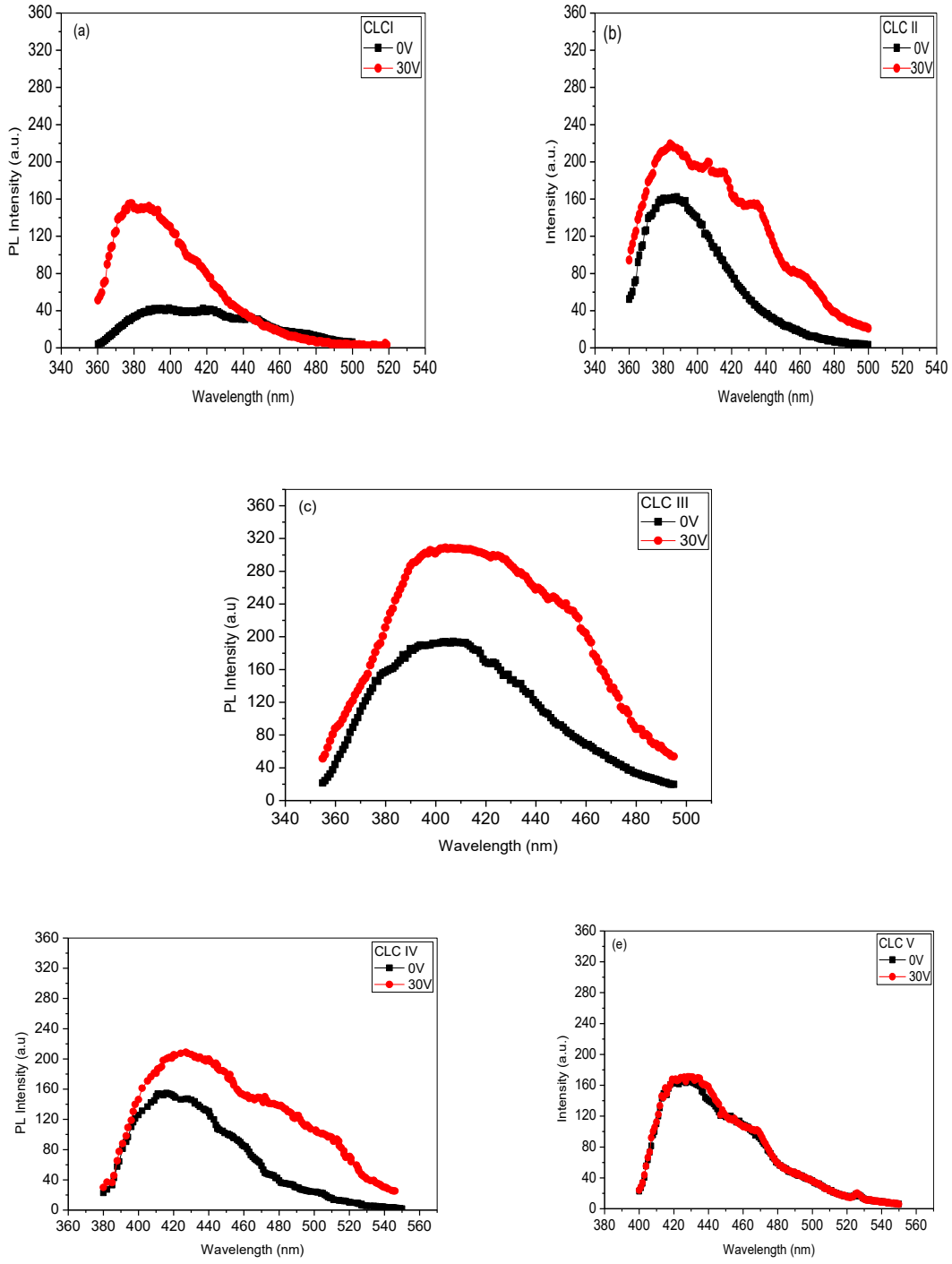

Fig. 3.8: Electrically controlled photoluminescence of (a)CLC I (b) CLC II (c) CLC III (d) CLC IV (e) CLC V.

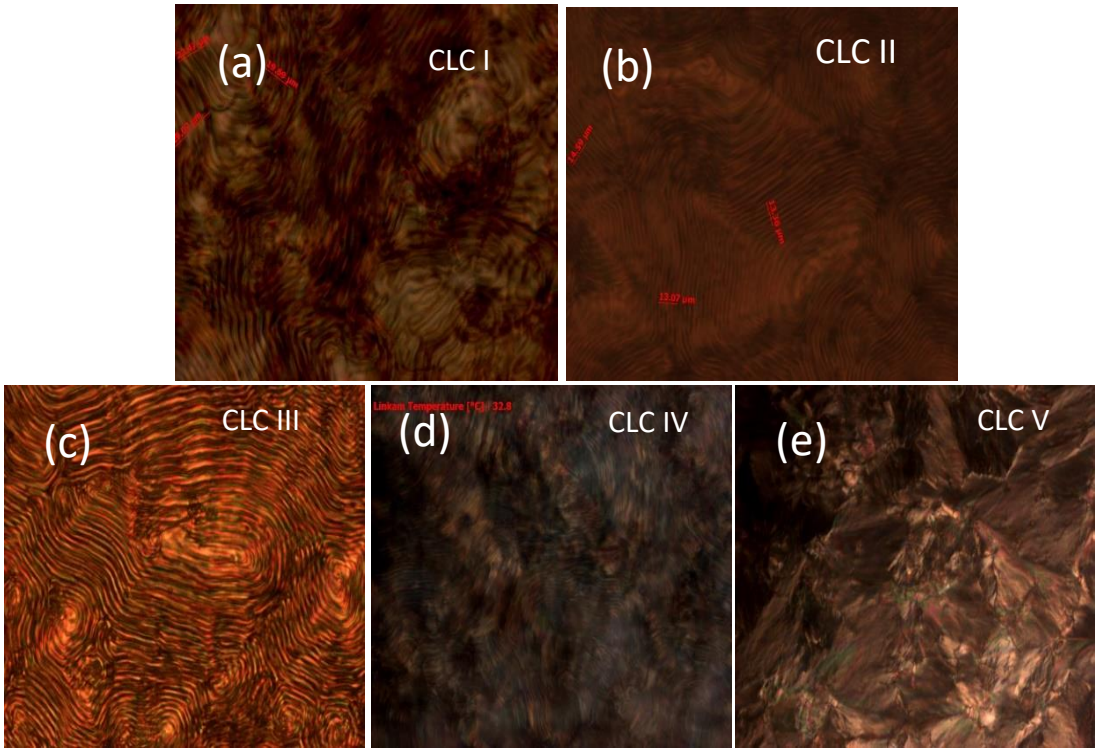

Fig. 3.9: Microscopic Textures representing (a) CLC I (b) CLC II (c) CLC III (d) CLC IV (e) CLC V confined in unaligned cells of 5 µm thickness.

Investigations for the morphological, optical, electro-optical and photoluminescence behavior carried out for the NLC doped with five different concentrations of chiral dopant indicate that **2.5 wt% sample (CLC III) is most appropriate for nanoparticles doping.** The following are the main features of this concentration (CLC III)

1. Morphology: Till this concentration, micro textures do not show any defects or discontinuities in the uniform texture, however after this, defects start appearing (CLC IV and CLC V)
2. Optical hysteresis: The optical hysteresis just starts coming in the sample, so there is a scope for its increase/decrease/disappearance of memory on nanoparticle doping.
3. PL intensity: The emission peak intensity is maximum for this sample as compared to other doped samples. This increases its prospects as a future optical material.
4. Electro-optical Response of PL emission peak: CLC III shows maximum response to the applied voltage. Hence a good electro-optic base material for Nano doping.

References

1. Chilaya GS, Lisetski LN. Cholesteric liquid Crystals: Physical properties and molecular-statistical theories. Mol. Cryst. Liq. Cryst. 1986;140:243–86.
2. Ginsburg GS, Atkinson D, Small DM. Physical properties of cholesteryl esters. Prog. Lipid Res. 1984;23:135–67.
3. Chilaya G. Induction of chirality in nematic phases. Rev. Phys. Appl. 1981;16:193–208.
4. Wang Y, Li Q. Light-driven chiral molecular switches or motors in liquid crystals. Adv. Mater. 2012;24:1926–45.
5. Chilaya G, Chanishvili A, Petriashvili G, Barberi R, De Santo MP, Matranga MA. Different approaches of employing cholesteric liquid crystals in dye lasers. Mater. Sci. Appl. 2011;02:116–29.
6. Huang Y, Zhou Y, Doyle C, Wu ST. Tuning the photonic band gap in cholesteric liquid crystals by temperature-dependent dopant solubility. Opt. Express. 2006;14:1236–42.
7. Kumar R, Raina KK. Enhanced ordering in polymer stabilised ferroelectric liquid crystal guest-host composites: evidence by polarised fluorescence spectroscopy. Liq. Cryst. 2014;41:694–700.
8. Malik P, Raina KK. Droplet orientation and optical properties of polymer dispersed liquid crystal composite films. Opt. Mater. (Amst). 2004;27:613–7.
9. Kumar R, Raina KK. Electrically modulated fluorescence in optically active polymer stabilised cholesteric liquid crystal shutter. Liq. Cryst. 2014;41:228–33.
10. Fuh AY, Wu Z, Cheng K, Liu C, Chen Y. Direct optical switching of bistable cholesteric textures in chiral azobenzene-doped liquid crystals. Opt. Express. 2013;21:21840–6.
11. Dierking I. Chiral liquid crystals: structures, phases, effects. Symmetry (Basel). 2014;6:444–72.
12. Ozaki M, Kasano M, Ganzke D, Haase W, Yoshino K. Mirrorless lasing in a dye-doped ferroelectric liquid crystal. Adv. Mater. 2002;14:306–9.
13. Shih CY, Yeh HC. Surface plasmon-enhanced lasing in dye-doped cholesteric liquid crystals. Opt. Express. 2012;20:20698.
14. Araoka F, Shin KC, Takanishi Y, Ishikawa K, Takezoe H, Zhu Z. How doping a cholesteric liquid crystal with polymeric dye improves an order parameter and makes

possible low threshold lasing. J. Appl. Phys. 2003;94:279–83.
15. Funamoto K, Ozaki M, Yoshino K. Discontinuous shift of lasing wavelength with temperature in cholesteric liquid crystal. japanese J. Appl. Physics, Part 2 Lett. 2003;42.
16. Kasano M, Ozaki M, Yoshino K, Ganzke D, Haase W. Electrically tunable waveguide laser based on ferroelectric liquid crystal. Appl. Phys. Lett. 2003;82:4026–8.
17. Ferjani S, Barna V, De Luca A, Versace C, Strangi G. Random lasing in freely suspended dye-doped nematic liquid crystals. Opt. Lett. 2008;33:557–9.
18. Takanishi Y, Ohtsuka Y, Suzaki G, Nishimura S, Takezoe H. Low threshold lasing from dye-doped cholesteric liquid crystal multi-layered structures. Opt. Express. 2010;18:12909–14.
19. Kelly SM, O'Neill M. Liquid crystals for electro-optic applications. Handb. Adv. Electron. Photonic Mater. Devices, Vol. 7 Liq. Crystals, Disp. Laser Mater. 2000.
20. Hsiao YC, Timofeev IV., Zyryanov VY, Lee W. Hybrid anchoring for a color-reflective dual-frequency cholesteric liquid crystal device switched by low voltages. Opt. Mater. Express. 2015;5:2715.
21. Caputo R, De Sio L, Cataldi U, Umeton C. Plasmon resonance tunability of gold nanoparticles embedded in a confined cholesteric liquid crystal host. Mol. Cryst. Liq. Cryst. 2012;559:194–201.
22. Yaroshchuk O, Tomylko S, Gvozdovskyy I, Yamaguchi R. Cholesteric liquid crystal-carbon nanotube composites with photo-settable reversible and memory electro-optic modes. Appl. Opt. 2013;52:E53–9.
23. Yoshida H, Inoue Y, Shiozaki Y, Takahashi M, Kubo H, Fujii A. Fast and continuous tunable lasing from a nano-pore embedded cholesteric liquid rystal Film. Mol. Cryst. Liq. Cryst. 2012;560:101–7.
24. Yoshida H, Tanaka Y, Kawamoto K, Kubo H, Tsuda T, Fujii A. Nanoparticle-stabilized cholesteric blue phases. Appl. Phys. Express. 2009;2.
25. Gharde RA, Thakare SY. Effects of concentration of multiwall carbon nanotube on cholesteric liquid crystal. 2015;4:68–74.
26. Castles F, Morris SM, Terentjev EM, Coles HJ. Thermodynamically stable blue phases. Phys. Rev. Lett. 2010;104.
27. Chang CK, Chiu SW, Kuo HL, Tang KT. Cholesteric liquid crystal-carbon nanotube

hybrid architectures for gas detection. Appl. Phys. Lett. 2012;100.
28. Coles HJ, Pivnenko MN. Liquid crystal “blue phases” with a wide temperature range. Nature. 2005;436:997–1000.
29. Furumi S. Recent progress in chiral photonic band-gap liquid crystals for laser applications. Chem. Rec. 2010;10:394–408.
30. Gardiner DJ, Morris SM, Castles F, Qasim MM, Kim WS, Choi SS. Polymer stabilized chiral nematic liquid crystals for fast switching and high contrast electro-optic devices. Appl. Phys. Lett. 2011;98.
31. Mitov M. Cholesteric liquid crystals with a broad light reflection band. Adv. Mater. 2012. p. 6260–76.
32. Yilmaz S. Optical properties of aligned nematic liquid crystals in electric field. J. Mod. Phys. 2011;02:248–55.
33. Reshetnyak VY, Shelestiuk SM, Sluckin TJ. Fredericksz transition threshold in nematic liquid crystals filled with ferroelectric nano-particles. Mol. Cryst. Liq. Cryst. 2006;454:201/[603] – 206/[608].
34. Ko SW, Huang SH, Fuh AYG, Lin TH. Measurement of helical twisting power based on axially symmetrical photo-aligned dye-doped liquid crystal film. Opt. Express. 2009;17:15926–31.
35. Yang DK, West JL, Chien LC, Doane JW. Control of reflectivity and bistability in displays using cholesteric liquid crystals. J. Appl. Phys. 1994;76:1331–3.
36. Kopp VI, Fan B, Vithana HK, Genack a Z. Low-threshold lasing at the edge of a photonic stop band in cholesteric liquid crystals. Opt. Lett. 1998;23:1707–9.
37. Winful HG. Nonlinear reflection in cholesteric liquid crystals: Mirrorless optical bistability. Phys. Rev. Lett. 1982;49:1179–82.
38. Hollins RC. Materials for optical limiters. Curr. Opin. Solid State Mater. Sci. 1999;4:189–96.
39. Bedanta S, Kleemann W. Supermagnetism. J. Phys. D Appl. Phys. 2009;42:13001.
40. Beeckman J, Neyts K, Vanbrabant PJM. Liquid-crystal photonic applications. Opt. Eng. 2011;50:081202 (17 pages).
41. Andreussi O, Biancardi A, Corni S, Mennucci B. Plasmon-controlled light-harvesting: Design rules for biohybrid devices via multiscale modeling. Nano Lett. 2013;13:4475–84.

42. Dong H, Zhu H, Meng Q, Gong X, Hu W. Organic photoresponse materials and devices. Chem. Soc. Rev. 2012;41:1754.
43. Clark M., Harrison K., Raynes E. Liquid crystal materials and devices. Phys. Technol. 1980;11:232–40.
44. Bisoyi HK, Li Q. Light-directing chiral liquid crystal nanostructures: From 1D to 3D. Acc. Chem. Res. 2014;47:3184–95.
45. Jakli A, Muller M, Kruerke D, Heppke G. First observation of electromechanical effects in a chiral ferroelectric columnar liquid crystal. Liq. Cryst. 1998;24:467–72.
46. Yaroshchuk O, Tomylko S, Dolgov L, Semikina T, Kovalchuk O. Carbon nanotubes doped liquid crystals: Robust composites with a function of electro-optic memory. Diam. Relat. Mater. 2010;19:567–72.
47. Lin GJ, Chen TJ, Lin YT, Wu JJ, Yang YJ. Effects of chiral dopant on electro-optical properties of nematic liquid crystal cells under in-plane switching and non-uniform vertical electric fields. Opt. Mater. Express. 2014;4:2468.
48. Garbovskiy Y, Glushchenko I. Nano-Objects and Ions in Liquid Crystals: Ion Trapping Effect and Related Phenomena. Crystals. 2015;5:501–33.
49. De Oliveira BF, Avelino PP, Moraes F, Oliveira JCRE. Nematic liquid crystal dynamics under applied electric fields. Phys. Rev. E - Stat. Nonlinear, Soft Matter Phys. 2010;82.
50. Huang CC, Chou TR, Chen JW, Chao CY. Enhancement of Photoluminescence Intensity of CdSe Nanorods Doped in Cholesteric Liquid Crystals. Brazilian J. Phys. 2014. p. 41–6.

CHAPTER -IV

EFFECTS OF CNT DOPING IN CHIRAL NEMATIC MEDIUM

Overview

The present chapter consists of two parts. The first part deals with the investigations and analysis of ODA functionalized SWCNTs in a CLC matrix and the second part consists of the study of the properties of chiral nematic liquid crystal doped with COOH capped MWCNT.

Octadecylamine functionalized Single-Walled Carbon Nanotubes (SWCNT) dispersion in the induced CLC influenced the collective orientation of nematic liquid crystal molecules in helical layers. By varying dopant concentration, we could manipulate the properties of the doped matrix. As confirmed by polarized fluorescence spectroscopy, highly anisotropic nature of single wall CNTs enhanced the anisotropy of liquid crystal. The $\pi-\pi$ interaction of SWCNTs present in the planar alignment layers and chiral nematic liquid crystal molecules, affects the molecular relaxation process. We also observed and quantified an electro-optical hysteresis of permanent nature.

The dispersal of COOH functionalized Multi-walled carbon nanotubes (MWCNT) into the induced chiral nematic liquid crystals confined in a planar aligned cell led to an improved electro-optic response regarding an increase in refractive index, and dielectric constant of the CLC. We investigated physical, optical and electro-optical behavior of doped samples with different dopant concentrations confined in similar boundary conditions. Polarized fluorescence spectroscopy established the anisotropic changes brought in by CNT doping with a significant increase in absorbance of doped samples. An early onset of Freedericksz transition also endorses the change in switching behavior of CLC after doping. The reorientation of liquid crystal director and CNTs with applied electric field was observed until the homeotropic state was achieved. We also noted an emanation of memory in doped samples after the withdrawal of electric field.

MEMORY EFFECTS IN CHIRAL NEMATIC LIQUID CRYSTALS DOPED WITH FUNCTIONALIZED SINGLE-WALLED CARBON NANOTUBES

In the last decade, researchers have shown an increasing interest in the field of nanoparticles doping in liquid crystals. Nano-doped composites have found significant applicability and attracted scientific understanding [1–6]. Self-organization of nanomaterials in flexible, yet organized structure of liquid crystals becomes intuitive because of the anisotropic nature of LC molecules. A large variety of nanoparticles is available in various shapes and sizes. Their incorporation in to an innumerous number of LC phases brings unprecedented variety in the device manufacturing and improvisation. We have used carbon nanotubes as well as spherical nanoparticles as dopants in CLCs.

There are reports of improved switching response, diffractive properties, and nonvolatile memory effects in the carbon nanotubes (CNTs) doped FLCs and nematic liquid crystals [7-11]. CNTs also find application in the field of biomedicine as protein biosensors, biocatalysts, bio separators and for drug storage and delivery [8]. They have also been instrumental in effectively reducing long standing problems related to display devices like optical flicker, image sticking, optical bounce, etc. [9,10]. Improvements in optical and electro-optic switching behaviour due to the addition of SWCNTs in ferroelectric liquid crystal (FLC) and an emergence of irreversible memory as a consequence of MWCNTs doping in FLC and nematic liquid crystals have been previously reported [11–14]. Memory responses in CNT-doped chiral liquid crystals were observed as the slower structural transition from homeotropic to the planar state [15]. Chang et al. observed an induced phase transition due to variation in acetone vapour concentration being accompanied by a decrease in electrical resistance of CLC-CNT hybrid, which makes it suitable for gas detection [16]. Lee et al. explored the possibility of reducing dc driving voltage and enhanced electro-optic switching behaviour by the addition of small amount of CNTs in TN cells [17]. CNTs, being highly anisotropic are well integrated into liquid crystal matrix, but the lack of uniformity in physical dimensions, poor solubility, and control of purity limit their applicability [18]. To redress these limitations and ensure a uniform dispersion of CNTs in the host medium, surface functionalization of carbon nanotubes was suggested [19–23]. The capping of CNTs also helped in improving their electro-optical properties and applicability. All these reports

claimed the lowering in electro-optical switching voltage and improved electro-optic switching behaviour of nematic liquid crystals and FLCs with CNT doping, but the understanding of manipulation of CNTs in the induced chiral liquid crystals (CLC) in the presence of strong Vander Waals forces still remains incomplete.

In the present study, we have attempted to investigate the effects of ODA functionalized SWCNT doping on the electro-optic and morphological behaviour of chiral nematic liquid crystals [24]. These investigations are expected to give a positive contribution in the field of research in functional materials.

4.1 Sample Preparation and Characterization

4.1.1 Functionalization of SWCNTs and their homogeneous mixing in CLC matrix: We used a nematic liquid crystal ZLI-4151 and added 2.5wt% of chiral dopant (CB15) mesogens in it. Octadecylamine (ODA)-functionalized SWCNTs [M/S Sigma Aldrich] having a diameter, d ≈ 2–10 nm and length, L ≈ 0.5–2μm were used as a dopant in host chiral nematic matrix. Figure 4.1 shows the molecular structure of ODA functionalized SWCNT and its Fourier transform infrared (FT-IR) spectra.

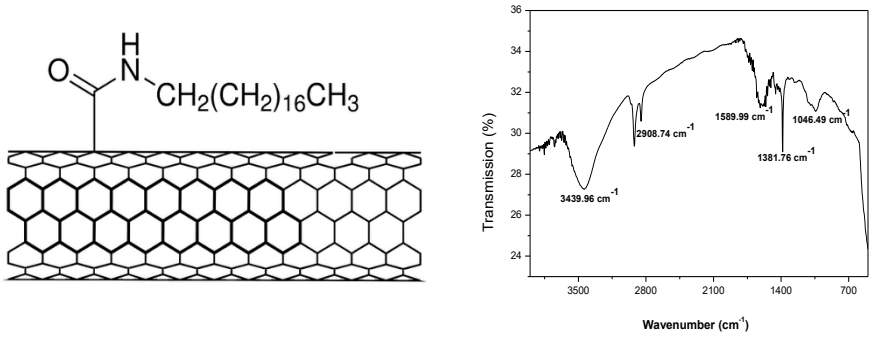

Figure 4.1: (a) Molecular structure (b) FTIR spectra of ODA functionalized SWCNTs.

4.1.2 Fourier transform Analysis: The spectra were studied using infrared spectrophotometer [Model-Perkin Elmer BX–II; Waltham, MA, USA]. In Figure 4.1(b), the dip at 1046.49 cm^{-1} represents the C–N stretching and the dip at 1381.76 cm^{-1} corresponds to simple bending vibrations of C–H bonds. The dip at 1589.99 cm^{-1} depicts the presence of C═O stretch, which confirms the successful attachment of functional group (ODA) to

SWCNTs. The dips at 2908.74 and 2842.10 cm^{-1} portray the asymmetric and symmetric vibrations of C-H bond. The dip at 3439.96 cm^{-1} corresponds to O-H stretch of vibration and wavenumber corresponding to dip at 3479 cm^{-1} shows the presence of N-H bond [25,26].

We prepared SWCNT doped chiral nematic liquid crystal composites by homogeneously dispersing 0.1, 0.3 and 0.4wt% ODA functionalized SWCNTs into the chiral nematic mixture followed by ultrasonication for about one hour. The samples were filled in the LC cells of 5µm thickness as per the procedure mentioned in Section 2.2 and following investigations were done to analyze their behavior.

4.1.3 Morphological Analysis: Fig. 4. 2 depicts the morphology of SWCNT doped chiral nematic liquid crystal samples under crossed polarizers at 100X magnification.

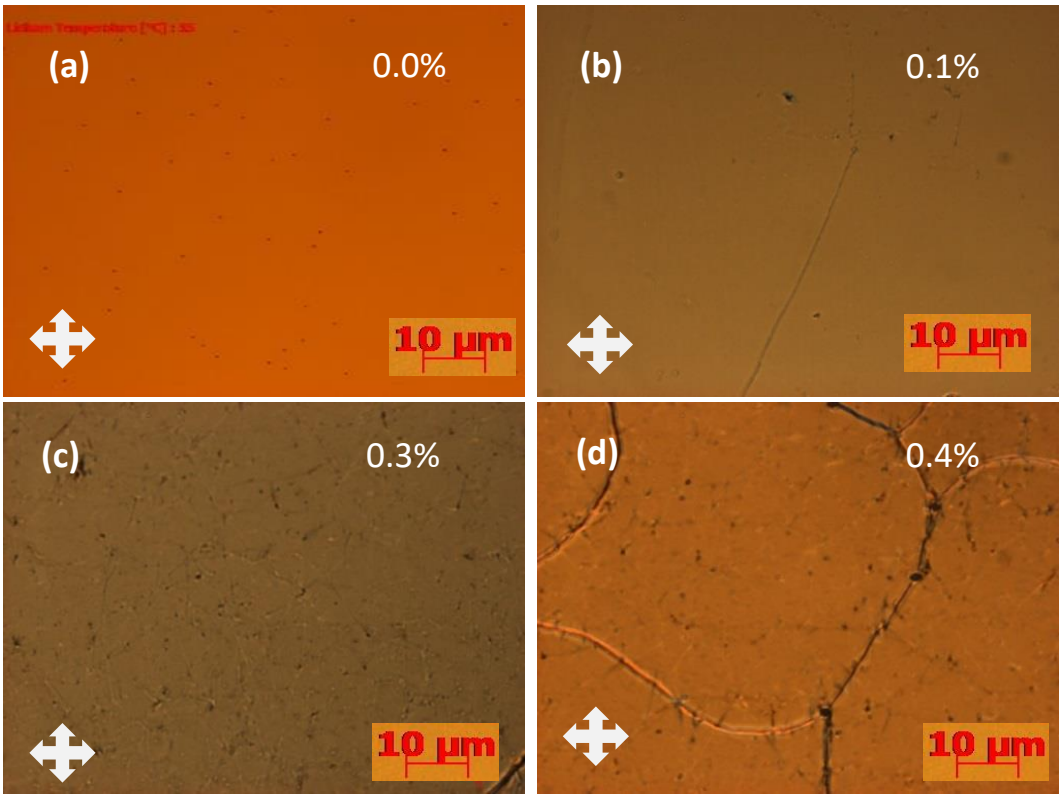

Figure 4.2: Optical micro textures of (a) 0.0 (b) 0.1 (c) 0.3 (d) 0.4wt% ODA functionalized SWCNT-doped CLC as a function of dopant concentration.

The planar Grandjean micro-texture in Fig. 4.2(a) represents the undoped CLC with its periodic helical supramolecules confined in planar boundary conditions of conducting substrates. The state corresponds to multiple Bragg reflections. The reflected wavelength is given by, $\lambda=np$, where n represents the refractive index and p is the pitch of the helix [27]. At 30^{o}C, 0.1wt% CNT-doped CLC sample shows a uniform change in colour [Fig. 4.2(b)]. The competition between elastic forces in the CNT doped medium, and surface anchoring force manifests itself in the form of appearance of disclinations in the microtexture. With further increase in concentration to 0.3wt%, we witnessed a multi domain formation oriented along modulated helical structure [Fig. 4.2(c)].

We believe that the presence of CNTs has disrupted the ordering at the interfaces by inducing anisotropic interactions with the CLC molecules. The formation of domains bounded by chain like boundaries takes place at 0.4wt% dopant concentration. These well defined domain boundaries appear to have confined the chiral nematic molecules, [Fig. 4.2(d)] and stabilized the liquid crystal matrix [28]. The functional group has probably aligned itself in the planes of supramolecular helical structure thus preventing CNTs from aggregate formation.

4.1.4 Electro-optic Switching: Fig. 4.3 depicts the electro-optical switching behaviour of SWCNTs doped CLC material under crossed polarizers.

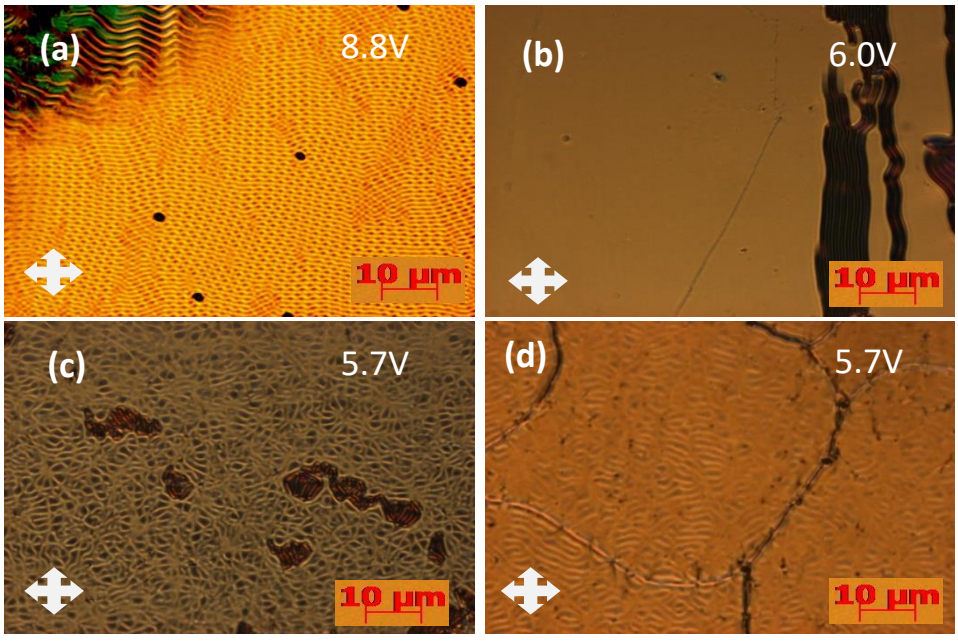

Figure 4.3: Microtextures of doped CLC for (a) 0.0 (b) 0.1 (c) 0.3 (d) 0.4wt%, dopant concentration during Freedericksz transition.

In case of the undoped chiral nematic system, a square grid texture marks the onset of Freedricksz transition [Fig. 4.3(a)]. We observed contrast inversion in optical textures due to the instability caused by CLC mesogens, at the onset of transition.

Electro-optical switching took place at a lower threshold field (1.20V/μm) in 0.1wt% doped sample [Fig. 4.3(b)] as compared to the undoped sample (1.76V/μm).

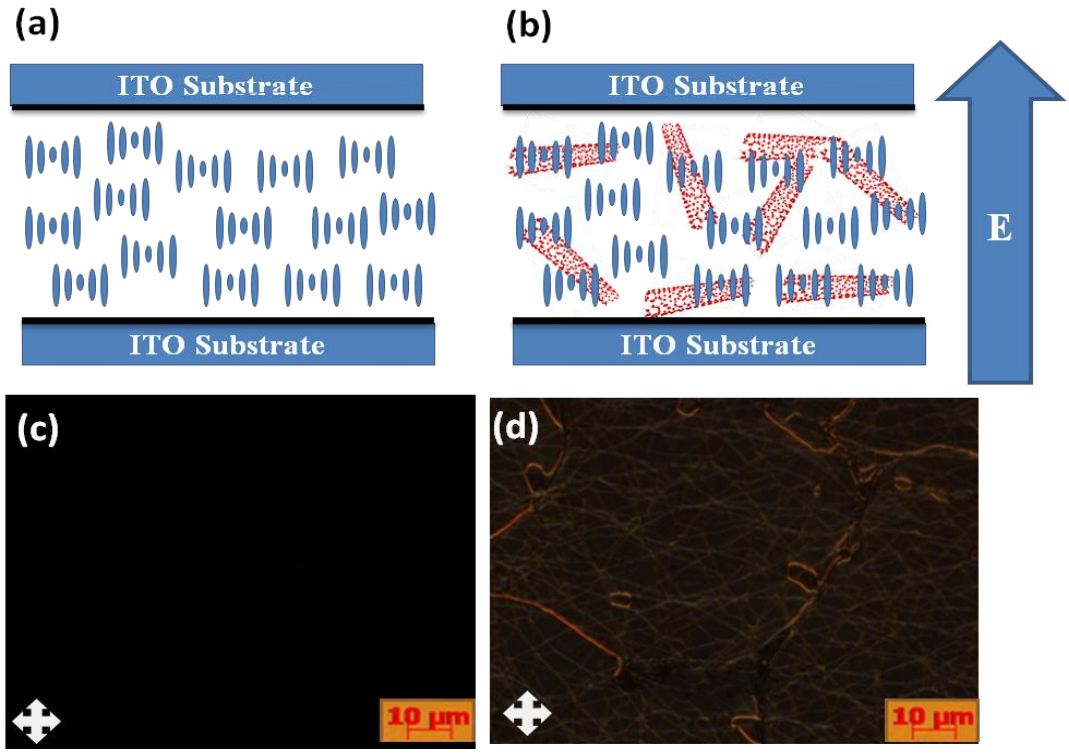

Figure 4.4: (a, b) Hypothetical model depicting the field induced molecular alignment in undoped and doped CLCs respectively, (c) Optical texture showing the homotropic (perfectly dark) state of undoped CLC, (d) Spatial distribution of CNTs visible in the homotropic state of doped CLC.

The fall in the threshold is quite significant. We observed ~30% decrease in switching threshold of 0.1wt% doped sample and ~40% in 0.3wt% doped sample [Fig. 4.3(c)]. The dielectric anisotropy of the medium plays a crucial role in deciding the switching response of LCs. As higher anisotropy of the matrix favours faster switching, the addition of anisotropic particles can contribute to increase LC dielectric anisotropy. CNTs being highly

anisotropic, are expected largely to influence the switching behavior of liquid crystal host. Moreover if reorientation of CNTs occurs at a lower voltage than that for LCs, then reorientation happens faster and the threshold field value decreases [29].

We observed a perfect dark homotropic state in the undoped sample [Fig. 4.4(c)], due to the perfect alignment of CLC molecules along the field direction, whereas a spatial distribution of SWCNT network was clearly observed under crossed polarizers in 0.3wt% and 0.4wt% doped samples [Fig. 4.4(d)] as perceived in hypothetical model [Fig. 4.4(a,b)].

Dielectric spectroscopy was done to check the influence of CNTs on ac conductivity of doped samples. We observed a nearly tenfold increase in conductance of doped samples (frequency range 100Hz-1kHz) as compared to the undoped one. The ac conductivity can be computed by [30]

$$\sigma_{ac} = \epsilon_o \epsilon'' \omega \ldots\ldots\ldots\ldots\ldots\ldots\ldots\ldots (4.1)$$

Where, ϵ_o is permittivity of the free space, Ɛ" is the imaginary part of permittivity (recorded experimentally) and ω is the angular frequency. Fig. 4.5 clearly depicts the role of SWCNTs in the enhancement of conductivity (σ_{ac}) of doped samples.

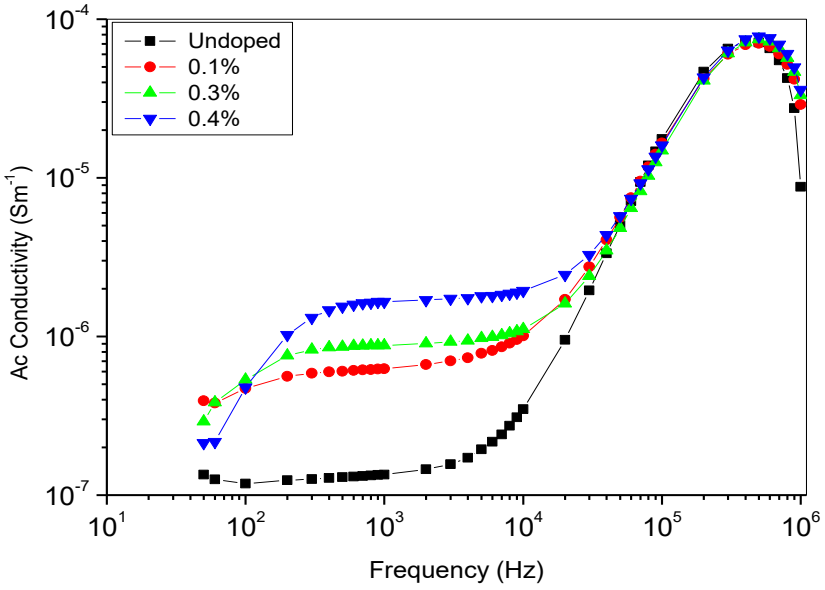

Figure 4.5: ac conductivity as a function of SWCNT doping concentration.

We believe that interaction between surface anchoring and π−π electron stacking enhances the ac conductivity by contributing towards space charge polarization at the interface [31].

The formation of an interface between CNTs and liquid crystal matrix could be responsible for the recorded increase. As reported earlier [20], sometimes a charge is accumulated at the alignment layer due to space charge polarization in the presence of CNTs. This interface formation leads to enhanced conductivity and affects the dielectric response of the material. Experiments are still ongoing to investigate the real role of CNT concentration in bringing about such a significant increase in conductivity.

4.1.5 Optical Investigations of Induced Memory: Fig. 4.6 depicts the optical transmission intensity as a function of applied electric field during the electro-optical transition. We placed the sample cells with their rubbing direction making an angle of 45° with either of the polarizers. We recorded the transmission responses by first stepwise increasing the applied voltage (solid curve) and then corresponding to a stepwise decrease of voltage (dotted curve). Before the application of field, CLC molecules are in a stable state. The molecular dipoles start aligning along the field direction under the influence of electric field. The transmittance increases gradually and saturates in the homeotropic state. The elastic forces of helical structure force the molecules to reorient on subsequent withdrawal of the field. Reorientation causes a decline in transmission intensity. We observed that transmittance does not follow the same path on its way back hinting at optical hysteresis in

the behaviour of sample.

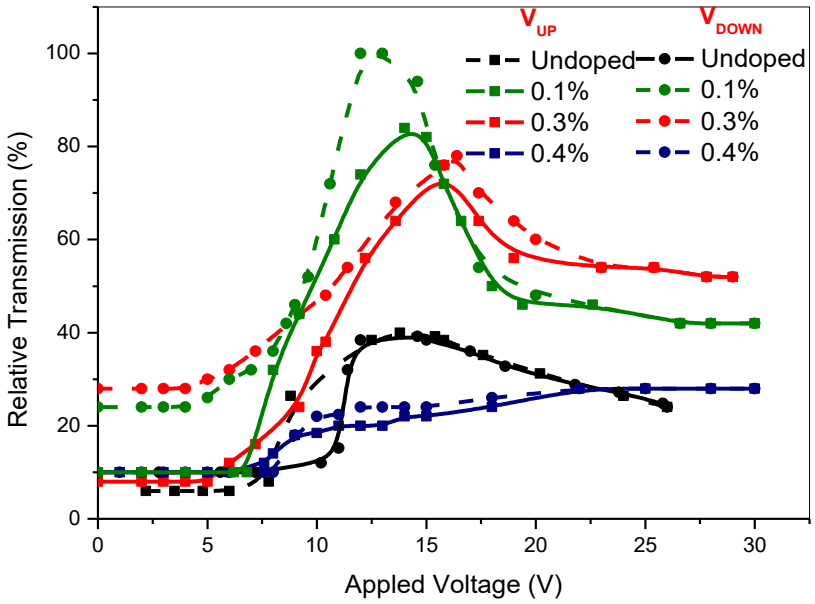

Figure 4.6: Electro-optic response of SWCNT-doped CLC samples, (solid curves represent increasing voltage while dotted ones represent decreasing voltage).

We believe that the reason for partial realignment is the stabilization of network of linear cholesteric domains by SWCNTs, which in turn supports planar orientation of CLCs after withdrawal of the electric field. Fig. 4.7 shows the variation in electro-optical memory as a function of ageing. These textures were captured by first subjecting the sample to $30V_{p\text{-}p}$ voltage, then abruptly switching off the field.

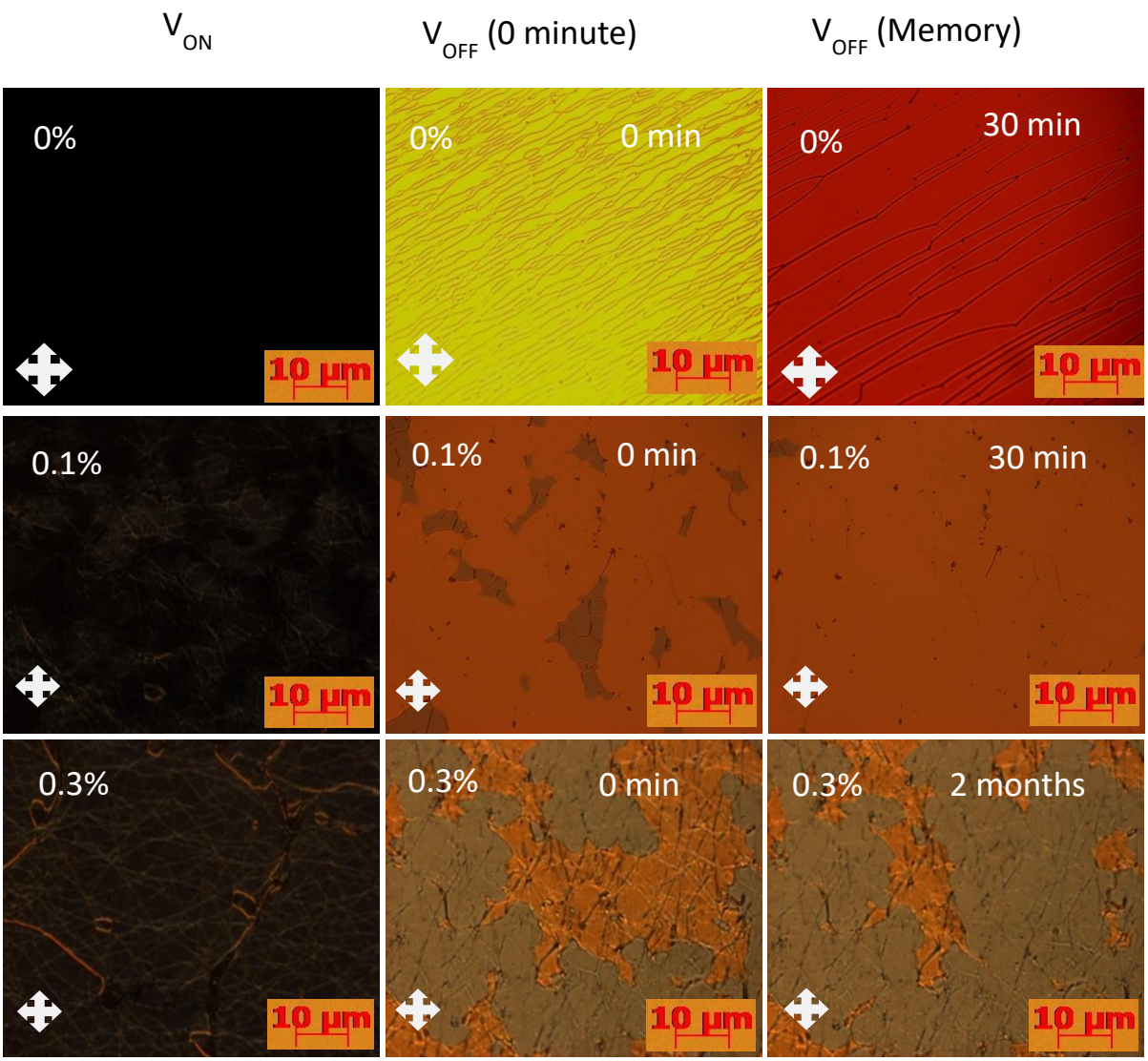

Figure 4.7: Illustration of memory effects in SWCNT-doped samples through optical textures.

The optical microtextures in Fig. 4.7 clearly show that doped samples did not regain their original textures. The presence of planar domains of a different colour indicates the irreversibility of electrically induced homeotropic-to-planar transition state of SWCNT doped chiral LC. These textures also predict irreversible electro-optic response of the material in field OFF state. Fig. 4.7 also displays enhancement in optical hysteresis with increased doping. The induced memory state persisted for two months of observation in 0.3wt% doped sample and could be erased only by heating the sample to its isotropic temperature [105^{o}C] and subsequent cooling. The samples were taken through repeated cycles of application and withdrawal of field to ensure the existence of memory. A loss in

transmission intensity leading to a decrease in memory parameter was observed for the higher value of doping concentration (0.4wt%). We believe that randomness generated in the sample at this (the relatively higher) concentration is responsible for the decrease.

Table 4.1: Optical characteristics of Undoped and SWCNT-doped CLC samples.

CNT Concentration (wt%)	**Memory Parameter**	**λ_{ex} (nm)**	**I_{ex} (a.u.)**	**λ_{em} (nm)**	**I_{em} (a.u.)**	**Anisotropy at λ_{em} (Δn) 10^{-3}**	**Refractive Index**
0.0	0.10	348.8	20.3	405.5	20.3	14	1.49
0.1	0.15	338.0	29.0	384.5	29.2	40	1.69
0.3	0.28	337.9	38.0	384.2	37.4	51	1.69
0.4	0.00	337.0	24.4	381.6	24.1	2	1.69

A decrease in anisotropy of the sample measured with fluorescence spectrophotometer also endorses the assertion [Table 4.1].

4.1.6 Effect of Doping on Refractive Index: The transparency/opacity and response of the material towards propagation of light through it was investigated using Abbe's refractometer. We measured the refractive indices of pure and doped samples and noted an enhancement of about 18% in the refractive index of doped samples. The observed enhancement promises for exploring better prospects and device usage of this optical material.

4.1.7 Fluorescence Anisotropy Measurements: Fig. 4.8 (a,b) depicts the PL excitation and emission spectra of doped samples respectively. We could get a better understanding of fluorescence emission due to orientation of supramolecular structure as a function of incident light wavelength for all the doped samples under investigation. The fluorescence anisotropy is computed as [27]

$$\Delta n = \frac{I_{\parallel} - gI_{\perp}}{I_{\parallel} + 2gI_{\perp}} \quad \text{..... (4.3)}$$

Where, 'g' represents the g-factor of the instrument, $I_{\parallel}$ and $I_{\perp}$ are the PL intensities corresponding to parallel and perpendicular directions relative to the LC director in a layer.

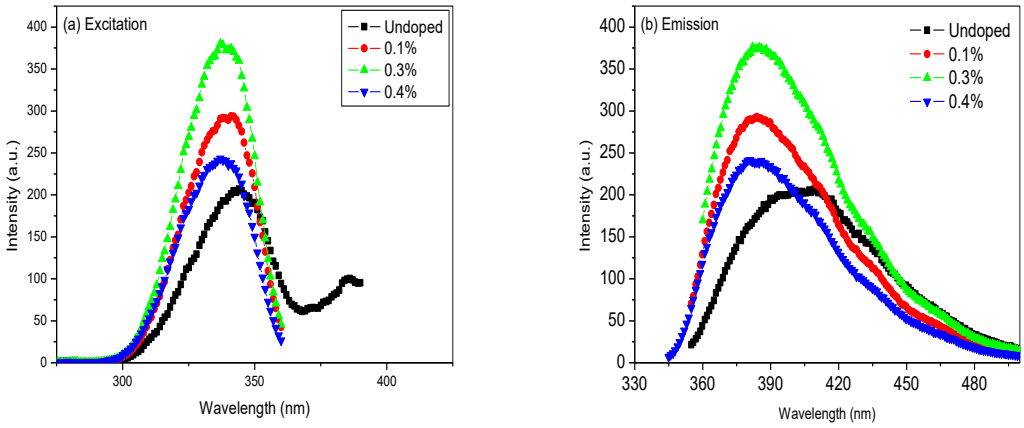

Figure 4.8. (a) excitation (b) emission fluorescence spectra of doped samples.

The fluorescence anisotropy findings also support the output responses of transmitted light as tabulated in Table-4.1. They further indicate that doping with CNTs has brought order in LC medium which shows up as anisotropy in its order parameter. The CNTs in CLC matrix follow the orientation of the surrounding supramolecular structure, which in turn has probably resulted in improved ordering [32].

The doping of SWCNTs in chiral nematic liquid crystals has improved the morphological and electro-optic switching behaviour of CLC host. The functional group has restricted the CNTs from aggregate formation. The faster reorientation and high anisotropicity of CNTs has influenced the switching behavior by significantly bringing down the threshold voltage. The dispersion of CNTs has also stabilized the sample which is indicated in the enhancement of electro-optic memory (significantly at 0.3wt% CNTs doping). The CNT doped CLCs can be of potential practical usage in optical memory devices and display technology.

IMPROVED ELECTRO-OPTICAL RESPONSE OF INDUCED CHIRAL NEMATIC LIQUID CRYSTAL DOPED WITH MULTI-WALLED CARBON NANOTUBES

The dispersal of Carbon nanotubes (CNTs) in liquid crystalline phases has received an increased interest of researchers [33–38]. Their anisotropic nature, inherent conductivity and self-alignment properties earn them a place as a potential dopant for liquid crystal matrices and as an alignment layer [39–41]. When used as a dopant in liquid crystals, CNTs have been reported to enhance the dielectric anisotropy of LC host. They bring about significant changes in overall Electro-optic and dielectric behavior regarding conductivity, threshold voltage and response times of the LC cells [1,17,42–45]. The doping of CNTs in various mesophases has been widely done, reported and reviewed [35,46,47]. CNTs have been reported to effectuate a lower switching voltage, widening of the reflection band, improved birefringence and enhanced dielectric anisotropy in FLCs [12,14,30,48–50]. The generation of themo-optical hysteresis above a certain concentration of CNTs, in the form of percolation network or cluster formation, realizing a permanent memory state of electrical conductivity was also reported [21,51–55]. The doping of MWCNTs to a CLC have been reported to modify the physical properties of the host [56].

In spite of the extensive use of CNTs as dopants in various LC phases, nothing much has been done to explore the behavior of an induced CLC doped with CNTs [57]. Chiral media are known for their inherent property of selective reflection and a helical pitch that can be easily influenced by external provocations [58]. On the other hand, CNTs are characteristically anisotropic due to their shape. The combination of two such materials seems logically sure to bring about unprecedented functionality and enhancement in the properties of liquid crystal host [31].

We, in the present work, have ensured the uniform dispersal of functionalized multi-walled carbon nanotubes in the induced chiral phases. We have observed the influence of CNT doping on electro-optical switching, anisotropy, dielectric properties and optical hysteresis of the CLC host for different concentrations of the dopant.

4.2 Sample Preparation and Analysis

4.2.1 Functionalization of MWCNTs: We used commercially available Multi-walled carbon nanotubes (MWCNT) with a hollow structure, having a diameter ≈110-170 nm, length 5-9 μm and 98% purity (Aldrich) as a dopant [Table 2.4]. They were functionalized before use, to ensure their homogeneous dispersal in the liquid crystal mixture. We chose the -COOH group for this purpose. The chemical functionalization was done through oxidation of the MWCNTs. We added 10mg of MWCNTs in a homogeneous mixture of H_2SO_4 and HNO_3 taken in a molar ratio (1:3). Ultrasonication of the mixture was done for 2 hours at 60^oC bath temperature. The mixture was then magnetically stirred for 24 hours at the same temperature. In the process of oxidation, π bond symmetry of sp^2 hybrids of carbon gets affected, and the carboxylic acid gets attached to the MWCNTs. Ultra-pure distilled water (250 ml) was added to the mixture after it got cooled down to room temperature. Functionalized MWCNTs were then separated out with a centrifuge (12000 rpm). Impurities were removed by washing them out thrice with acetone. The functionalized MWCNTs are then dispersed into chloroform, to be used for characterization of functional group.

4.2.2 Fourier Transform Analysis: FTIR analysis confirmed the attachment of functional group [Fig. 4.9].

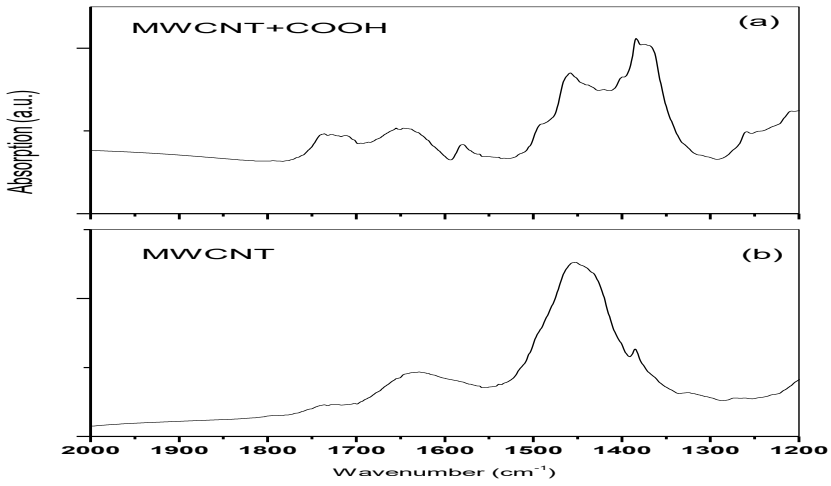

Figure 4.9: FTIR spectra of (a) COOH functionalized MWCNTs (b) Untreated MWCNTs.

We got strong absorbance even for very small concentrations due to the black colour of the CNTs. The absorption peak at 1740 cm^{-1} in the FTIR of functionalized MWCNTs represents elongated C=O stretching of a carboxylic group and the peak at 1385 cm^{-1} stands for the O-H bond. These peaks were not present in the spectrum of uncapped MWCNTs. Their presence in the IR analysis of treated MWCNTs confirms the attachment.

The doped suspensions were prepared by adding different concentrations (0.01, 0.10, 0.50 and 1.00wt%) of MWCNTs to the induced chiral nematic mixture as specified in section 2.2 of the second chapter of the thesis.

4.2.3 Morphological Analysis: Fig. 4.10 depicts the morphology of the doped samples under crossed polarizers at 100X magnification. The undoped chiral liquid crystal [Fig. 4.10(a)] is characterized by a planar Grandjean texture. Due to the periodicity and chirality in its structure, the chiral liquid crystal Bragg reflects the circularly polarized light incident on it. It reflects the one component while transmitting the opposite [59][24].

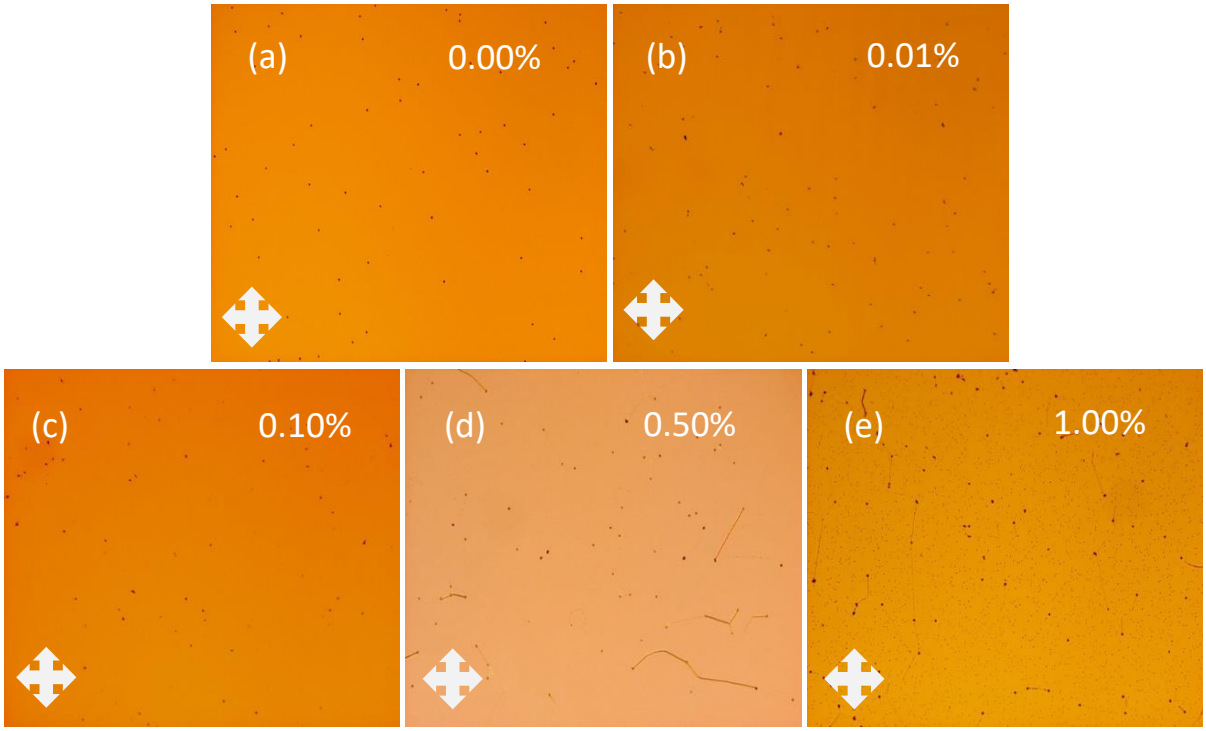

Figure 4.10: Optical micro textures of doped CLC as a function of MWCNT concentration (a) 0.00 (b) 0.01 (c) 0.10 (d) 0.50 (e) 1.00wt% respectively.

The selective reflection bandwidth $\Delta\lambda$ of reflection peak depends on optical anisotropy (Δn) and pitch (p) of the helix as per the following relation

$$\Delta\lambda = \Delta n.\ P \ldots\ldots\ldots\ldots\ldots\ldots \quad (4.4)$$

Where, $\Delta n = n_{\parallel} - n_{\perp}$, ($n_{\parallel}$ and $n_{\perp}$ are the refractive indices of the material in a direction parallel and perpendicular to the director, respectively) [60]. The Fig. 4.10 (b-c) reveals that low concentration of CNTs does not significantly influence the pitch of the helix as there is no noticeable change in colour of the lightly doped samples.

The micro texture representing 0.50wt% dopant concentration exhibits planar regions and slightly curved linear disclinations suggesting the emergence of two twist states separated from one another by the defect boundaries. A close look at the microtexture corresponding to 1.0wt% doping reveals an evenly spanned network in the form of pores, along with disclinations [Fig. 4.10 (e)] (zoom). This type of morphology indicates the formation of a percolating network by CNTs in liquid crystal matrix at this concentration.

Table 4.2: Phase transition temperatures for undoped and MWCNT-doped samples.

Liquid Crystal Type	T_{ISO} (K)	T_N*(K)
Nematic (N)	385	372
Undoped (CLC)	390	368
CLC+0.01wt%CNTs (MW1)	404	381
CLC+0.10wt%CNTs (MW2)	403	373
CLC+0.50wt%CNTs (MW3)	402	365
CLC+1.00wt%CNTs (MW4)	402	363

Fig. 4.11 displays the nucleation state of the doped and undoped samples and Table 4.2 shows the corresponding phase transition temperatures. Cholesteric platelets with two different colours, separating from the isotropic melt in the undoped sample [Fig. 4.11 (a)] represent two independent twist states of chiral nematic liquid crystal matrix [61]. The

smooth and defect-free surface of droplets in case of the undoped sample indicates that here, surface anchoring forces have minimal effect on the twist state of chiral mesogens. In 0.01-0.10wt% doped samples, colour of the droplets transforms to uniform single colour [Fig. 4.11 (b, c)]. The change hints at the role of CNTs in influencing the twist state of the matrix from double to single.

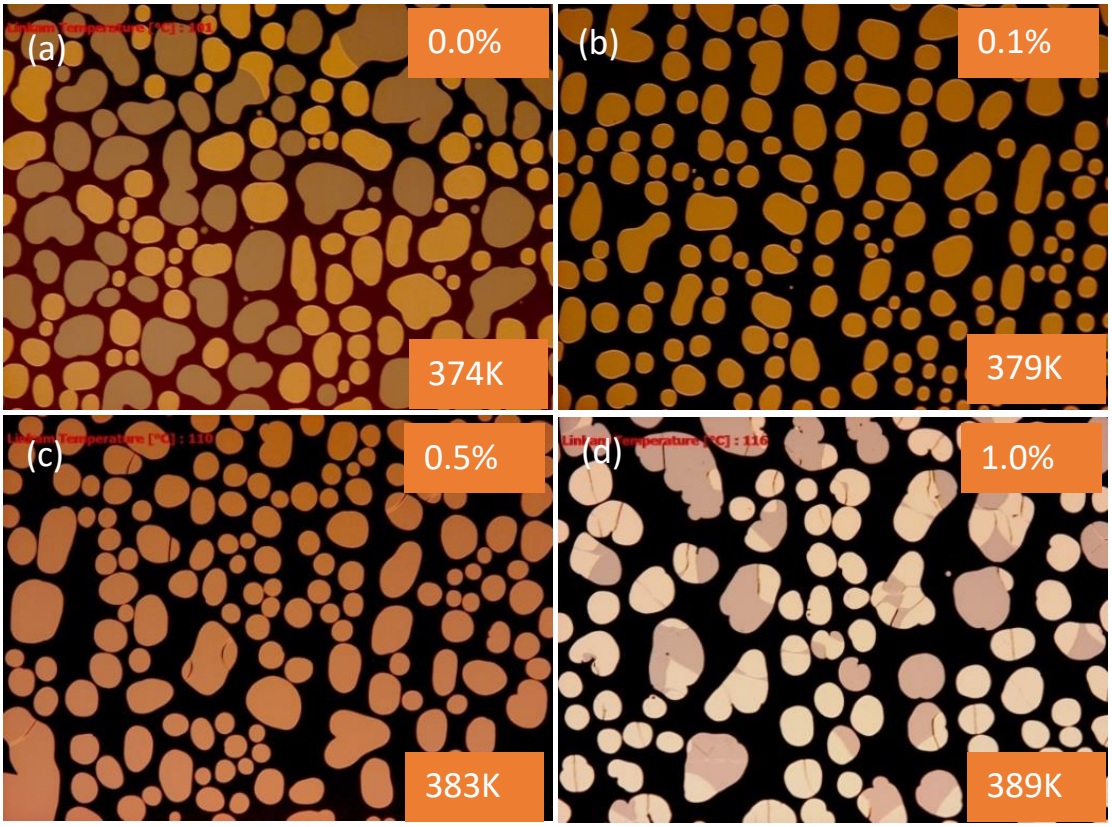

Figure 4.11: Optical micro textures depicting the nucleation process in (a) 0.00 (b) 0.10 (c) 0.50 (d) 1.00wt% MWCNT-doped samples.

Further increase in dopant concentration leads to a different twist state but here the two colours appear on a single droplet and at the disclination boundaries, which we believe, is due to the decreased influence of CNTs which are now lying agglomerated and/or confined to the defects generated in the medium [Fig. 4.11 (d)]. The defects seen on the surface of platelets may have been generated because of the π–π interaction of dopant structures with

liquid crystal molecules in the presence of elastic forces of rewinding helices and the surface anchoring forces.

4.2.4 Photoluminescence Studies: The relative orientation of helical structure as a function of wavelength spectrum of incident radiation for different dopant concentrations [Fig.4.12] was studied by computing PL anisotropy 'Δn' as given in Equation 4.3 [24]. A significant decrease in the intensity of emission peak of 0.01wt% doped sample as compared to the undoped sample [Table 4.3] indicates that doping with MWCNTs causes an increase in absorption and an increase in the doping amount further decreases PL intensity [Fig. 4.12].

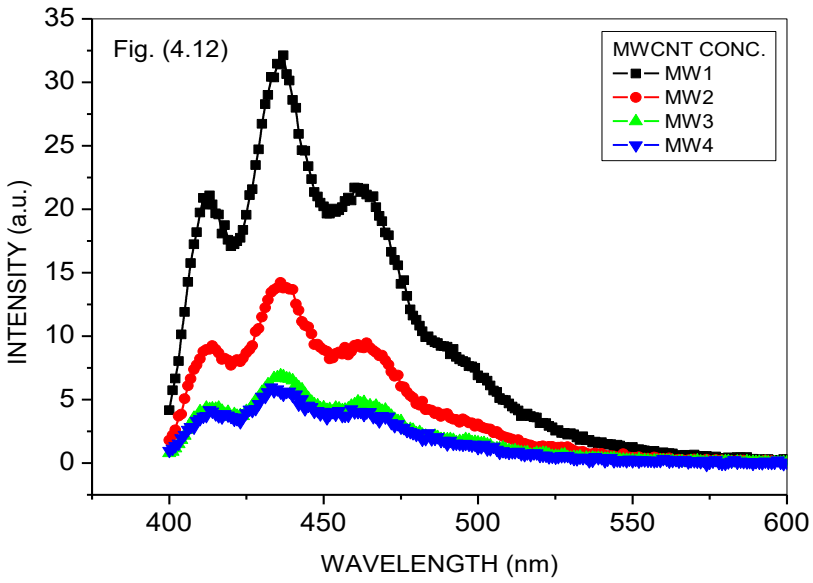

Figure 4.12: Emission spectra of MWCNT-doped samples.

The meagre horizontal shift in the emission peaks of the doped samples explains the trivial change in colour of the reflected light from different samples. The response of the medium to incident light was studied in terms of refractive indices of undoped and doped samples by Abbe's refractometer [Fig. 4.13(a)].

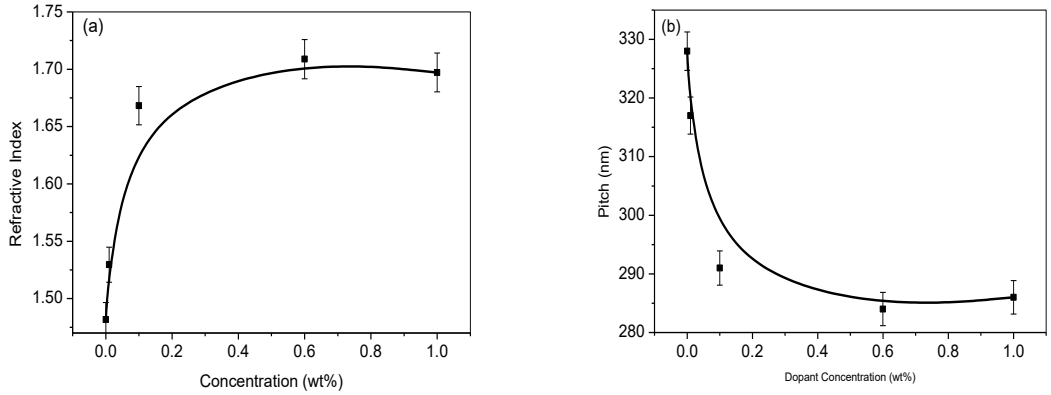

Figure 4.13: Variation of (a) Refractive Index (b) Pitch of the doped samples with MWCNT concentration.

A significant increase (up to 13%) in refractive index of doped samples as compared to the undoped was recorded [Table 4.3]. As there is almost no shift in reflected wavelength, we believe that pitch of the doped samples may have decreased [Fig. 4.13(b)].

Table 4.3: Optical characteristics of Undoped and MWCNTs-doped CLC samples.

Parameter	**Chiral 0.00wt%**	**Mw1 0.01wt%**	**Mw2 0.10wt%**	**Mw3 0.50wt%**	**Mw4 1.00wt%**
Refractive Index	1.48	1.51	1.66	1.70	1.70
Threshold Voltage (V)	8.8	5.8	5.3	6.9	6.9
Anisotropy at 436 nm (10^{-3})	2	4	19	3	2
Emission peak position (nm)	407.0	437.0	436.4	436.4	434.0
Peak PL Intensity (a. u.)	190	32	14	7	6
Conductivity (10^{-7} $Sm^{-1)}$	0.09	0.36	0.49	1.32	1.56
Ɛ’ (at 40^{O}C) 1kHz	5.8	5.9	6.1	6.3	6.3

The fluorescence anisotropy findings as tabulated in Table-4.3 validate other findings. All the investigations suggest that MWCNTs do influence the order of host liquid crystal medium by aligning themselves in alignment layers.

4.2.5 The Electro-Optical Switching Behaviour: The application of electric field above a threshold value (1.06V/μm) forces the liquid crystal molecules to make an orientation along the field by applying a torque on polarized molecules. The CNTs present in doped samples also move to the directionally aligned conductive state as explained in section (4.1.3) [29]. We observed lowering of the switching threshold with CNT doping in case of lower concentrations which seems to be due to high anisotropy of CNTs contributing to the anisotropy of the composite. Corresponding to higher concentration of CNTs, the transition takes place at a higher value. We believe that this is because of the stabilization of cholesteric domains by the percolation network of CNTs [Table 4.3].

4.2.6 Electrical Conductivity and Dielectric Response: The electric field induced behavior of CNT-doped LC media has always attracted interest of the people working in this field. It has been widely reported in literature that a minimal change in CNT concentration can significantly alter the electro-physical behavior of LC composite [34,62,63].

Dielectric spectroscopy of MWCNT doped samples was done by a parallel RC circuit and changes in the capacitance and dissipation were recorded to compute the ac conductance σac, using Equ 4.1 [64]. The variation of conductivity with frequency corresponding to different dopant concentrations has been plotted in Fig. 4.14(a). The effect of dopant concentration on the conductivity of doped samples has been shown in Fig. 4.14(b) A notable increase (five - tenfold) in the ac conductivity of doped samples at 50 Hz shows the influence of CNTs.

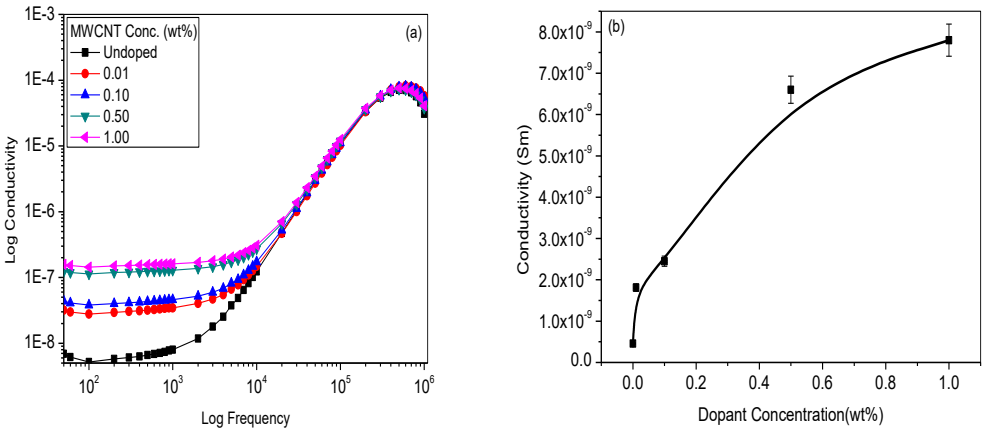

Figure 4.14: ac conductivity of MWCNT-doped CLC samples as a function of (a) field frequency at various dopant concentrations (b) Doping Concentration.

The cause of observed increase in conductivity of MWCNTs doped samples [Table 4.3] can be attributed to the conductive behaviour of CNTs which provide an easy path for conduction at low concentrations and finally form interconnection of aggregates and percolating network permeating into LC matrix at 1.0wt% concentration.

Figure 4.15 (a, b) show a substantial increase in Ɛ' at low (50-100 Hz) frequencies with rise in temperature. The real part of dielectric permittivity shows about 19-fold increase [Table 4.3] corresponding to a rise in temperature of about 60K at 50 Hz and about 40% increase at 1kHz frequency for 1.00wt% doped sample, indicating the sensitivity of its dielectric behavior towards temperature. The dielectric constant is not influenced much by doping with MWCNTs. It only shows a notable change corresponding to 1.0wt% doped sample at 50 Hz. With increase in frequency, doping with MWCNTs does not seem to have any impact on the dielectric constant. [Fig. 4.15 (c, d)].

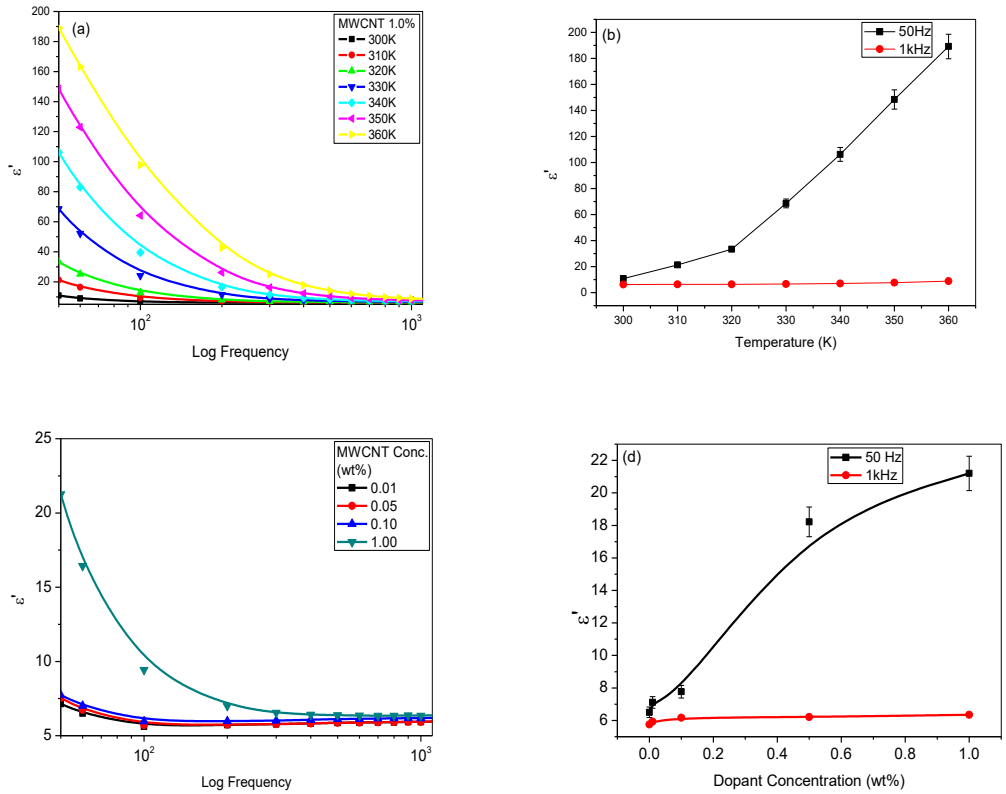

Figure 4.15: Effect of (a, b) Temperature (c, d) Dopant concentration on dielectric permittivity of MWCNT-doped samples.

4.2.7 Measurement of Optical Hysteresis through Transmission Studies: Microphotographs in Fig. 4.16 show the electric field induced director orientation of the undoped and doped samples. It reveals that after the withdrawal of once applied field, the undoped chiral system completely regains its original morphology through a mechanical rotation. The microtextures corresponding to CNTs doped samples exhibit the formation of field responsive anisotropic domains which persist even in the field-OFF state [Fig. 4.16 (a-f)]. Samples do not relax back for days of observation. They do so only after reheating the samples to high temperatures of the order of 75-100^{0}C. We further noted that temperature at which the samples regain their original morphology increases with increase in dopant concentration [Fig. 4.16 (g-i)].

The findings of the present study indicate that CNTs play an important role in changing the behavior of the sample. The COOH functionalized MWCNTs doping in induced CLCs has

altered the morphological and electro-optic switching behaviour of liquid crystal host material. A uniform dispersal of CNTs was ensured through attachment of

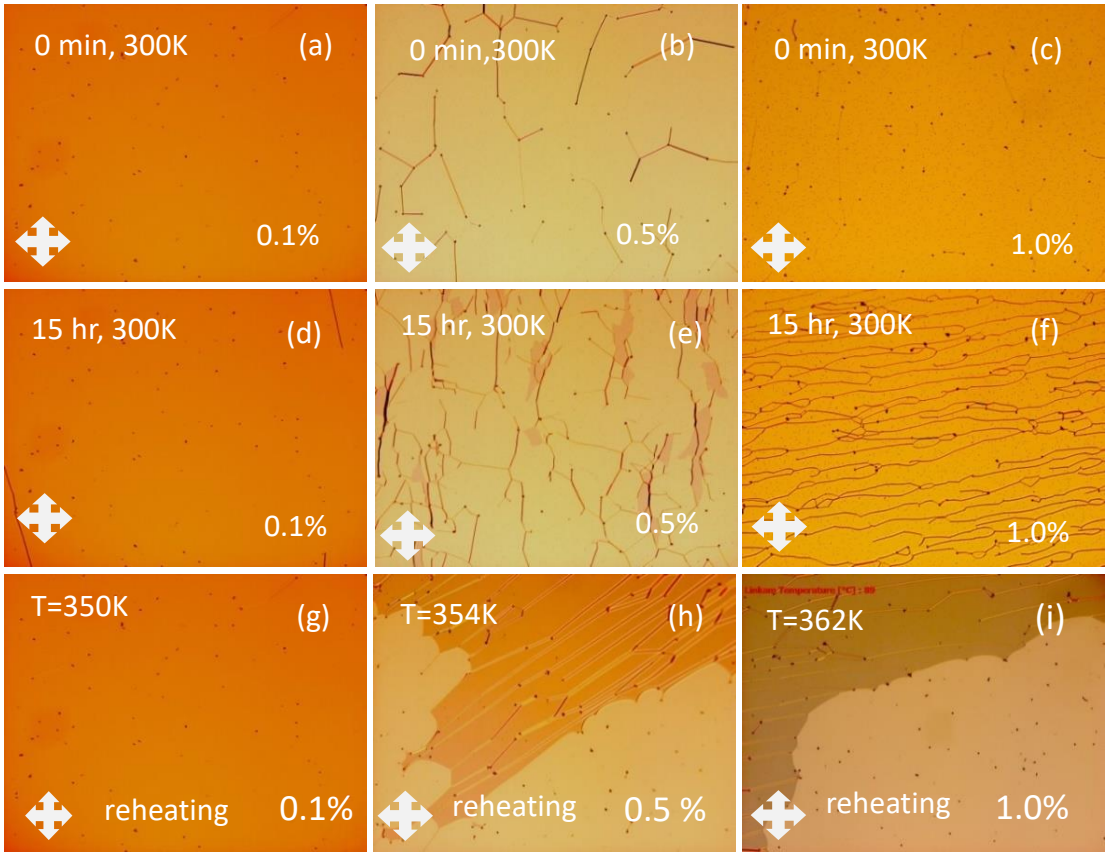

Figure 4.16: Illustration of memory effects in the doped samples through optical textures.

functional group. It was observed that CNT doping could significantly reduce the threshold electric field for Freedericksz transition and has potentially improved the optical anisotropy and dielectric properties of the material. The PL spectroscopy has established that besides being good absorbers (MWCNTs), the CNTs tend to stabilize the LC matrix and enhance its electro-optic memory.

Equipped with these properties, MWCNT doped LCs can be of potential use for fabrication of switching devices and owing to the optical hysteresis displayed by them, they can also be used in optical memory devices.

References:

1. Joshi T, Kumar A, Prakash J, Biradar AM. Low power operation of ferroelectric liquid crystal system dispersed with zinc oxide nanoparticles. Appl. Phys. Lett. 2010;96:5–7.

2. Lee WK, Choi JH, Na HJ, Lim JH, Han JM, Hwang JY. Low-power operation of vertically aligned liquid-crystal system via anatase-TiO(2) nanoparticle dispersion. Opt. Lett. 2009;34:3653–5.

3. Kumar A, Biradar AM. Effect of cadmium telluride quantum dots on the dielectric and electro-optical properties of ferroelectric liquid crystals. Phys. Rev. E - Stat. Nonlinear, Soft Matter Phys. 2011;83.

4. Joshi T, Kumar A, Prakash J, Biradar AM, Taylor P. Low frequency dielectric relaxations of gold nanoparticles/ferroelectric liquid crystal composites. Liq. Cryst. 2010;37:1433–8.

5. Hegmann T, Qi H, Marx VM. Nanoparticles in liquid crystals: Synthesis, self-assembly, defect formation and potential applications. J. Inorg. Organomet. Polym. Mater. 2007;17:483–508.

6. Kumar R, Raina KK. Morphological control and switchable photoluminescence responses of silica nanoparticles-modified polymer-dispersed liquid crystal composite films. Liq. Cryst. 2015;42:119–26.

7. Neeraj, Raina KK. Nickel nanoparticles doped ferroelectric liquid crystal composites. Opt. Mater. (Amst). 2013;35:531–5.

8. Woltman SJ, Jay GD, Crawford GP. Liquid-crystal materials find a new order in biomedical applications. Nat. Mater. 2007;6:929–38.

9. Ponevchinsky VV, Goncharuk AI, Denisenko VG, Lebovka NI, Lisetski LN, Nesterenko MI. LC nanocomposites: induced optical singularities, managed nano/micro structure, and electrical conductivity.1303.0560. 2013;1–10.

10. Lim YJ, Bhattacharyya SS, Tie W, Park HR, Lee YH, Lee SH. Effects of carbon nanotubes on electro-optic characteristics in vertically aligned liquid crystal display. Liq.

Cryst. 2013;40:1202–8.

11. Dolgov L, Yaroshchuk O, Lebovka M. Effect of electro-optical memory in liquid crystals doped with carbon nanotubes. Mol. Cryst. Liq. Cryst. 2008;496:212–29.

12. Shukla RK, Raina KK, Hamplová V, Kašpar M, Bubnov A. Dielectric behaviour of the composite system: Multiwall carbon nanotubes dispersed in ferroelectric liquid crystal. Phase Transitions. 2011;84:850–7.

13. Dolgov L, Yaroshchuk O, Tomylko S, Lebovka N. Electro-optical memory of a nematic liquid crystal doped by multi-walled carbon nanotubes. Condens. Matter Phys. 2012;15.

14. Gupta SK, Singh DP, Manohar R. SWCNT doped ferroelectric liquid crystal: The electro-optical properties with enhanced dipolar contribution. Curr. Appl. Phys. Elsevier B.V; 2013;13:684–7.

15. Huang CY, Pan HC, Hsieh CT. Electrooptical properties of carbon nanotube doped twisted nematic liquid crystal cell. Jpn. J. Appl. Phys. 2006;45:6392–4.

16. Chang CK, Chiu SW, Kuo HL, Tang KT. Cholesteric liquid crystal-carbon nanotube hybrid architectures for gas detection. Appl. Phys. Lett. 2012;100.

17. Lee W, Wang CY, Shih YC. Effects of carbon nanosolids on the electro-optical properties of a twisted nematic liquid-crystal host. Appl. Phys. Lett. 2004;85:513–5.

18. Ma PC, Siddiqui NA, Marom G, Kim JK. Dispersion and functionalization of carbon nanotubes for polymer-based nanocomposites: A review. Compos. Part A Appl. Sci. Manuf. 2010;41:1345–67.

19. Liu CX, Choi JW. Improved Dispersion of Carbon Nanotubes in Polymers at High Concentrations. Nanomaterials. 2012;2:329–47.

20. Manjuladevi V, Kumar J, Gupta RK. Functionalized cnt and liquid crystals. 2012;2:30–5.

21. Neeraj, Raina KK. Multiwall carbon nanotubes doped ferroelectric liquid crystal composites: A study of modified electrical behavior. Phys. B Condens. Matter. Elsevier;

2014;434:1–6.

22. Cheng HKF, Basu T, Sahoo NG, Li L, Chan SH. Current advances in the carbon nanotube/thermotropic main-chain liquid crystalline polymer nanocomposites and their blends. Polymers (Basel). 2012;4:889–912.

23. Manjuladevi V, Gupta RK, Kumar S. Effect of functionalized carbon nanotube on electro-optic and dielectric properties of a liquid crystal. J. Mol. Liq. 2012;171:60–3.

24. Middha M, Kumar R, Raina KK. Memory effects in chiral nematic liquid crystals doped with functionalised single-walled carbon nanotubes. Liq. Cryst. 2015;42:1028–35.

25. Kaur R, Raina KK. Influence of single-wall carbon nanotubes on Langmuir-Blodgett films of ferroelectric liquid crystals as studied by atomic force microscopy. Liq. Cryst. 2014;41:1065–72.

26. Yu JG, Huang KL, Liu SQ, Tang JC. Preparation and characterization of soluble methyl-β-cyclodextrin functionalized single-walled carbon nanotubes. Phys. E Low-dimensional Syst. Nanostructures. 2008;40:689–92.

27. Kumar R, Raina KK. Enhanced ordering in polymer stabilised ferroelectric liquid crystal guest-host composites: evidence by polarised fluorescence spectroscopy. Liq. Cryst. 2014;41:694–700.

28. Lu SY, Chien LC. Carbon nanotube doped liquid crystal OCB cells: physical and electro-optical properties. Opt. Express. 2008;16:12777–85.

29. Schymura S, Scalia G. On the effect of carbon nanotubes on properties of liquid crystals On the effect of carbon nanotubes on properties of liquid crystals. RSA. 2013;

30. Malik P, Chaudhary A, Mehra R, Raina KK. Electro-optic, thermo-optic and dielectric responses of multiwalled carbon nanotube doped ferroelectric liquid crystal thin films. J. Mol. Liq. 2012;165:7–11.

31. Yaroshchuk O, Tomylko S, Gvozdovskyy I, Yamaguchi R. Cholesteric liquid crystal-carbon nanotube composites with photo-settable reversible and memory electro-optic

modes. Appl. Opt. 2013;52:E53–9.

32. Basu R, Iannacchione GS. Nematic anchoring on carbon nanotubes. Appl. Phys. Lett. 2009;95.

33. Lynch MD, Patrick DL. Organizing carbon nanotubes with liquid crystals. Nano Lett. 2002;2:1197–201.

34. Dierking I, Scalia G, Morales P. Liquid crystal-carbon nanotube dispersions. J. Appl. Phys. 2005;97.

35. Rahman M, Lee W. Scientific duo of carbon nanotubes and nematic liquid crystals. J. Phys. D. Appl. Phys. 2009;42:063001.

36. Scalia G. Alignment of carbon nanotubes in thermotropic and lyotropic liquid crystals. ChemPhysChem. 2010;11:333–40.

37. Puech N, Blanc C, Grelet E, Zamora-Ledezma C, Maugey M, Zakri C. Highly ordered carbon nanotube nematic liquid crystals. J. Phys. Chem. C. 2011;115:3272–8.

38. Schymura S, Kühnast M, Lutz V, Jagiella S, Dettlaff-Weglikowska U, Roth S. Towards efficient dispersion of carbon nanotubes in thermotropic liquid crystals. Adv. Funct. Mater. 2010;20:3350–7.

39. Ji Y, Huang YY, Terentjev EM. Dissolving and aligning carbon nanotubes in thermotropic liquid crystals. Langmuir. 2011;27:13254–60.

40. Vimal T, Pandey S, Gupta SK, Singh DP, Manohar R. Enhanced negative dielectric anisotropy and high electrical conductivity of the SWCNT doped nematic liquid crystalline material. J. Mol. Liq. 2015;204:21–6.

41. Middha M, Kumar R, Raina KK. Improved electro-optical response of induced chiral nematic liquid crystal doped with multi-walled carbon nanotubes. Ferroelectrics. 2016;495:75–86.

42. García-García A, Vergaz R, Algorri JF, Quintana X, Otón JM. Electrical response of liquid crystal cells doped with multi-walled carbon nanotubes. Beilstein J. Nanotechnol.

2015;6:396–403.

43. Qi H, Hegmann T. Impact of nanoscale particles and carbon nanotubes on current and future generations of liquid crystal displays. J. Mater. Chem. 2008;18:3288.

44. Chen HY, Lee W, Clark NA. Faster electro-optical response characteristics of a carbon-nanotube-nematic suspension. Appl. Phys. Lett. 2007;90.

45. Malik P, Chaudhary A, Mehra R, Raina KK. Dielectric studies and memory effect in nanoparticle doped ferroelectric liquid crystal films. Mol. Cryst. Liq. Cryst. 2011;541:243/[481] – 251/[489].

46. Weiss V, Thiruvengadathan R, Regev O. Preparation and characterization of a carbon nanotube-lyotropic liquid crystal composite. Langmuir. 2006;22:854–6.

47. Lagerwall JPF, Scalia G. Carbon nanotubes in liquid crystals. J. Mat. Chem. 2008;18:2890–8.

48. Podgornov FV, Suvorova AM, Lapanik AV, Haase W. Electrooptic and dielectric properties of ferroelectric liquid crystal/single walled carbon nanotubes dispersions confined in thin cells. Chem. Phys. Lett. 2009;479:206–10.

49. Prakash J, Choudhary A, Mehta DS, Biradar AM. Effect of carbon nanotubes on response time of ferroelectric liquid crystals. Phys. Rev. E - Stat. Nonlinear, Soft Matter Phys. 2009;80.

50. Malik A, Prakash J, Kumar A, Dhar A, Biradar AM. Copper oxide decorated multi-walled carbon nanotubes/ferroelectric liquid crystal composites for faster display devices. J. Appl. Phys. 2012.

51. Stauffer D, Aharony A. Introduction to Percolation Theory. Taylor Fr. 1991;192.

52. Mamunya YEP, Lebovka NI, Lisunova MO, Lebedev EV, Rybak A, Boiteux G. Conductive polymer composites with ultralow percolation threshold containing carbon nanotubes. J. Nanostructured Polym. Nanocomposites. 2008;4:21–7.

53. Koval A, Dolgov L, Yaroshchuk O. Dielectric studies of dispersions of carbon

nanotubes in liquid crystals 5CB. Quantum Electron. 2008;337–41.

54. Lisetski LN, Minenko SS, Fedoryako AP, Lebovka NI. Dispersions of multiwalled carbon nanotubes in different nematic mesogens: The study of optical transmittance and electrical conductivity. Phys. E Low-Dimensional Syst. Nanostructures. 2009;41:431–5.

55. Ponevchinsky VV, Goncharuk AI, Vasil'ev VI, Lebovka NI, Soskin MS. Cluster self-organization of nanotubes in a nematic phase: The percolation behavior and appearance of optical singularities. JETP Lett. 2010;91:241–4.

56. Gharde RA, Thakare SY. Effects of Concentration of Multiwall Carbon Nanotube on Cholesteric Liquid Crystal. 2015;4:68–74.

57. Malik P, Raina KK, Bubnov A, Prakash C. Dielectric spectroscopy of a high-polarization ferroelectric liquid crystal. Phase Transitions. 2006;79:889–98.

58. Kato T, Mizoshita N, Kishimoto K. Functional liquid-crystalline assemblies: Self-organized soft materials. Angew. Chemie - Int. Ed. 2005. p. 38–68.

59. Furumi S. Self-assembled organic and polymer photonic crystals for laser applications. Polym. J. 2012;45:579–93.

60. Hernández RJ, Mazzulla A, Pane A, Volke-Sepúlveda K, Cipparrone G. Attractive-repulsive dynamics on light-responsive chiral microparticles induced by polarized tweezers. Lab Chip. 2013;13:459–67.

61. Dierking I. Chiral liquid crystals: structures, phases, effects. Symmetry (Basel). 2014;6:444–72.

62. Atkuri H, Cook G, Evans DR, Cheon CI, Glushchenko A, Reshetnyak V. Preparation of ferroelectric nanoparticles for their use in liquid crystalline colloids. J. Opt. A Pure Appl. Opt. 2009;11:024006.

63. Dhar R, Pandey AS, Pandey MB, Kumar S, Dabrowski R. Optimization of the display parameters of a room temperature twisted nematic display material by doping single-wall carbon nanotubes. Appl. Phys. Express. 2008;1:1215011–3.

64. Khushboo, Jayoti D, Malik P, Chaudhary A, Mehra R, Raina KK. Properties of ferroelectric liquid crystal/multiwall carbon nanotube doped composite. Integr. Ferroelectr. 2014;158:123–30.

CHAPTER 5

EFFECTS OF NANOPARTICLES DOPING IN CHIRAL NEMATIC LIQUID CRYSTALS

Overview

The first part of this chapter comprises of two studies. The first is about the effects of varying concentration of silver nanoparticles on the properties of CLC matrix and the second includes results of doping an equal amount of silver nanoparticles on nematic and chiral matrices confined under same boundary conditions.

In the second part, study of the effects of functionalized Aluminum-doped ZnO nanoparticles doping on the optical and electro-Optical behaviour of a CLC have been discussed.

Electrically induced Optical hysteresis and enhanced photoluminescence were observed in the samples doped with Dodecanethiol functionalized silver nanoparticles, which virtually vamooses at 0.020wt% dopant concentration. We have recorded an uptrend of enhancement in emission peak intensity till 0.015wt% dopant concentration above which, we noticed a fall in the peak intensity. We also detected a significant shift in the peak position with chiral dopant concentration.

Another study reveals the Impact of chirality on nematic liquid crystal matrix doped with Dodecanethiol-capped silver nanoparticles (AgNPs). The temperature dependent morphological behaviour of both: the doped NLC and CLC was investigated by polarized optical microscopy. We recorded lowering of the threshold of Freedericksz transition and about a tenfold rise in dielectric constant of CLC samples with rising temperature. We also observed a pronounced surge in photoluminescence in addition to an irreversible memory in the chiral medium.

Emergence of optical hysteresis and enhanced photoluminescence was observed in chiral medium dispersed with functionalized Aluminum-doped ZnO nanoparticles. We recorded lowering of the threshold for Freedericksz transition and a nearly tenfold rise in dielectric

constant with temperature. An irreversible memory in the doped chiral medium was measured with transmission studies.

PHOTOLUMINESCENCE TUNING AND ELECTRO-OPTICAL MEMORY IN CHIRAL NEMATIC LIQUID CRYSTALS DOPED WITH SILVER NANOPARTICLES

In recent years, there is an immense growth in research activities in the field of ‘active plasmonics’ by nanofabrication in liquid crystal (LC) materials [1–5]. The emerging field, known as ‘nanophotonics,' is a meaningful amalgamation of the functionality and versatility of soft matter and the optoelectronic properties of nanoparticles. The incorporation of nanostructures in liquid crystals has opened up new perspectives for the evolution of plasmonic devices with enhanced performance [6,7]. Kumar et al. have reported ninefold enhancement in photoluminescence (PL) intensity of gold NP-doped in deformed helix ferroelectric liquid crystals (DHFLC) [8]. A build-up of luminescence intensity following the doping of metal nanoparticles in polymers, dye molecules, and ferroelectric liquid crystals (FLCs) has been observed and widely reported [9–11].

Popov et al. [12] suggested that photon scattering, which is responsible for random lasing in Rh6G dye-doped LC laser, is enhanced by surface plasmons generated by active gold nanoparticles. Pratibha et al. [13] explained the polarization-sensitive surface plasmon resonance and corresponding red-shift in liquid crystal matrix with concentration of gold nanospheres, by the Maxwell-Garnet effective medium theory. Caputo et al. [14] reported vehement influence of gold NPs doping in chiral liquid crystal (CLC), on the position of plasmonic absorption peak, leading to a broad tunability with temperature, in the presence of external electric fields. Hung et al. reported an enhancement of optical diffraction due to silver nanoparticles induced surface plasmon resonance (SPR) in CLCs [15]. Enhanced photoluminescence leading to an augmentation of excitation and emission rate of liquid crystal molecules due to localized electromagnetic fields in silver nanoparticle doped nematic liquid crystals, graphene quantum dots doped FLC molecules, and AgNP doped RHO6G dye has additionally been reported [16–19]. Middha et al. observed improved ordering due to self-organization of single walled carbon nanotubes in CLC matrix leading to enhanced photoluminescence [20]. Many researchers have reported emergence of memory in NLCs and FLCs doped with nanoparticles. Yoshida et al. have reported stabilization of blue phase and elongation of the pitch of a chiral medium doped with gold

nanoparticles [21]. Parkash et al. have reported non-volatile memory effect based on a gold nanoparticle-doped deformed helix ferroelectric liquid crystal DHFLC [22]. They have attributed the observed memory effect to the electric field induced interaction of molecular polarization of LC mesogens with gold nanoparticles. There are reports of induction of an irreversible memory as a result of adding an optimum concentration of CdTe quantum dots in FLC (LAHS19) [23]. We have also reported the emergence of memory in due to carbon nanotubes doped CLCs in our earlier works [20,24]. Podoliak et al. observed a high optical nonlinearity in nematic liquid crystals doped with TOAB-coated gold nanoparticles [25].

Although a lot of work has been done in this field, not much has been reported on the effect of silver nanoparticles doping on optical and electro-optical properties of chiral nematic liquid crystals [26]. The purpose of this work was to investigate the comportment of dodecanethiol (DDT)-functionalized silver nanoparticles in soft, super helical structures of induced CLCs and report the emerging optical, morphological and switching behaviour.

5.1 Sample Characterization

For the present study, we used Dodecanethiol (DDT) functionalized silver nanoparticles of size 5-15nm, obtained from Sigma-Aldrich as a dopant in the host chiral nematic matrix. We prepared the doped CLC composites by dispersing 0.005, 0.010, 0.015 and 0.020wt% of DDT-functionalized silver nanoparticles into the induced CLC mixture followed by ultrasonication for about one hour. The composites, at their isotropic temperature, were filled in LC cells as per the procedure described in Chapter 2.

5.1.1 Morphological Analysis: Figure 5.1 depicts the optical textures exhibited by Ag nanoparticles dispersions in chiral nematic phase of a liquid crystal mixture under crossed polarizers of a polarized optical microscope fixed at 100X magnification. Planar Grandjean texture in [Fig. 5.1 (a)] characterizes an uninterrupted helical structure in the undoped sample. The helical pitch is related to the reflected colour as $\lambda = np$, where symbols have their meaning as mentioned in section 4.1.2. The optical textures of doped samples with 0.005 to 0.015wt% AgNP concentration, are marked by defects and a change in colour which indicates that silver doping has modified the symmetry of helical structure and deformed its pitch [Fig. 5.1 (b-d)].

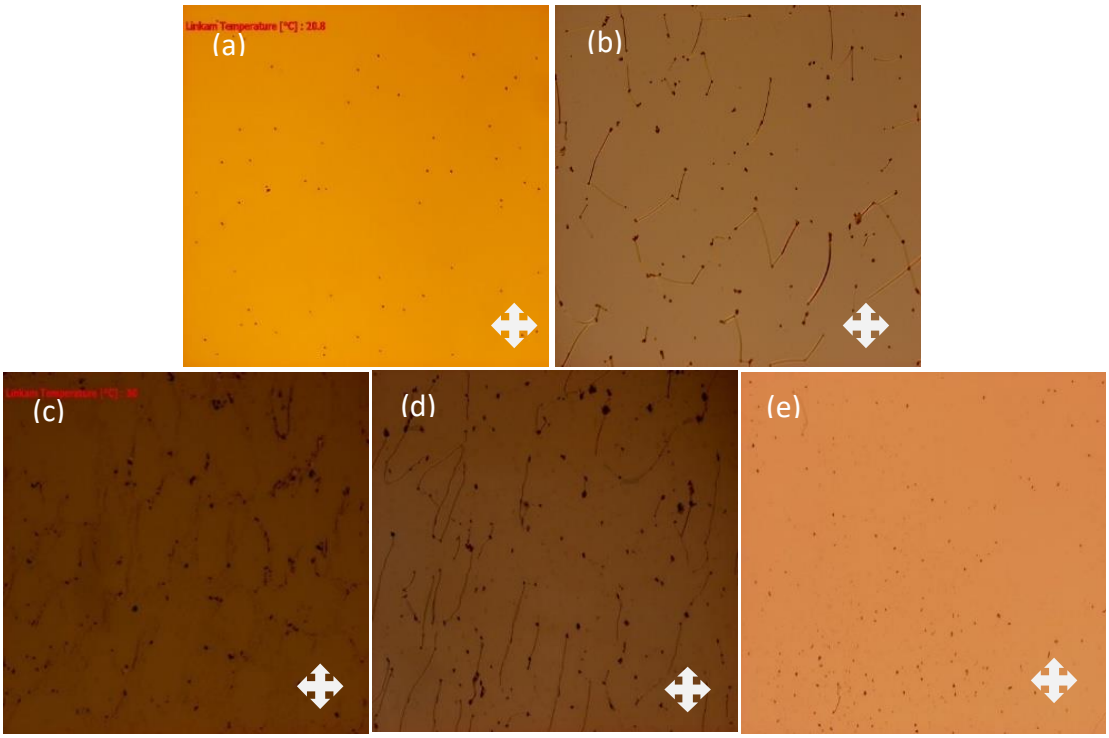

Figure 5.1: Optical micrographs of the scattering state of freshly doped CLCIII with increasing concentration of silver NPs (a) Undoped (b) 0.005 (c) 0.010 (d) 0.015 (e) 0.020wt%, before the application of bias.

With further increase in concentration of nanoparticles to 0.020wt%, we observed a change in color of the texture and disappearance of disclinations indicating the decreased effect of AgNPs, possibly because they have started agglomerating at this concentration. [Fig. 5.1(e)] The thermo-optical behavior of the samples was investigated by heating them to their isotropic temperature at a constant rate of 1K/minute and then cooling to room temperature at the same rate. Thermo-optical hysteresis was noticed from the morphology which, we believe is a result of competition between the planar surface anchoring forces of the cell surfaces and thermo-elastic forces induced in the helical structure.

Figure 5.2 (a-e) shows the microtextures at room temperature taken about 24 hours after the withdrawal of externally applied square wave ac electric field of magnitude 6V/µm. These microphotographs show the emergence of electro-optical memory in AgNPs doped samples. A close look at them reveals that the samples did not return to their original form even after a daylong observation. The prima facie genesis of the induced memory is the incapability

of helical superstructures to completely rewind after the withdrawal of the field due to the presence of AgNPs in the matrix [21].

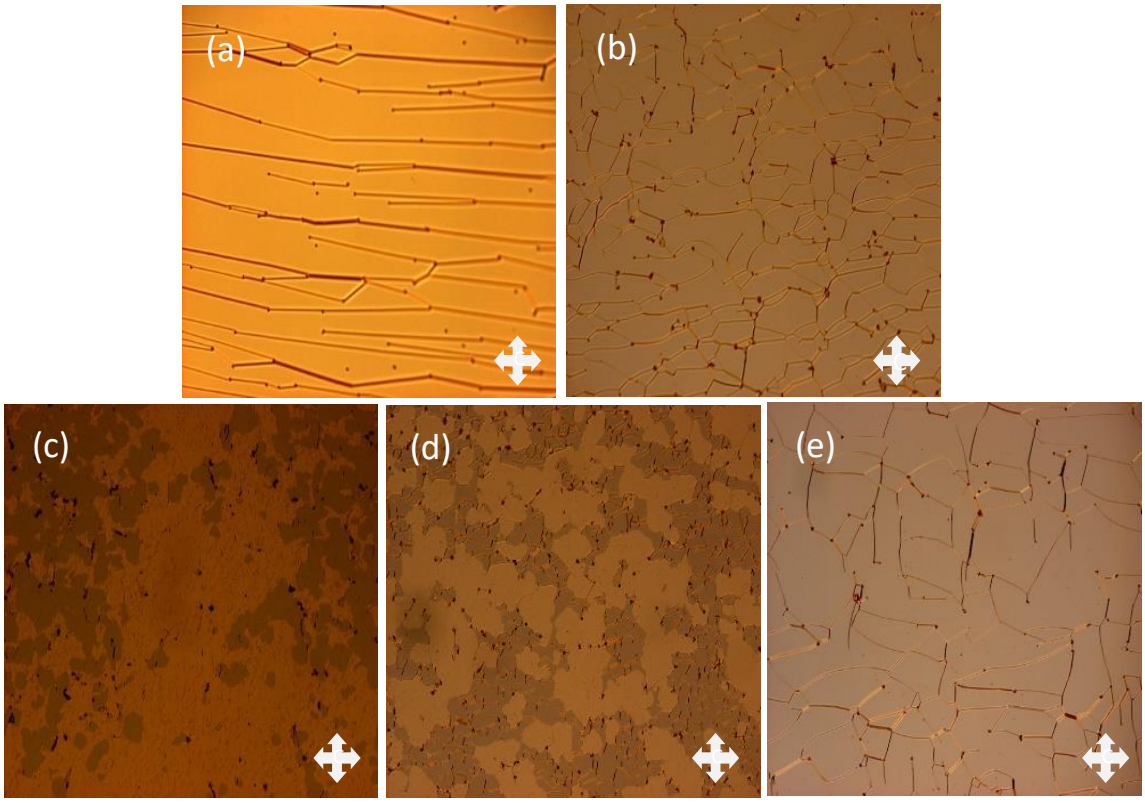

Figure 5.2: Optical textures of electrically induced memory effects after the withdrawal of electric field in the doped CLCIII samples with increasing concentration (a) Undoped CLCIII (b) 0.005 (c) 0.010 (d) 0.015 (e) 0.020 wt% of silver NPs.

The silver nanoparticles trapped in the defects of doped matrix had apparently reduced the free energy and stabilized the orientation state of the doped matrix [22,23]. The memory stored in these deformed helices is permanent in nature. The observations were repeated even after a period of ten days. The observed hysteresis was measured and subsequently confirmed by photoluminescence measurements.

5.1.2 Photoluminescence Studies: We recorded the PL spectrum of Dodecanethiol-capped silver nanoparticles before dispersing them into the chiral nematic liquid crystal mixture. The maximum PL intensity emission peak was positioned at 403nm [Fig. 5.3(a)]. PL excitation spectrum of undoped and doped samples was recorded by using fluorescence spectrophotometry. The basic parameters of slit width, excitation step, etc. were kept

constant for all the samples. We found that the doped sample has the absorption peak at 350nm. We, thus performed photo-induced luminescence of the doped samples for 350nm excitation wavelength. The photoluminescence spectrum of undoped chiral liquid crystals was recorded from 380nm to 550nm.

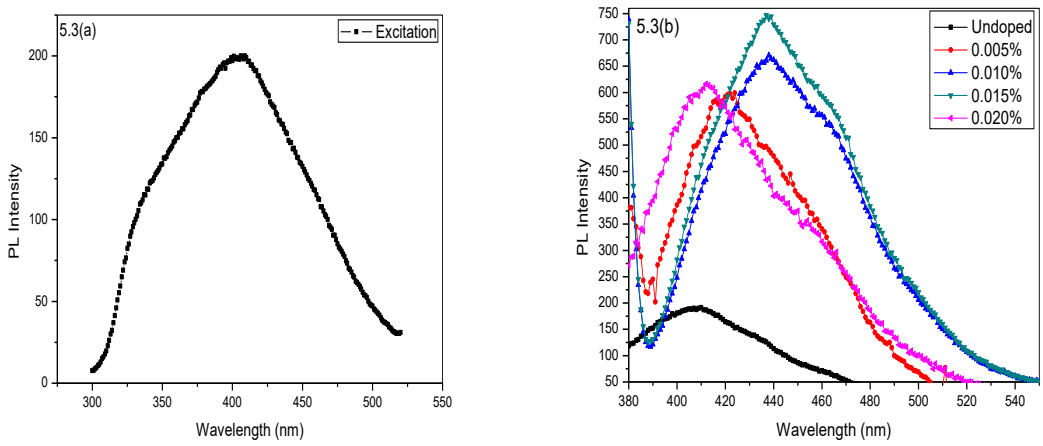

Figure 5.3: Photoluminescence spectra of (a) functionalized silver nanoparticles (b) Silver nanoparticles-doped CLCIII samples for various dopant Concentrations.

We located the peak position on the emission spectrum of undoped chiral medium at 407nm. In a quest to investigate the effect of silver nanoparticles on the photoluminescence of chiral liquid crystals, we recorded photoluminescence spectra of chiral liquid crystals doped with various concentrations of silver nanoparticles for the same range of wavelengths [Fig. 5.3(b)].

Table 5.1. Photoluminescence Response of Undoped and Doped CLC samples for various concentrations of silver nanoparticles.

Silver Nanoparticle Concentration (wt%)	Excitation Wavelength (nm)	Maximum Emission Wavelength (nm)	PL Intensity
UNDOPED	318	407	190
0.005	350	422	597

0.010	350	437	668
0.015	350	438	746
0.020	350	413	615

The shape of the photoluminescence spectra of doped chiral liquid crystals in the presence of silver nanoparticles hints of the well-organization of silver nanoparticles in CLC. As the concentration of dopant is increased from 0.005 to 0.015wt%, an increase in the Pl intensity is observed. Table 5.1 depicts the peak-intensity of photoluminescence as a function of concentration. Peak intensity reaches a maximum at 0.015wt% concentration and shows around threefold enhancement of intensity. We believe that enhancement of the peak PL intensity because of local surface plasmon resonance in the 0.005 to 0.015wt% concentration range. When light falls on spherical silver nanoparticles, the electron cloud inside the surface of metallic nanoparticles starts oscillating in harmony with electric field of the incident electromagnetic wave. This induced resonance is known as localized surface Plasmon resonance (SPR) [27,28]. This manifestation brings about an enhancement of the electromagnetic field on the surface of silver nanoparticles. The large optical fields generated by surface plasmons, increase the fluorescence intensity of doped chiral liquid crystal superstructures.

The local surface plasmon resonance effect, induced in chiral superstructures by silver nanoparticles becomes more pronounced with increase in concentration of silver nanoparticles from 0.005- 0.015wt%. The PL spectrum also shows a shifting (≈ 17 nm) of the peak towards higher wavelengths on addition of silver nanoparticles (AgNPs), and on increasing the concentration from 0.005 to 0.015wt% [Table 5.1]. This can be because of lengthening of the pitch due to the presence of nanoparticles; as reported earlier in case of nanoparticle-doped CLCs by M. Mitov et al. [29]. With further increase in concentration of silver nanoparticles from 0.015 to 0.020wt%, a decline in the peak intensity was noticed. We believe that this decrease in PL intensity is because of the fractional energy transfer among the liquid crystal molecules and conglomerated silver nanoparticles [30,31].

5.1.3 Electro-optic Switching and Conductivity Analysis: We investigated the switching behaviour of Dodecanethiol-capped silver nanoparticles doped samples by applying a square wave pulse of magnitude 0-30V. As compared to undoped CLC, doped samples (0.015- 0.020wt%) exhibited almost double resistivity at 100Hz [Fig 5.4 (a)]. As reported in earlier studies, genesis of the observed fall in conductivity lies in the fact that functional group, by forming an organic layer around the surface of Agnps traps the positive and negative ions [32–34]. Due to this ion trapping by the molecules of capping agent, we observe a rise in resistivity. AgNPs have also shown their influence on the switching behavior of doped samples. We observed a lowering in the threshold voltage required to bring about Freedericksz transition in Ag-doped CLC samples [Fig. 5.4(b)].

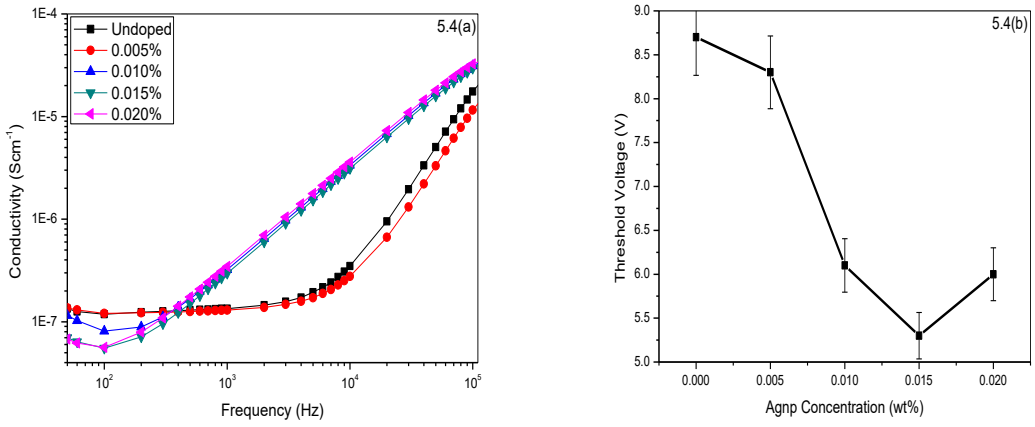

Figure 5.4: Plot of (a) ac conductivity versus frequency (b) threshold voltage at 50 Hz, for various concentrations of silver nanoparticles.

We believe that the following two phenomena are responsible for the observed downtrend. Firstly, in the absence of applied field, the screening effect due to space charge formation is vanquished by ion capturing as explained earlier and secondly when field is applied, electric flux density is augmented in the vicinity of spherical silver nanoparticles. The increased density of flux around the metallic nanoparticles contributes to the increased effective field strength which helps cause the electric field induced switching and unwinding of helices in doped samples at a lower voltage.

5.1.4 Electro-optical Hysteresis: We analyzed the PL emission spectrum of Ag-doped CLC samples subjected to a stepwise increase in alternating electric field ranging from 0V/μm to 6V/μm and back to 0V/μm. The histogram in Fig. 5.5 (a) reveals that emission spectrum of the undoped and doped samples are voltage dependent, and the peak intensity of all the samples gets modified by changing applied voltage. In addition to this, we observed switching behaviour of the samples in PL intensity profile. Until the switching voltage is reached (which is different for every sample), PL intensity remains almost constant. On increasing the applied voltage above the threshold, PL intensity increases further till the phase change continues. Once the sample goes homotropic, intensity remains constant. We observed that in this state when applied voltage was switched off, Pl intensity did not attain its previous value. We repeated the observations after 24 hours of withdrawal of electric field and plotted

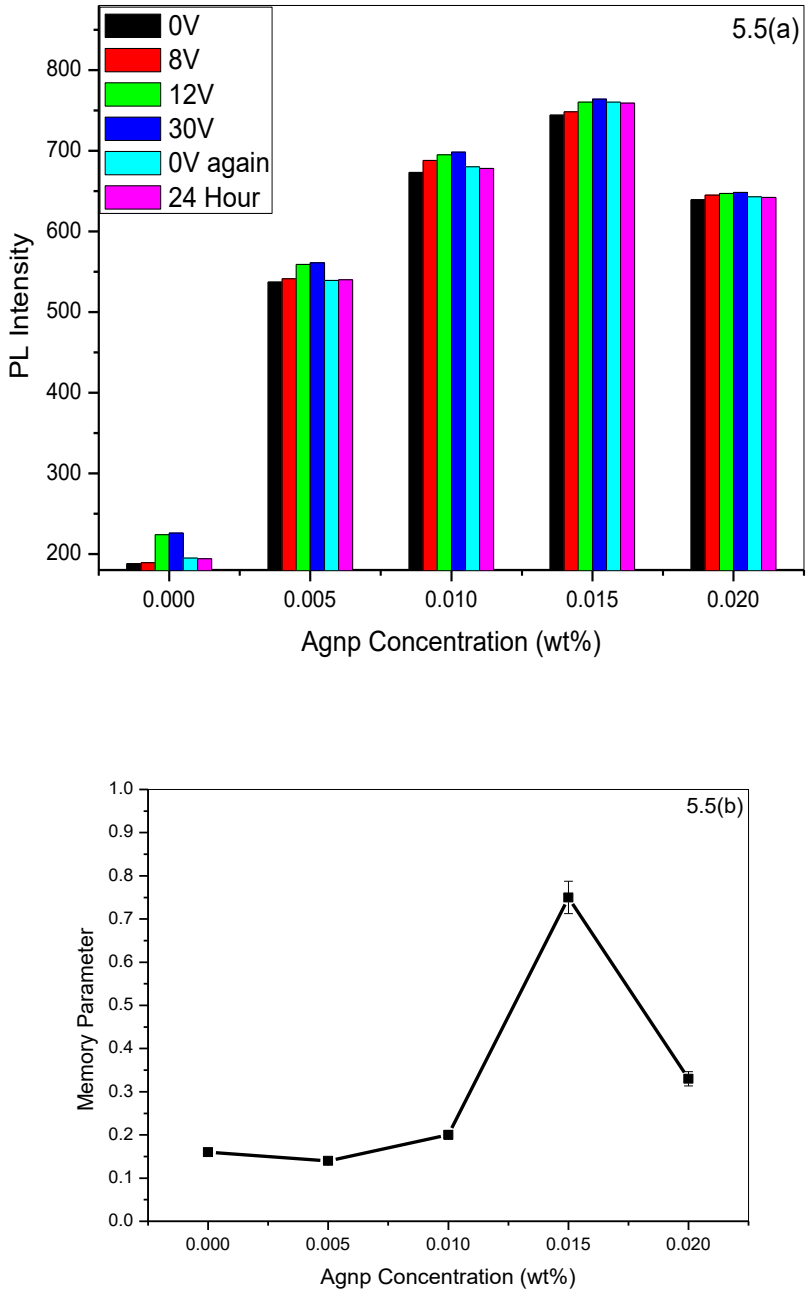

Figure 5.5: (a) PL response of silver nanoparticle-doped CLC with the application and withdrawal of ac electric field (b) Variation of the memory parameter as a function of dopant concentration.

Them as memory parameter vs. dopant concentration graph [Fig. 5.5(b)]. We calculated the memory parameter as

$$Memory\ Parameter = \frac{I_{final} - I_{initial}}{I_{max} - I_{initial}} \qquad \text{.....(5.1)}$$

The observation of such memory effect in case of silver nanoparticle doped CLC further endorses the presence of collective oscillations of an electronic cloud of metallic silver nanoparticles and electromagnetic field of the incident light wave. The abnormally high electric field is generated out of this interaction, which is capable enough to delay the relaxation of liquid crystal molecules back to the scattering state. This intrinsic field generated optical hysteresis increases with increase in concentration of silver nanoparticles from 0.005-0.015wt%.

We also believe that silver nanoparticles have organized themselves into the defects generated in chiral helical structure in such a way that their presence stabilizes the medium [20]. Because of this, helical symmetry of the doped matrix gets deformed, and the process of relaxation of molecules is slowed. The LC molecules are left impuissant to attain the original configuration. In case of higher concentration (0.020%), the decline in these exclusive properties like lower switching threshold and the memory parameter, endorse the formation of agglomerates of silver nanoparticles at this concentration.

We, thus conclude that the photoluminescence behaviour of a chiral liquid crystal has successfully been modulated by adding different concentrations of silver nanoparticles into them. The 0.005-0.020wt% of AgNPs doped composites show the complete organization of silver nanoparticles in the liquid crystal matrix. Because of the perfect self-organization of silver nanoparticles in CLC matrix, the tuning of luminescence properties of chiral liquid crystal was possible.

The organization of silver nanoparticles into CLC also brings hysteresis in the doped sample cells. The enhanced intrinsic field created by silver NPs in the presence of incident em wave contributed to the improved electro-optical response and a strong memory effect in the doped matrices. Improved electro-optical response in the form of reduced threshold voltage and better optical contrast, ensure the plausible use of this nanocomposite as a tunable

optical functional material with electro-optical memory. Noticeable improvement in the properties of silver doped chiral nematic liquid crystal material has ensured striking appositeness of the composite for its plausible use in the fabrication of memory and high contrast display devices.

EFFECT OF CHIRALITY ON OPTICAL AND ELECTRO-OPTIC BEHAVIOUR OF NEMATIC LIQUID CRYSTALS DOPED WITH FUNCTIONALIZED SILVER NANOPARTICLES

Chirality in Liquid Crystals is an interesting phenomenon with a prospective to induce new phases and textures like Blue phase, TGB phase, Focal conic texture and many others with helical ordering [35]. The sensitivity of the cholesteric pitch to external provocations brings versatility in chiral phases. Nanoparticle induction in chiral media has resulted in a prominent number of effects leading to improvisation and fabrication of new devices of display market and biomedical use. The optimum dispersion of chiral mesogens in nematic liquid crystals (NLC) brings about significant improvement in its properties. Their improvised behaviour makes them suitable for developing new optical devices [36,37]. Owing to the tremendous applicability and relatively simple structure of nematic liquid crystals, nanoparticle doping was previously done in nematic liquid crystals only. Recently cholesteric liquid crystals (CLC) are also being used for doping of NPs. Doped CLCs showed improvements in optical response and driving voltage [38]. There are many reports of distinctive effects because of induction of nanoparticles in chiral liquid crystals, some of which were rarely seen in nematics. Stabilization of blue phase, augmentation of photoluminescence and emergence of reversible and irreversible memory are a few examples [21,26,39].

Although a lot of work has been done in the past decade in the field of nanoparticles doping in nematic and ferroelectric liquid crystals, a comparative study throwing a spotlight on the effects of introducing chirality in nanoparticle-doped achiral systems has been underexplored. Our motive behind carrying out the present piece of research was to explore the prospective and tenability of bringing helical symmetry in a nematic system composed of uniaxial anisotropic mesogens aligned along the director. It seemed engaging about how induced chiral mesogens, confined in a helical symmetry would respond to the interaction between electromagnetic field of the incident light wave and the surface plasmons generated by silver nanoparticles. A comparison of their behavior with less orderly nematic molecular organization under similar conditions was still more interesting to pursue.

We, in the present case, have doped an equal amount of Dodecanethiol functionalized silver nanoparticles (AgNPs) in nematic as well as induced chiral nematic liquid crystals and compared their morphological, optical, and electro-optic behavior.

5.2 Sample preparation and characterization

We prepared silver nanoparticle doped composites by dispersing 0.002wt% of silver nanoparticles (AgNPs) into nematic as well as chiral nematic mixtures. Pure and AgNP-doped LC mixtures were filled in the LC cells as per the procedure mentioned earlier in the second chapter.

5.2.1 Thermo-optical Studies through POM: We used a POM with crossed polarizers set at 100X magnification and attached to a temperature controlled hot stage to record micro textures of the sample cells while increasing their temperature till isotropic and cooling down to room temperature at a rate of 1K/min.

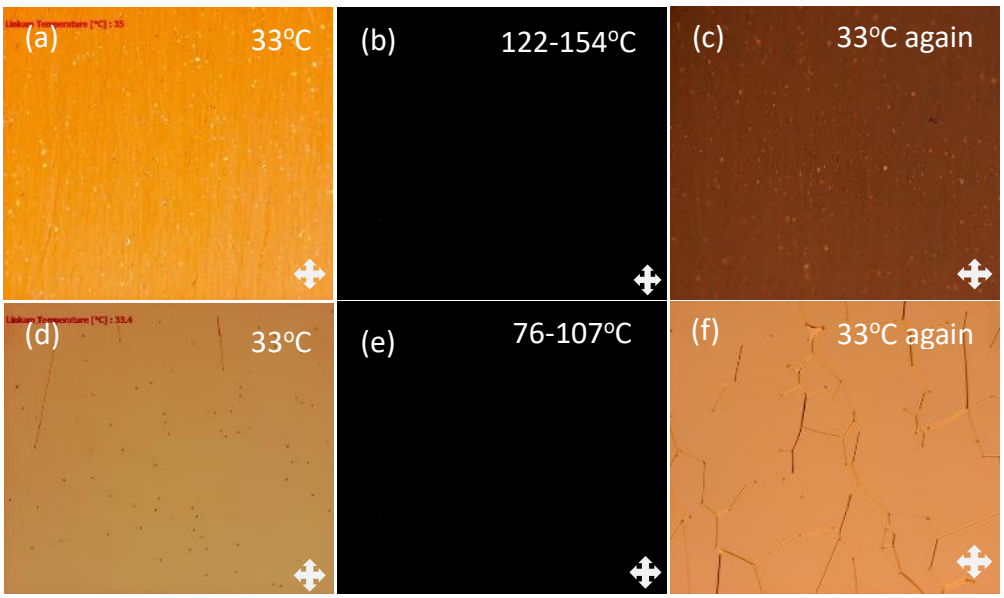

Figure 5.6: Phase transition of silver nanoparticles-doped (a,b,c) Nematic and (d,e,f) Chiral LCs with temperature.

The doping with AgNPs brings about visible colour changes in both; nematic as well as chiral matrices. In undoped samples, phase transition to isotropic takes place at a slightly (4°C) lower temperature in chiral nematic as compared to nematic. The difference increases

to 47°C with AgNPs doping [Fig. 5.6 a,b,d,e)]. The occurrence of phase transition at a lower temperature in doped CLC in comparison to doped NLC suggests that doping with AgNPs has brought in order in nematic system while they seem to have brought down the symmetry of the chiral medium.

A detailed look at figure 5.6 (c,f) reveals that while samples are being brought to room temperature, doped NLC completely regains its original configuration. Appearance of defects due to incomplete reorganization of molecules in the matrix of doped chiral sample, at the same time, confirms the deformed helical structure.

We believe that the observed thermo-optical hysteresis is due to the slowing down of the process of elastic rewinding of helices by the nanoparticles present in the matrix. The nanoparticles confined in the anchored surfaces, in the process of their self-organization within the helical arrangement end up stalling the elastic forces of the helical structure.

5.2.2 Electro-Optical Switching: Figure 5.7 (a,b,d,e) unveils the additament of nanoparticles by a decreased value of switching threshold for electro-optical transition in both nematic as well as chiral samples by approximately 25% [Table 5.2].

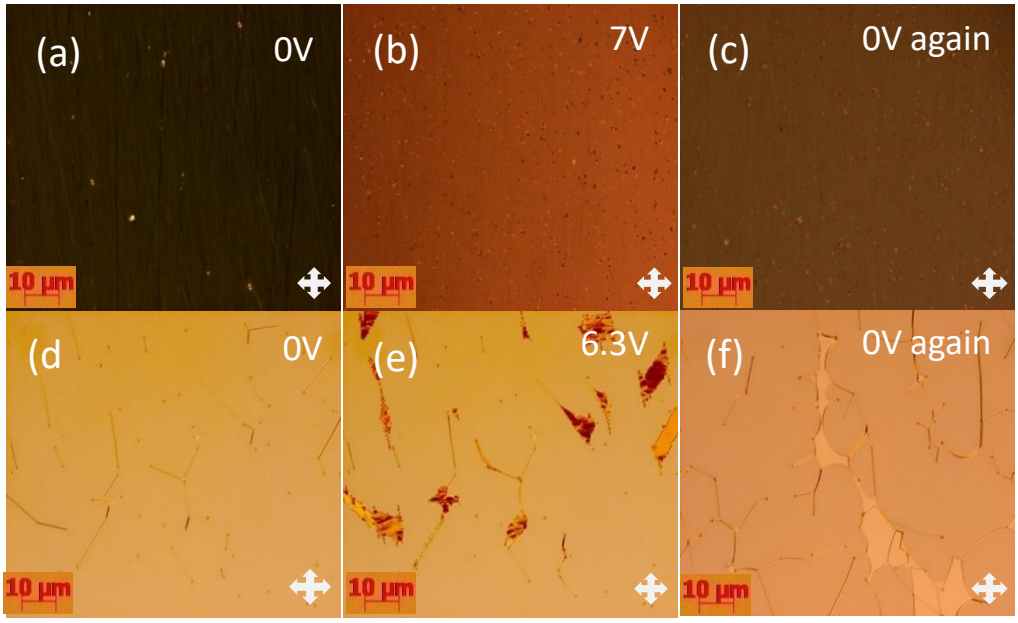

Figure 5.7 Freedericksz Transition in silver nanoparticles-doped (a,b,c) Nematic and (d,e,f) Chiral LCs.

Silver nanoparticles being metallic in nature, enhance the effect of applied field by trapping of ions in their vicinity. Many researchers have earlier reported presence of ions in LC cells results in the charge screening effect [33,40]. When such a cell is subjected to an external electric field, space charge separation of the matrix takes place, which lowers the effectiveness of applied field. Silver nanoparticles, by trapping of ions in their vicinity, polarize the liquid crystal molecules surrounding them. The process leads to an increase in the effectiveness of applied electric field and helps the switching to take place at a lower value [6,41].

Fig. 5.7 (c,f) depicts the emanation of electro-optic memory following AgNPs doping in chiral medium. Self-organization of silver nanoparticles in the defects has stabilized the orientational state of doped chiral matrix by reducing the free energy [42,43]. The memory stored in these deformed helices is of permanent nature and was present even after ten days of observation.

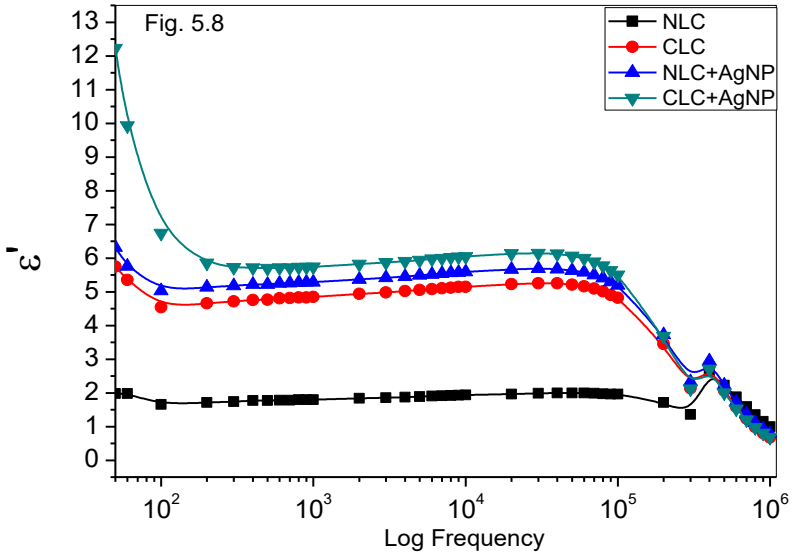

Figure 5.8: Variation of the dielectric constant of the undoped and silver nanoparticles-doped samples with applied electric field frequency.

5.2.3 Dielectric investigations: Fig. 5.8 shows the frequency (50 Hz to 100 kHz) response of dielectric permittivity at room temperature. Additament of AgNPs has brought about

200% increase in the dielectric constant of NLC and 100% increase in CLC (at 60Hz). The enhancement was observed for relatively low frequencies only while in the higher frequency range (≥ 1kHz), doped samples did not show any notable change.

We believe that this type of frequency dependent behavior is due to the ionic conductivity or low frequency dielectric dispersion. At low frequency, dipoles can follow the oscillations of applied field while at higher frequencies, ionic conductivity loses its significance [46]. After the application of electric field, polarization takes some time to build up and ε' decreases with increasing frequency. The increase can also be due to the fact that organization of AgNPs in LC matrix is such that the dipole moment of nanoparticles adds to the dipole moment of liquid crystal molecules [47]. Moreover, presence of charges at the nanoparticle-LC molecular interface causes overall enhancement of the polarization of matrix which leads to higher dipole moment.

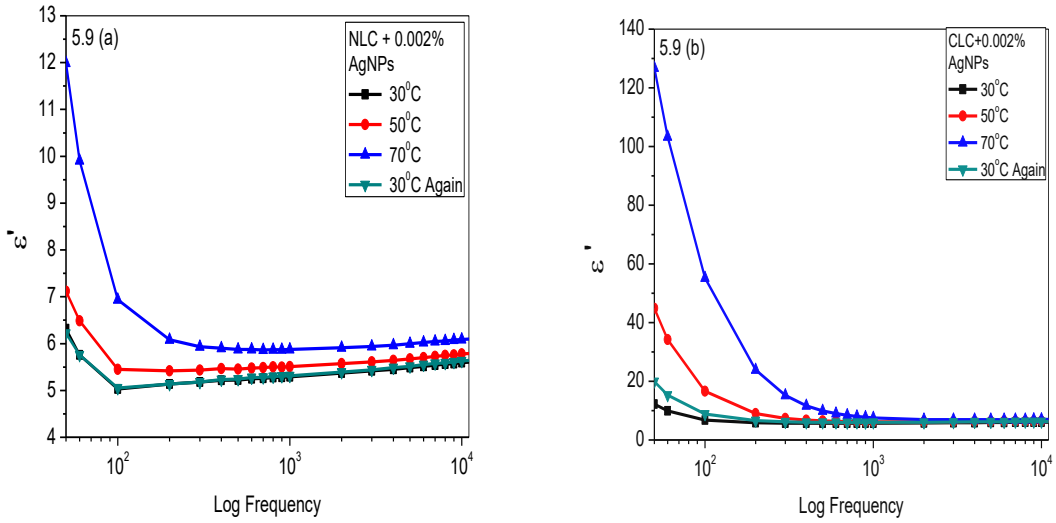

Figure 5.9: Variation of dielectric constant of silver nanoparticles-doped (a) NLC (b) CLC samples with applied electric field frequency at different temperatures.

Fig. 5.9 (a, b) depicts the frequency response of dielectric constant of doped samples corresponding to a rise in temperature. We observed a nearly twofold increase in the dielectric constant for a 40K rise in temperature above the room temperature at 50 Hz for doped nematic sample [Fig. 5.9 (a)]. We also recorded about five to tenfold enhancement

in case of doped chiral sample [Fig. 5.9 (b)] for the corresponding range of temperature. We believe that enhancement in the value of Ɛ' for the doped sample is because of the spontaneous polarization of silver nanoparticles [48]. The dielectric constant of a polar medium increases because of the increased polarization. Temperature induced unwinding of the helices further augments the polarization process. The LC director may also have coupled itself parallel to the dipoles of silver NPs in the matrix, thus contributing to the enhancement of real part of the permittivity.

The thermo-optical hysteresis generated due to partial rewinding of the helices is also reflected in the dielectric behavior of doped chiral samples [Fig. 5.9 (b)].

5.2.4 Conductivity Measurements: Figure 5.10 demonstrates an increase in the conductivity of doped samples over pure NLC and CLC hosts. The increase is significantly lower in the case of doped CLC (≈ 30%) as against the doped NLC (≈ 400%) [Table 5.2].

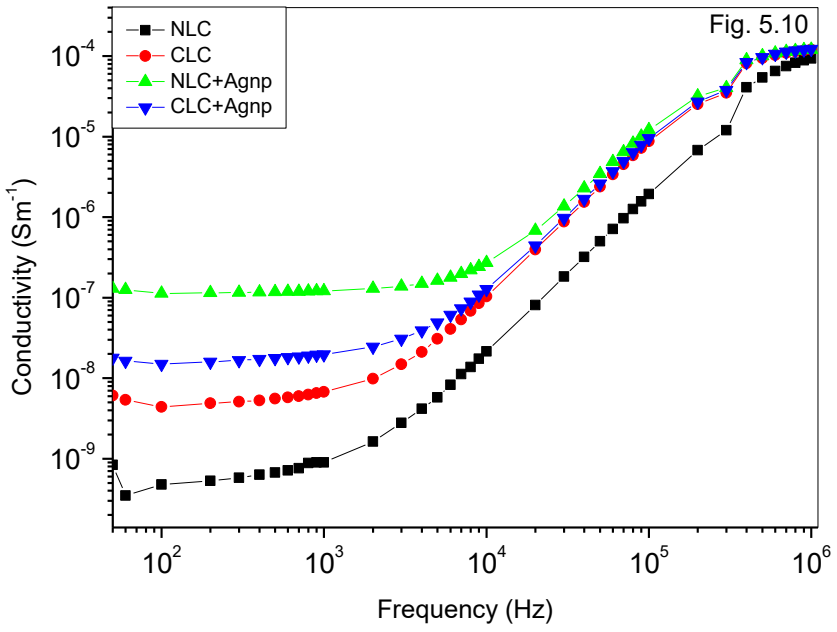

Figure 5.10 Variation of the conductivity of undoped and AgNP-doped NLC and CLC samples.

As we know the source of electrical conductivity in pure liquid crystals is mainly ionic. The residual impurities, aging and, contamination of cell surfaces or material are a few of the

various possible sources of existence of ions. The formation of chains or network by dispersed metallic nanoparticles can also contribute to the conductivity of doped samples. Moreover, electrons present in metallic nanoparticles also contribute to the electrical conductivity of the doped samples [29]. The segregation or restricted dispersal of silver nanoparticles due to their trapping in the defects of chiral supramolecular structures can be the reason behind limited contribution of AgNPs to the conductivity of doped CLC [47,48].

Table 5.2: Summary of Thermo-optic, Electro-optic, and Photoluminescence response of the undoped and silver nanoparticles-doped NLC and CLC samples.

Sample	Planar→ Iso (^{O}C)	Conductivity 60 Hz (10^{-7})	$(\varepsilon')_{30}{}^{o}C$ at 60Hz	Threshold Voltage(V)	Peak PL intensity	λ_{max}
NLC	95-121	0.003	1.97	10.0	140	384
CLC	95-117	0.060	5.46	8.8	190	407
NLC+Agnp	122-154	1.230	5.75	7.0	290	410
CLC+Agnp	76-107	0.159	10.02	6.3	617	413

5.2.5 Photoluminescence Studies: We recorded PL emission spectra of undoped and doped samples at room temperature while keeping the basic instrumental parameters, viz., slit-width, excitation step, etc. constant for all the samples [50-53].

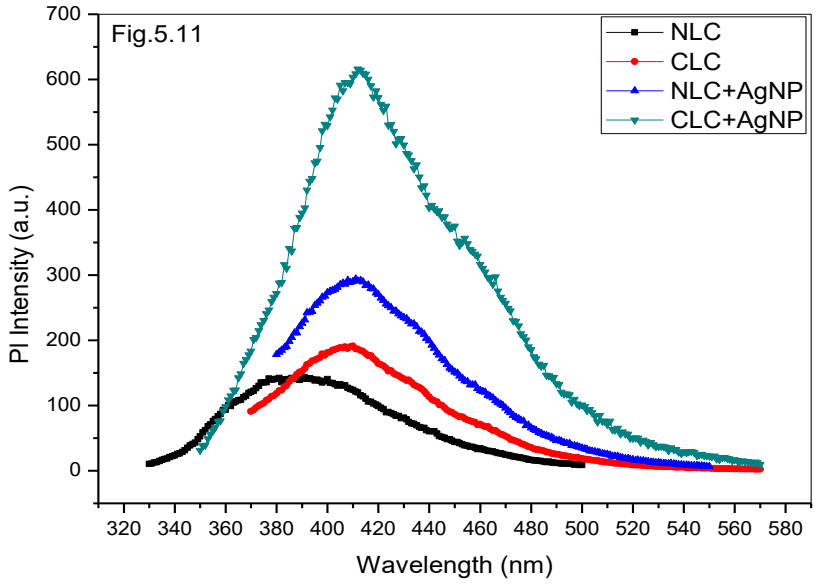

Figure 5.11: PL emission spectrum of the undoped and silver nanoparticles-doped NLC and CLC samples.

The wavelength corresponding to the maximum PL intensity of emission spectrum was found to occur at 408 nm. We thus performed the photo-induced luminescence of the doped chiral liquid crystals by fixing the excitation wavelength at 350 nm. The photoluminescence spectra of chiral liquid crystal molecules in the presence of silver nanoparticles have an almost similar profile as the spectrum of undoped liquid crystals, indicating the complete organization of silver nanoparticles in liquid crystal matrix. [Fig. 5.11] The addition of chiral molecules affects the refractive index of the medium and doping with nanoparticles also causes an elongation of the pitch, as observed by the reflection peak appearing at longer wavelengths: this is consistent with a previous study [8] which reported helical pitch elongation in nanoparticle-doped CLCs [Table 5.2]. We also observed a pronounced enhancement in the peak intensity of photoluminescence because of AgNP doping in chiral medium. We have successfully investigated the role of chirality in modifying the behavior of AgNPs doped nematic liquid crystals. We recorded a significant enhancement in photoluminescence, electro-optical and thermoelectric behaviour of doped samples after the

introduction of chirality. Electro-optical hysteresis has been observed in the doped chiral sample while this was absent in the doped nematic sample.

We consider the local surface plasmon resonance effect of silver nanoparticles present in chiral superstructures of doped CLC sample to be responsible for the enhancement of fluorescence as compared to the doped NLC cell. When frequency of photons of the incident light matches the natural frequency of surface electrons oscillating in the restoring force field of positive nuclei, the condition for resonance is established. There are earlier reports about the optical absorption of a particle being maximum at the plasmon resonant frequency, which is sensitive to the refractive index changes in the medium [49]. We believe that the reason behind shifting of the peak in PL spectrum is the change in plasmon frequency due to refractive index changes on addition of chiral molecules [50,51]. The overall behavior of the AgNP doped chiral sample indicates its potentiality as a functional material for memory devices. The sensitivity of surface plasmons generated photoluminescence in the nanocomposite based chiral medium to its refractive index (a function of the pitch of helix), envisages the potential for its use as an optical sensor with functionality.

EFFECT OF ALUMINUM DOPED ZINC OXIDE NANOPARTICLES DOPING ON THE ELECTRO-OPTICAL AND PHOTOLUMINESCENCE BEHAVIOUR OF A CHIRAL MATRIX

Recently zinc oxide nanoparticles have widely been reported to possess several favorable properties, including good transparency [49,50] high electron mobility (2000 cm^2/Vs at 80K) [51], wide band gap (3.37 eV) and strong room-temperature luminescence [52]. Zinc oxide (ZnO) is an intrinsic n-type semiconductor having a band gap in the ultraviolet (UV) region which makes ZnO a unique candidate for UV light lasers and detectors working in the range of 368–390 nm [53]. ZnO nanomaterials have been found very useful in several optoelectronic applications such as optical sensors [51], light emitters [54], surface acoustic wave (SAW) devices [55], gas sensing [56] and piezoelectric devices [57].

There are reports about further widening of the band gap with Al doping [58] as aluminum serves as a donor in ZnO lattice and makes it useful for the fabrication of optoelectronics devices and detectors [59]. The addition of aluminum improves the electrical and optical properties of ZnO [60]. Bahedi et al. reported that Al-doped ZnO gives strong PL intensity in UV region in crystalline samples [61-62]. All these properties of AZO (Aluminium doped ZnO) particles make them suitable to be used as transparent electrodes in liquid crystal displays (LCD) [61], energy saving and heat protecting windows, thin film transistors [62] and light emitting diodes (LED) [63,64].

Inspired by the properties of AZO nanoparticles and the results of our previous studies [20,24] regarding carbon nanotubes and silver nanoparticles doping in CLC matrix, we were genuinely motivated to further our efforts. We were interested in exploring the perspectives of doping our base matrix with AZO nanoparticles. Also as the AZO nanoparticle doping in nematic LCs, having uniaxial symmetry, was giving promising results [1,65,66] , their incorporation in the medium having helical symmetry seemed interesting to investigate.

The present study includes the effects of doping on the optical and electro-optical properties of chiral nematic liquid crystals with different concentrations of Octadecylamine capped AZO nanoparticles. The concentration dependent morphological behaviour was investigated by polarized optical microscopy. We confirmed the electro-optic switching

behavior of the liquid crystalline helix with an active chiral dopant. An improvement in the electro-optical behavior of AZO NPs doped CLC medium in the frequency range 50 Hz-1MHz was recorded. A lowering in the electro-optical switching threshold and a nearly tenfold rise in the dielectric constant with temperature was noted. We observed a pronounced surge in the photoluminescence emission peak of the doped samples. Optical hysteresis was recorded in the doped samples and measured with transmission studies.

5.3 Sample Preparation and Characterization

5.3.1 Functionalisation of AZO Nanoparticles: We used 6% aluminum doped zinc oxide (AZO) nanoparticles having size < 50 nm (Sigma-Aldrich). We functionalized them with octadecyl amine (ODA) by a chemical route. A 0.54 gm of ODA was dissolved in 180 ml of chloroform before adding 1 gm of AZO to the solution. Sonication followed the mixing for two hours. We precipitated the functionalized AZO particles from chloroform by adding 400 ml anhydrous ethanol along with deionized water. The clear solution was decanted to get the precipitate which, after drying was used as a dopant in the CLC matrix [69].

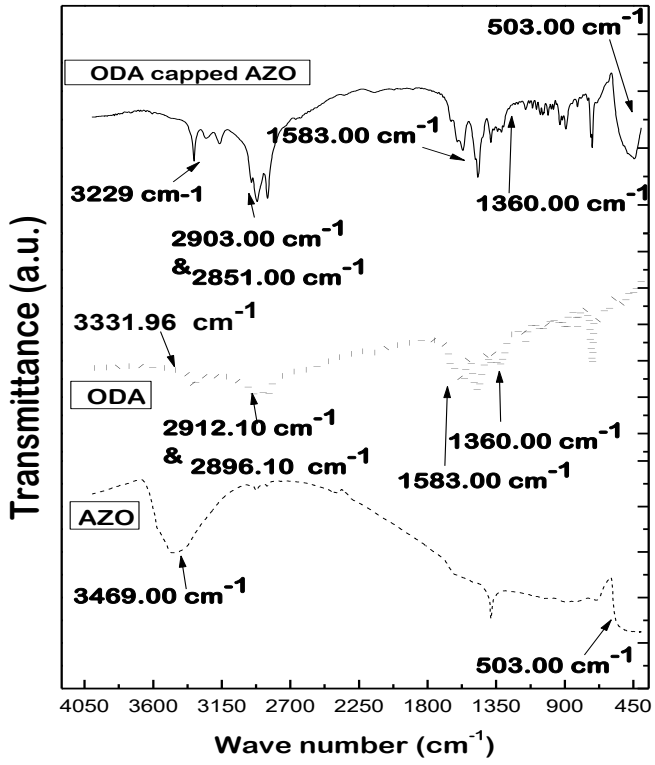

Figure 5.12: FTIR spectroscopy profile of ODA functionalized AZO nanoparticles.

5.3.2 Fourier Transform Infrared Spectroscopy: The attachment of functional group was confirmed by FTIR spectroscopy [69]. FTIR spectrum of ODA [Fig.5.12] is marked by absorption peaks corresponding to the amine group (3331.96 cm^{-1}) and carbon atoms belonging to the octadecyl chain. The craggy absorptions at 2912.13 cm^{-1} and 2896.10 cm^{-1} corresponded to C-H stretching. Absorption at 1583.00 cm^{-1} corresponds to the carbonyl C═O bond stretching of the amine group. Simple bending vibrations of C−H bonds are represented by the dip at 1380.00 cm^{-1}. Absence of a broad absorption 3469.00 cm^{-1} in ODA capped AZO and its presence in the FTIR of AZO confirms chemical functionalization through oxidation. The shifting of the dip at 3331.00cm^{-1} corresponding to the presence of a free NH_2 group in the ODA spectrum to 3229.00cm^{-1} in the functionalized AZONP spectrum indicates successful functionalization of AZO.

5.3.3 Transmission Electron Microscopy: TEM investigations were done to verify the size of nanoparticles.

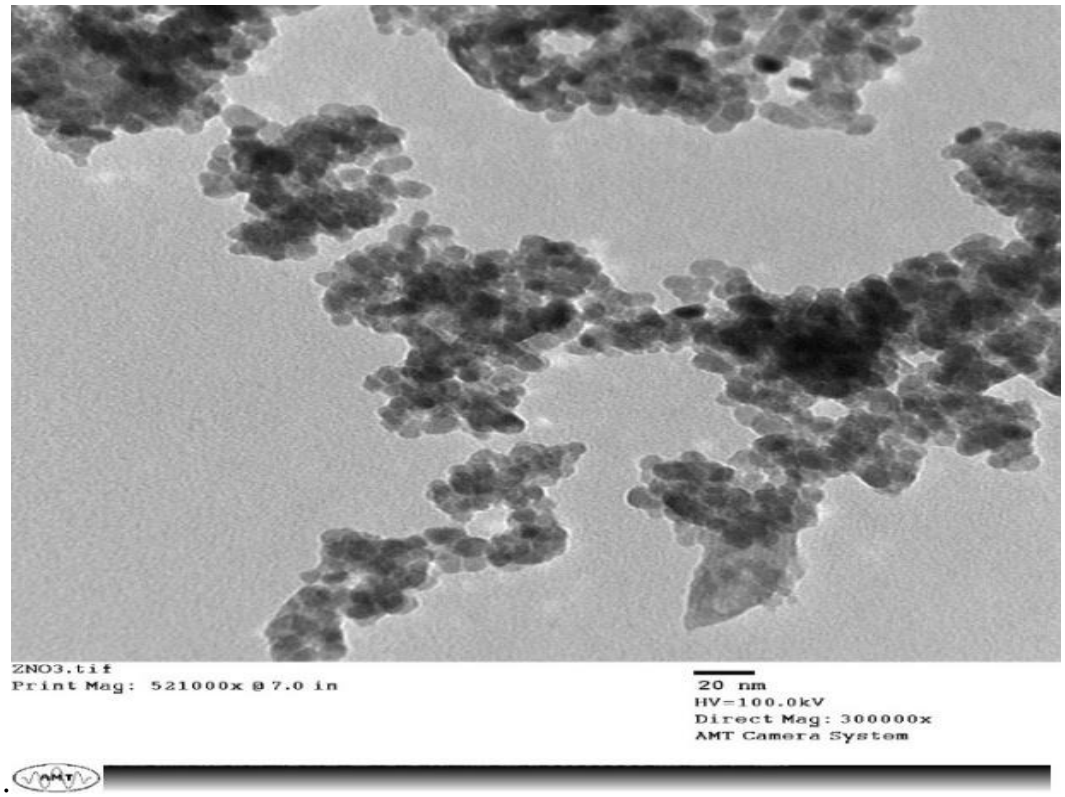

Figure 5.13 TEM micrograph of AZO NPs dispersed in ethanol solution.

A sufficient number of microphotographs taken from different areas of the sample reveal that average size of the functionalized nanoparticles is 7.8 nm. AZO particles doped CLC composites were prepared by homogeneously dispersing 0.01, 0.015, and 0.020wt% of AZO NPs in chiral nematic mixture and filled in LC cells of 5μm (as used in our previous studies) in their isotropic state.

5.3.4 Morphological Studies: The POM with crossed polarizers at 100X magnification was used to record micro textures of AZO doped sample cells. Figure 5.14 (a) shows scattering state of the chiral medium confined in antiparallel aligned ITO coated substrates. Fig. 5.14 (b,c) shows that doping with AZO NPs has generated defects in helical symmetry of the chiral medium.

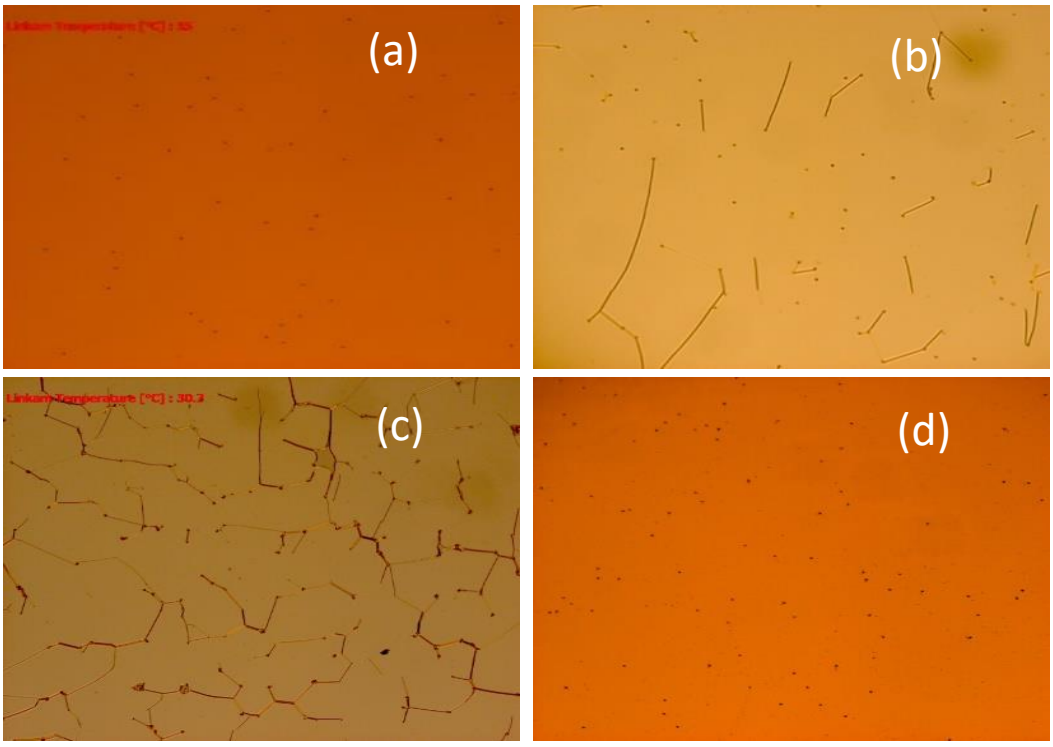

Figure 5.14: Optical micrographs of the scattering state of doped CLC samples with increasing concentration of AZO NPs (a) Undoped (b) 0.01 (c) 0.015 and (e) 0.020 wt%, in freshly filled cells.

The number of disclinations increases with increasing the concentration of nanoparticles. Fig. 5.14(d) depicts the formation of agglomerates at 0.02wt% concentration of dopant. The difference in colour of the light reflected from the samples with different concentrations of AZO NPs indicates that self-organization of AZO NPs has also influenced the pitch of the chiral matrix as per the Bragg's relation given in equation 4.4.

5.3.5 Electro-optical Studies: Figure 5.15 depicts electro-optic switching behaviour of AZO NPs doped CLC samples. We applied a square wave pulse of 0-30V amplitude and 50 Hz frequency to the sample filled, antiparallel aligned planar cells maintained at room temperature (30^{o}C). We observed that AZO nanoparticles doped CLC cells switch at lower threshold voltages as compared to the undoped sample [Table1]. The lowering of the threshold of Freedericksz transition owes its genesis to ion transport mechanism in the material. As reported earlier by many researchers, ions are always present in LC cells due to several reasons (explained in section 5.1) [33,68,71]. When we apply a square wave pulse

to a sample filled aligned CLC cell, hydrodynamic instabilities are induced [Fig. 5.15] and unwinding of helices accompanied by space charge separation takes place.

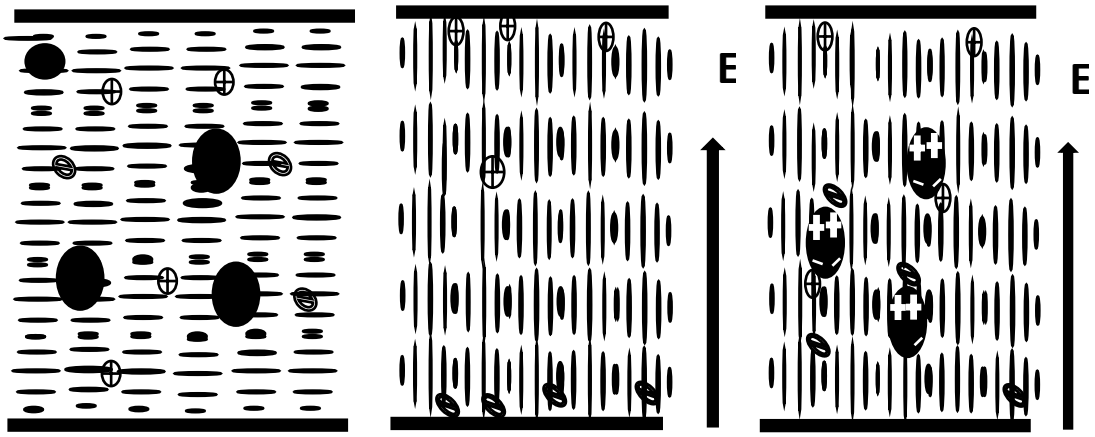

Fig. 5.15. Model depicting ion transport mechanism in (a) AZO NP-doped CLC cell before the application of electric field (b) undoped and (c) AZO-NPs doped CLC cell undergoing Freedericksz transition.

The ions drift towards the alignment layers, and polarization of the dopant nanoparticles takes place. Polarized dopants molecules interact with the ion impurities through Colombian interaction and physically trap the ions. This trapping of ions reduces the number of ions reaching alignment layers and limits the effectiveness of charge screening [70]. Hence, lower threshold voltage is required to make a transition from planar to electro-optically switched state [Table1].

5.3.6 Dielectric Response of the Doped samples: It has been widely reported in literature and our earlier works that an insignificant change in nanoparticle concentration brings about noticeable and sometimes even pronounced changes in the electro-physical behaviour of the host LC [24,66,71]. We studied the dielectric behavior of a planar-aligned cell as a function of applied frequency by using a parallel RC circuit and scanned the capacitance and dissipation parameters for a range of frequencies from 50Hz to 1MHz. The real ε' (capacitative) and imaginary ε" (ac conductance) components of permittivity of the sample were computed after that.

At lower frequencies 50-100 Hz, magnitude of the real part of dielectric permittivity (Ɛ’) decreased for 0.01 and 0.015wt% doped samples and was lower in comparison to undoped

CLC, while it was higher in case of 0.02wt% doped sample. At higher frequencies (100 Hz-1MHz) the value of Ɛ' is almost same for all the samples [Fig. 5.16].

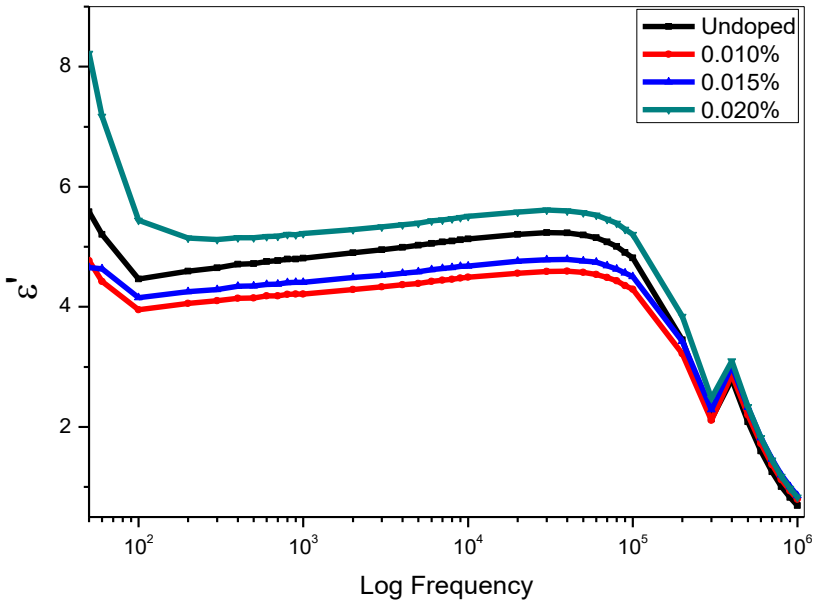

Fig. 5.16: Variation of the real part of dielectric permittivity with frequency for different dopant concentration for the doped samples.

With doping of semiconducting AZO nanoparticles in CLC, dipolar interaction among liquid crystal molecules organized in chiral symmetry and the dopant nanoparticles starts taking place. This strong dipolar interaction disrupts the symmetry of chiral medium by changing orientation of the molecules. Moreover, ions present in the undoped CLC get trapped by dopant nanoparticles and cannot reach the electrodes: resulting in lower values of dielectric constant. As the doping concentration increases to 0.02wt%, forces among the nanoparticles dominate and the number of ions produced also multiplies due to higher doping concentration [65], therefore the magnitude of dielectric permittivity shows an increase in the value of the dielectric constant.

The expression for ionic contributions to dielectric dispersion in a LC cell subjected to an electric field of frequency 'f' is given as [72]

$$\in' = \frac{nq^2 D^{3/2}}{\pi^{3/2} \in_0 d K_B T} f^{-3/2} + \in'_{lc} \qquad \text{.....(5.2)}$$

Where n is the concentration, q is the charge, D is the diffusion constant for mobile ions, d is the thickness of the cell, ε_0 is the permittivity in free space, K_B is the Boltzmann constant, T is the absolute temperature, and ε'_{lc} is the inherent dielectric constant of LC matrix. As per above expression, ionic contribution decreases with increasing frequency and it is the second term which mainly contributes to the dielectric constant. This is because at high frequency, trapped ions are unable to follow the speed of polarity reversal of the applied field and reach the substrates to contribute to the dipole moment. Hence ion trapping effect dominates at higher frequencies (100 kHz-1MHz) [33] and the value of dielectric constant falls and is also almost same for all the samples.

Thermo-electric Response: Dielectric spectroscopy was done to investigate the effect of temperature on dielectric permittivity of supramolecular helical matrix doped with self-

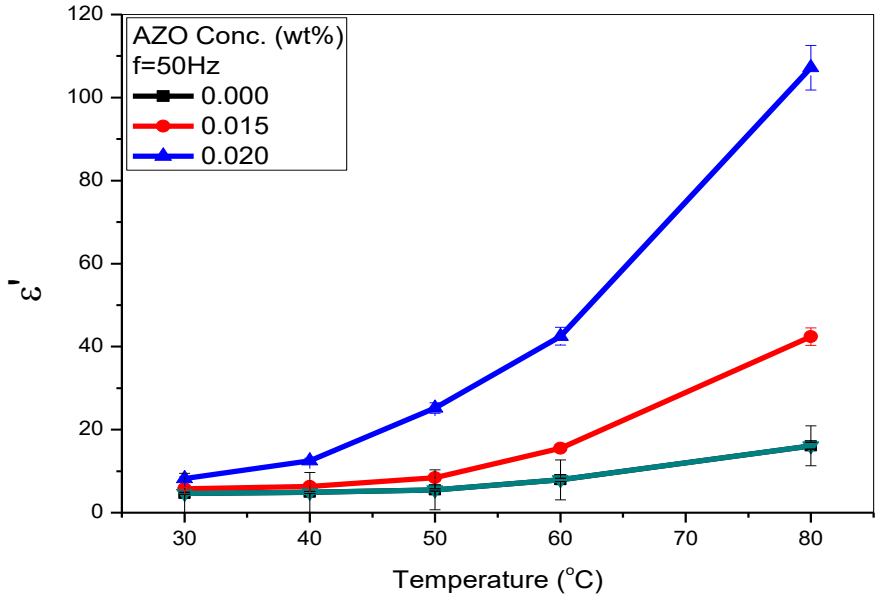

Fig. 5.17: Temperature dependence of dielectric permittivity of AZO-doped chiral nematic composite systems.

assembled AZO NPs. Fig, 5.17 shows about three to thirteen-fold increase in the value of Ɛ' for a 50^{o}C rise in temperature.

As the temperature rises, unwinding of helices promotes the polarization process and helps the director to orient parallel to the applied electric field. The mobility of ions, present in the medium, increases and more and more ions are now able to reach the alignment layers and contribute to the overall dipole moment. As the AZO nanoparticles are semiconducting in nature, they also see an upsurge in their polarization. The overall increase in polarization of the matrix is responsible for the observed enhancement in the real part of the dielectric permittivity with temperature.

5.3.7 Electrical Conductivity Measurements: Fig. 5.18 (a) depicts the response of conductivity of doped samples to the applied electric field frequency. Fig. 5.18 (b) shows the impact of AZO doping on the conductivity of doped samples as a function of dopant concentration. Equ 4.1computed the sample conductivity σac [73].

$$\sigma_{ac} = \epsilon_o \epsilon'' \omega \qquad \text{.....(4.1)}$$

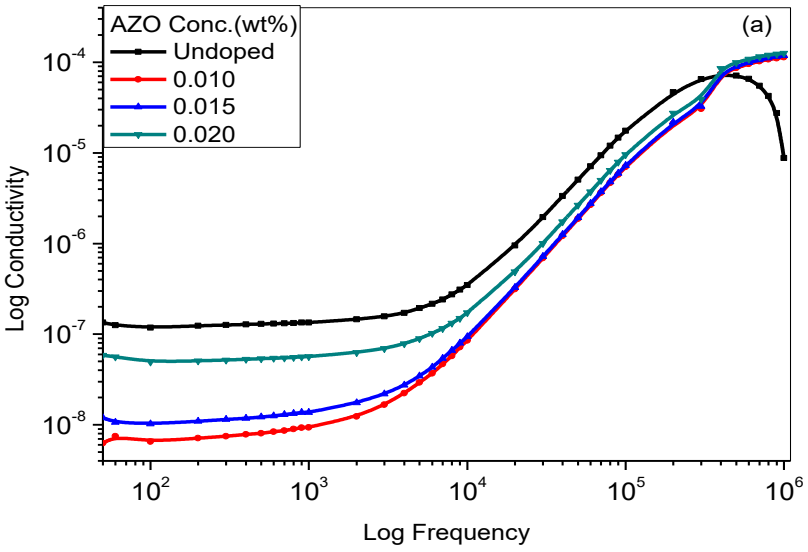

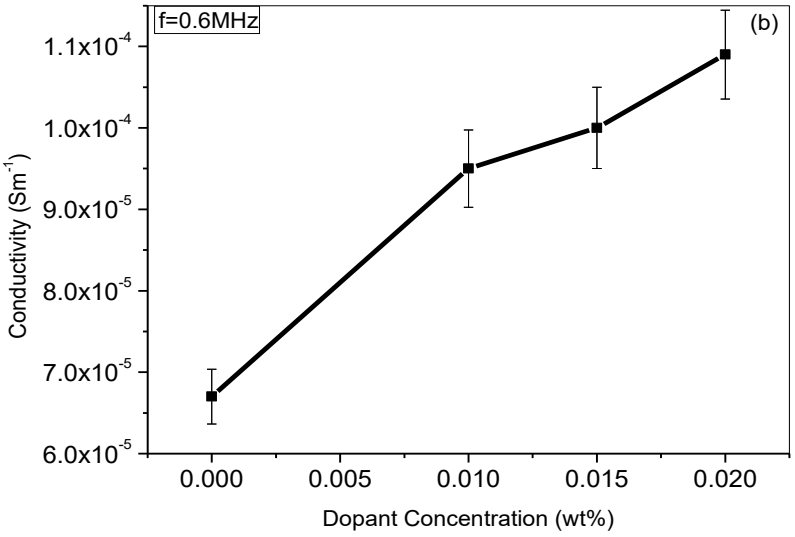

Fig. 5.18: ac conductivity of doped CLC samples as a function of (a) Frequency (b) Doping concentration.

Where, 'σ_{ac}' is the ac conductivity, ω = 2πf and ϵ_o is the permittivity of free space. For a nano-doped LC system, mainly two factors (ionic and the electronic) contribute towards the value of ac conductivity. Out of the two, ionic part is independent of frequency and electronic part changes with the change in frequency.

Table: 5.3 Electro-optical and optical properties of AZO-doped CLC samples.

Dopant Concentration (wt%)	Threshold Voltage (V)	Memory Parameter	Max PL Intensity
0.000	8.8	0.01	190 at 407
0.010	6.7	0.05	627 at 434
0.015	6.1	0.22	698 at 436
0.020	5.9	0.00	723at 436

We observed that at low frequencies, there was a decrease in the conductivity of doped samples as compared to undoped samples. We believe this is because of the decreased number of the freely available ions. At high frequencies, (› 0.5MHz) conductivity of the doped samples increases above that of the undoped sample and reaches a value nearly double as compared to the undoped sample at 0.6MHz, in the case of 0.02wt% doped sample.

The source of this increase in the value of conductivity at high frequency can be electronic hopping. Due to the large size of nanoparticles, the distance of hopping between the neighbouring nanoparticles decreases, and they find it easy for ionic charge transfer mechanism. The charge transfer now takes place through nanoparticles and contributes to the conductivity.

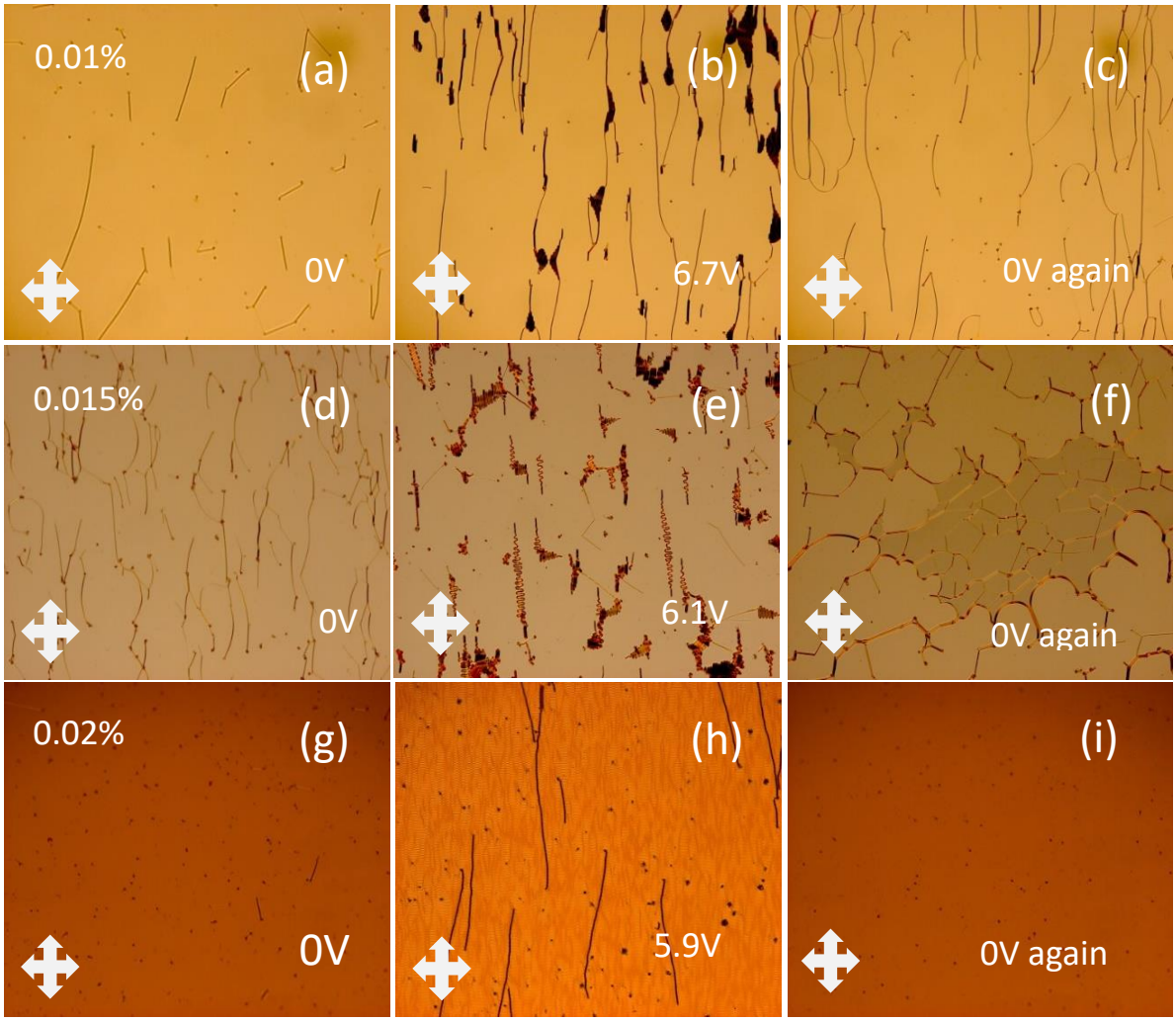

Figure 5.19: Illustration of Electro-optical memory effects in the AZO-doped samples through optical microtextures.

5.3.8 Investigations for Electro-Optical Hysteresis: Figure 5.19 (f,i) depicts the inception of electro-optic memory in case of doped CLC samples through micro-textures. Most likely the AZO particles, being large as compared to LC molecules, have obstructed the rewinding of helical supramolecules, which presents itself in the form of disclinations and planar regions intercepting the planar symmetry. Transmission studies were carried out to quantify the irreversible memory as memory parameter 'M' as explained in Chapter 2

$$M = \frac{T_f - T_i}{T_{max} - T_i} \ldots\ldots\ldots\ldots\ldots \quad (2.19)$$

Where T_i is the initial value of transmittance while increasing voltage from 0V and T_f is the final value of transmittance at the zero applied fields while decreasing the amplitude of voltage. T_{max} is the transmittance corresponding to peak value. We plotted optical transmission from doped samples as a function of applied electric field in Fig. 5.20.

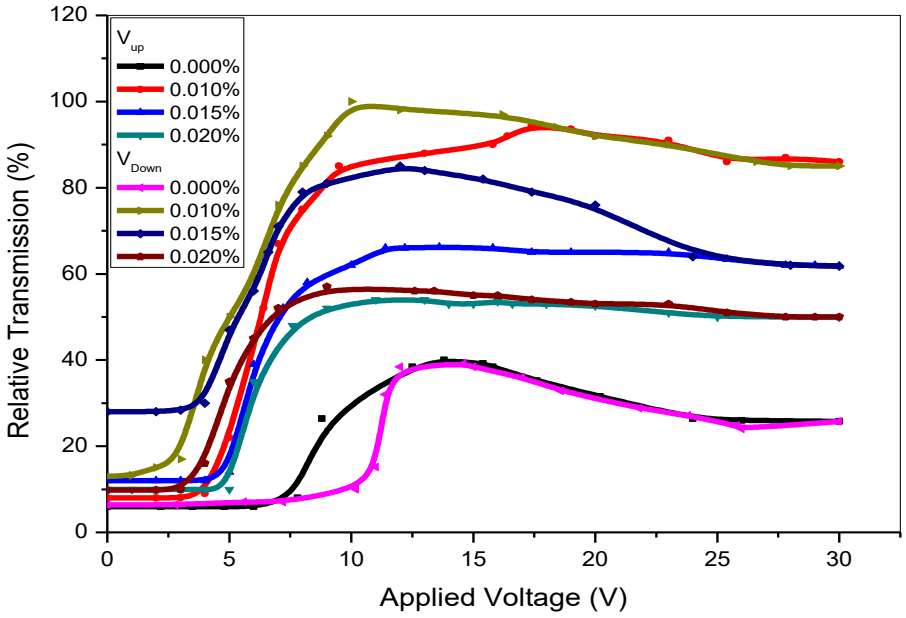

Fig. 5.20: Normalized transmission as a function of applied voltage for AZO doped samples.

The measurements were taken as mentioned in section 2.3.7. In the absence of an external field, the liquid crystal molecules are stable. In the ON state, as the field reaches its threshold value, molecules start aligning with the field direction. The transmitted intensity starts increasing gradually with changing phase and saturates in the homeotropic state. While decreasing the voltage, transmittance also decreases but does not follow the same path, hinting at optical hysteresis in the behaviour of the sample.

5.3.9 Photoluminescence Studies

To check the optical quality and possible effects of AZONPs doping on photoluminescence behaviour, emission spectra of doped samples were plotted at room temperature [Fig. 5.21] in the wavelength range of 300-600nm by fluorescence spectrophotometer and compared

with those of the undoped CLC. While recording the spectra, all other instrumental parameters such as the slit width, excitation step etc. were kept constant. The PL spectra of doped chiral liquid crystals were then taken by fixing the excitation wavelength at 350 nm.

The signatures of three visible emission bands corresponding to 412, 436, 462nm are dominant in the PL spectra of AZO doped CLC, which resulted from intrinsic defects in ZnO nanomaterials.

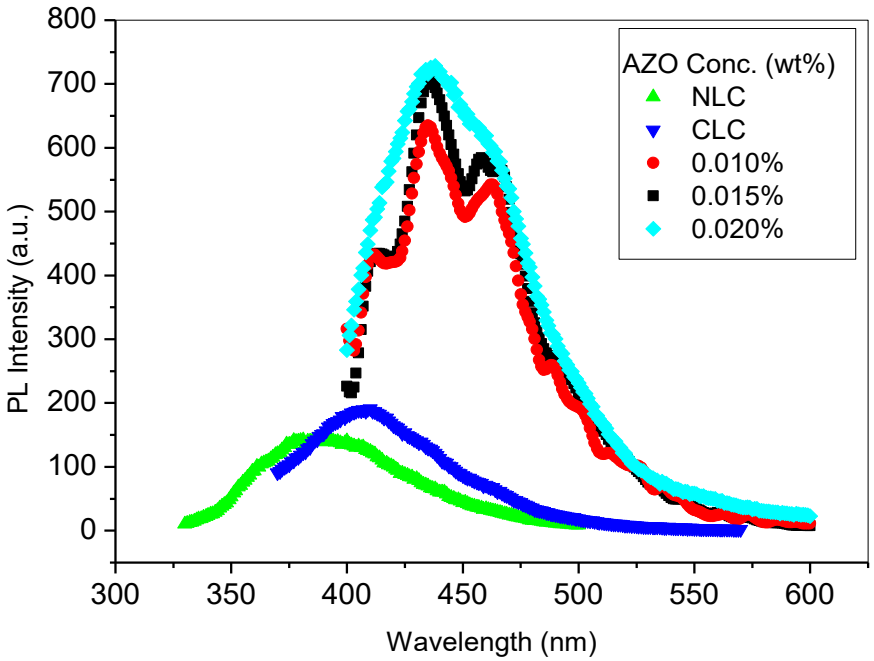

Fig. 5. 21: PL spectra of undoped and AZO nanoparticles doped CLCs.

The intrinsic defects in ZnO nanostructure are related to mainly Zn vacancies (V_{Zn}), O vacancies (V_O), interstitial Zn (Zn_i), interstitial O (O_i) and substitution of O at Zn position (O_{Zn}). These intrinsic defects cognate with emissions from deeper levels such as oxygen vacancies or zinc interstitials. It has been reported earlier [74] that a blue emission of ~412 nm in the PL spectra was attributed to O_i levels defects in ZnO, whereas the blue emission corresponding to ~436 nm and ~462 nm can be attributed to energy of transition of electron from Zn_i to VB and Zn_i to V_{Zn}, respectively. With increasing the concentration of AZO NPs in CLC, bands corresponding to 412nm and 462nm get merged and only the blue emission

corresponding to 436nm dominates. Comparative study of the PL spectra of AZO doped CLC with undoped CLC clearly depicts the absence of all these three blue emission bands in case of undoped sample.

The doping of AZO NPs in CLC samples has improved the blue emission and hence contributed to the enhancement of optical properties of CLC samples. The overall enhancement of peak intensity is also remarkable in doped samples [Table 5.3]. More than three-fold enhancement in the peak intensity was recorded for 0.01wt% doping of AZO nanoparticles. These properties ensure its use as a promising optical material.

References:

1. Joshi T, Kumar A, Prakash J, Biradar AM. Low power operation of ferroelectric liquid crystal system dispersed with zinc oxide nanoparticles. Appl. Phys. Lett. 2010;96:5–7.

2. Kumar R, Raina KK. Morphological control and switchable photoluminescence responses of silica nanoparticles-modified polymer-dispersed liquid crystal composite films. Liq. Cryst. 2015;42:119–26.

3. Kumar R, Raina KK. Enhanced ordering in polymer stabilised ferroelectric liquid crystal guest-host composites: evidence by polarised fluorescence spectroscopy. Liq. Cryst. 2014;41:694–700.

4. Joshi T, Prakash J, Kumar A, Gangwar J, Srivastava AK, Singh S. Alumina nanoparticles find an application to reduce the ionic effects of ferroelectric liquid crystal. J. Phys. D. Appl. Phys. 2011;44:315404.

5. Si G, Zhao Y, Leong ESP, Liu YJ. Liquid-crystal-enabled active plasmonics: A review. Materials (Basel). 2014. p. 1296–317.

6. Zhang Y, Liu Q, Mundoor H, Yuan Y, Smalyukh II. Metal nanoparticle dispersion, alignment, and assembly in nematic liquid crystals for applications in switchable plasmonic color filters and E-polarizers. ACS Nano. 2015;9:3097–108.

7. Jamil M, Ahmad F, Rhee J. Nanoparticle-doped polymer-dispersed liquid crystal display. Curr. Sci. 2011;101:1544–52.

8. Kumar A, Prakash J, Mehta DS, Biradar AM, Haase W. Enhanced photoluminescence in gold nanoparticles doped ferroelectric liquid crystals. Appl. Phys. Lett. 2009;95.

9. Tripathi S, Ganguly P, Haranath D, Haase W, Biradar AM. Optical response of ferroelectric liquid crystals doped with metal nanoparticles. Appl. Phys. Lett. 2013;102.

10. Sun Y, Tian Y, He M, Fan D, Liu Y, Zhang Q. Effect of Silver Nanoparticles on the photo-induced orientation of liquid crystalline polymer based on the surface plasmon resonance. 2011;29:161–5.

11. Shih CY, Yeh HC. Surface plasmon-enhanced lasing in dye-doped cholesteric liquid crystals. Opt. Express. 2012;20:20698.

12. Popov O, Zilbershtein A, Davidov D. Random lasing from dye-gold nanoparticles in polymer films: Enhanced gain at the surface-plasmon-resonance wavelength. Appl. Phys. Lett. 2006;89.

13. Pratibha R, Park K, Smalyukh II, Park W. Tunable optical metamaterial based on liquid crystal-gold nanosphere composite. Opt. Express. 2009;17:19459–69.

14. Caputo R, De Sio L, Cataldi U, Umeton C. Plasmon resonance tunability of gold nanoparticles embedded in a confined cholesteric liquid crystal host. Mol. Cryst. Liq. Cryst. 2012;559:194–201.

15. Huang SY, Peng CC, Tu LW, Kuo CT. Enhancement of luminescence of nematic liquid crystals doped with silver nanoparticles. Mol. Cryst. Liq. Cryst. 2009;507:301–6.

16. Gorkunov MV, Osipov MA. Mean-field theory of a nematic liquid crystal doped with anisotropic nanoparticles. Soft Matter. 2011;7:4348.

17. Kumar V, Kumar A, Biradar AM, Reddy GB, Sachdev D, Pasricha R. Enhancement of electro-optical response of ferroelectric liquid crystal: the role of graphene quantum dots. Liq. Cryst. 2014;41:1719–25.

18. Kalele S, Deshpande AC, Singh SB, Kulkarni SK. Tuning luminescence intensity of RHO6G dye using silver nanoparticles. Bull. Mater. Sci. 2008;31:541–4.

19. Hung WC, Cheng WH, Lin YS, Jang DJ, Jiang IM, Tsai MS. Surface plasmons induced extra diffraction band of cholesteric liquid crystal grating. J. Appl. Phys. 2008;104:1–5.

20. Middha M, Kumar R, Raina KK. Memory effects in chiral nematic liquid crystals doped with functionalised single-walled carbon nanotubes. Liq. Cryst. 2015;42:1028–35.

21. Yoshida H, Tanaka Y, Kawamoto K, Kubo H, Tsuda T, Fujii A, et al. Nanoparticle-stabilized cholesteric blue phases. Appl. Phys. Express. 2009;2.

22. Prakash J, Choudhary A, Kumar A, Mehta DS, Biradar AM. Nonvolatile memory effect based on gold nanoparticles doped ferroelectric liquid crystal. Appl. Phys. Lett. 2008;93:91–4.

23. Kumar A, Biradar AM. Effect of cadmium telluride quantum dots on the dielectric and electro-optical properties of ferroelectric liquid crystals. Phys. Rev. E - Stat. Nonlinear, Soft Matter Phys. 2011;83.

24. Middha M, Kumar R, Raina KK. Improved electro-optical response of induced chiral nematic liquid crystal doped with multi-walled carbon nanotubes. Ferroelectrics. 2016;495:75–86.

25. Podoliak N, Bartczak D, Buchnev O, Kanaras AG, Kaczmarek M. High optical nonlinearity of nematic liquid crystals doped with gold nanoparticles. J. Phys. Chem. C. 2012;116:12934–9.

26. Middha M, Kumar R, Raina KK. Photoluminescence tuning and electro-optical memory in chiral nematic liquid crystals doped with silver nanoparticles. Liq. Cryst. 2016;1–7.

27. Kelly KL, Coronado E, Zhao LL, Schatz GC. The optical properties of metal nanoparticles: The influence of size, shape, and dielectric environment. J. Phys. Chem. B. 2003;107:668–77.

28. Kaur S, Singh SP, Biradar AM, Choudhary A, Sreenivas K. Enhanced electro-optical properties in gold nanoparticles doped ferroelectric liquid crystals. Appl. Phys. Lett. 2007;91:18–21.

29. Mitov M, Portet C, Bourgerette C, Snoeck E, Verelst M. Long-range structuring of nanoparticles by mimicry of a cholesteric liquid crystal. Nat. Mater. 2002;1:229–31.

30. Goel P, Arora M. Mechanism of photoluminescence enhancement and quenching in Nd_2O_3 nanoparticles–ferroelectric liquid crystal nanocomposites. RSC Adv. 2015;5:14974–81.

31. Zhou XD, Xiao XH, Xu JX, Cai GX, Ren F, Jiang CZ. Mechanism of the enhancement and quenching of ZnO photoluminescence by ZnO-Ag coupling. EPL (Europhysics Lett. 2011;93:57009.

32. Mandal PK, Lapanik A, Wipf R, Stuehn B, Haase W. Sub-hertz relaxation process in chiral smectic mixtures doped with silver nanoparticles. Appl. Phys. Lett. 2012;100:1–4.

33. Garbovskiy Y, Glushchenko I. Nano-Objects and ions in liquid crystals: Ion trapping effect and related phenomena. Crystals. 2015;5:501–33.

34. Ha YS, Kim HJ, Park HG, Seo DS. Enhancement of electro-optic properties in liquid crystal devices via titanium nanoparticle doping. Opt. Express. 2012;20:6448–55.

35. Lin GJ, Chen TJ, Lin YT, Wu JJ, Yang YJ. Effects of chiral dopant on electro-optical properties of nematic liquid crystal cells under in-plane switching and non-uniform vertical electric fields. Opt. Mater. Express. 2014;4:2468.

36. Lee HH, Yu JS, Kim JH, Yamamoto SI, Kikuchi H. Fast electro-optic device controlled by dielectric response of planarly aligned cholesteric liquid crystals. J. Appl. Phys. 2009;106.

37. Castles F, Morris SM, Coles HJ. Flexoelectro-optic properties of chiral nematic liquid crystals in the uniform standing helix configuration. Phys. Rev. E - Stat. Nonlinear, Soft Matter Phys. 2009;80.

38. Mulder DJ, Schenning A, Bastiaansen C. Chiral-nematic liquid crystals as one dimensional photonic materials in optical sensors. J. Mater. Chem. C. Royal Society of Chemistry; 2014;2:6695–705.

39. Tripathi S, Prakash J, Chandran A, Joshi T, Kumar A, Dhar A. Enhanced dielectric and electro-optical properties of a newly synthesised ferroelectric liquid crystal material by doping gold nanoparticle-decorated multiwalled carbon nanotubes. Liq. Cryst. 2013;40:1255–62.

40. Vijayaraghavan A, Kar S, Soldano C, Talapatra S, Nalamasu O, Ajayan PM. Charge-injection-induced dynamic screening and origin of hysteresis in field-modulated transport in single-wall carbon nanotubes. Appl. Phys. Lett. 2006;89.

41. Garbovskiy Y, Glushchenko I. Ion trapping by means of ferroelectric nanoparticles, and the quantification of this process in liquid crystals. Appl. Phys. Lett. 2015;107.

42. Ponevchinsky VV, Goncharuk AI, Denisenko VG, Lebovka NI, Lisetski LN, Nesterenko MI. LC nanocomposites: induced optical singularities, managed nano/micro structure, and electrical conductivity. eprint arXiv:1303.0560. 2013;1–10.

43. Gharde RA, Thakare SY. Effects of concentration of multiwall carbon nanotube on cholesteric liquid crystal. 2015;4:68–74.

44. Manjuladevi V, Gupta RK, Kumar S. Effect of functionalized carbon nanotube on electro-optic and dielectric properties of a liquid crystal. J. Mol. Liq. 2012;171:60–3.

45. Naemura S, Sawada A. Ionic conduction in nematic and smectic a liquid crystals. Mol. Cryst. Liq. Cryst. 2003;400:79–96.

46. Malik P, Raina KK, Bubnov A, Chaudhary A, Singh R. Electro-optic switching and dielectric spectroscopy studies of ferroelectric liquid crystals with low and high spontaneous polarization. Thin Solid Films. 2010. p. 1052–5.

47. Liu M, Kitai AH, Mascher P. Point defects and luminescence centres in zinc oxide and zinc oxide doped with manganese. J. Lumin. 1992;54:35–42.

48. Thandavan TMK, Gani SMA, Wong CS, Nor RM. Enhanced photoluminescence and Raman properties of Al-doped ZnO nanostructures prepared using thermal chemical vapor deposition of methanol assisted with heated brass. PLoS One. 2015;10.

49. Arya SK, Saha S, Ramirez-Vick JE, Gupta V, Bhansali S, Singh SP. Recent advances in ZnO nanostructures and thin films for biosensor applications: Review. Anal. Chim. Acta. 2012;1–21.

50. Özgür Ü, Alivov YI, Liu C, Teke A, Reshchikov MA, Doğan S. A comprehensive review of ZnO materials and devices. J. Appl. Phys. 2005;1–103.

51. Makino T, Chia CH, Tuan NT, Segawa Y, Kawasaki M, Ohtomo A. Radiative and nonradiative recombination processes in lattice-matched (Cd,Zn)O/(Mg,Zn)O multiquantum wells. Appl. Phys. Lett. 2000;77:1632–4.

52. Look DC. Recent advances in ZnO materials and devices. Mater. Sci. Eng. B Solid-State Mater. Adv. Technol. 2001;80:383–7.

53. Ozgür M, Hofstetter D, Morkoç H. ZnO Devices and Applications: A review of current status and future prospects. Proc. IEEE. 2010;98:1255–68.

54. Liu X, Pan K, Li W, Hu D, Liu S, Wang Y. Optical and gas sensing properties of Al-doped ZnO transparent conducting films prepared by sol-gel method under different heat treatments. Ceram. Int. 2014;40:9931–9.

55. Kumar R, Al-Dossary O, Kumar G, Umar A. Zinc oxide nanostructures for NO2 gas–sensor applications: A review. Nano-Micro Lett. 2014;1–24.

56. Sernelius BE, Berggren KF, Jin ZC, Hamberg I, Granqvist CG. Band-gap tailoring of ZnO by means of heavy Al doping. Phys. Rev. B. 1988;37:10244–8.

57. Zhang WY, He DK, Liu ZZ, Sun LJ, Fu ZX. Preparation of transparent conducting Al-doped ZnO thin films by single source chemical vapor deposition. Optoelectron. Adv. Mater. Commun. 2010;4:1651–4.

58. Mridha S, Basak D. Aluminium doped ZnO films: electrical, optical and photoresponse studies. J. Phys. D. Appl. Phys. 2007;40:6902–7.

59. Bahedi K, Addou M, Jouad M El, Sofiani Z, Bayoud S, Haouti M El. Structural, optical and photoluminescence properties of Al doped ZnO thin films by spray pyrolysis. 3rd Ict.

Mediterr. Winter Conf. 2009;26–9.

60. Oh BY, Jeong MC, Moon TH, Lee W, Myoung JM, Hwang JY. Transparent conductive Al-doped ZnO films for liquid crystal displays. J. Appl. Phys. 2006;99:124505/1–124505/4.

61. Hoffman RL, Norris BJ, Wager JF. ZnO-based transparent thin-film transistors. Appl. Phys. Lett. 2003;82:733–5.

62. Choi YS, Kang JW, Hwang DK, Park SJ. Recent advances in ZnO-based light-emitting diodes. IEEE Trans. Electron Devices. 2010;57:26–41.

63. Ben Ayadi Z, El Mir L, Djessas K, Alaya S. Electrical and optical properties of aluminum-doped zinc oxide sputtered from an aerogel nanopowder target. Nanotechnology. 2007;18:445702.

64. Tripathi PK, Misra AK, Manohar S, Gupta SK, Manohar R. Improved dielectric and electro-optical parameters of ZnO nano-particle (8% Cu2+) doped nematic liquid crystal. J. Mol. Struct. 2013;1035:371–7.

65. Manohar R, Srivastava AK, Tripathi PK, Singh DP. Dielectric and electro-optical study of ZnO nano rods doped ferroelectric liquid crystals. J. Mater. Sci. 2011;46:5969–76.

66. Kaur R, Raina KK. Effects of nanoparticle doping on the phase transitional behaviour of ferroelectric liquid crystal Langmuir-Blodgett composite films. Phase Transitions. 2015;88:1213–24.

67. Costa MR, Altafim RA. C, Mammana AP. Ionic impurities in nematic liquid crystal displays. Liq. Cryst. 2001;28:1779–83.

68. Colpaert C, Maximus B, Meyere A. De. Adequate measuring techniques for ions in liquid crystal layers. Liq. Cryst. 1996;21:133–42.

69. Chen WT, Chen PS, Chao CY. Effect of doped insulating nanoparticles on the electro-optical characteristics of nematic liquid crystals. Jpn. J. Appl. Phys. 2009;48.

70. Shukla RK, Raina KK, Haase W. Fast switching response and dielectric behaviour of fullerene/ferroelectric liquid crystal nanocolloids. Liq. Cryst. 2014;41:1726–32.

71. Lin FC, Wu PC, Jian BR, Lee W. Dopant effect and cell-configuration-dependent dielectric properties of nematic liquid crystals. Adv. Condens. Matter Phys. 2013;2013.

72. Yaroshchuk O, Tomylko S, Gvozdovskyy I, Yamaguchi R. Cholesteric liquid crystal-carbon nanotube composites with photo-settable reversible and memory electro-optic modes. Appl. Opt. 2013;52:E53–9.

73. Vadivel M, Babu RR, Ramamurthi K. Studies on the structural, optical and magnetic properties of Al doped ZnO nanoparticles. 2015;7:1206–11.

CHAPTER 6
SUMMARY AND FUTURE SCOPE

A concentration based study on the impact of nanoparticles (SWCNTs, MWCNTs, Agnps, and AZOnps) doping on supramolecular helical organization of chiral nematic liquid crystals was conducted. The agglomeration-free homogeneous mixing was ensured by ultrasonication and confirmed by polarized optical microscopy. The thermo-optical and electro-optical switching behavior of nano-doped samples confined in antiparallel aligned planar liquid crystal cells was investigated by polarized optical microscopy. Significant lowering of the threshold of Freedericksz transition was observed in the doped samples. Emergence of defects with nanoparticle doping was a characteristic of all the doped samples. A pronounced surge in photoluminescence emission intensity was observed in all the nano-doped samples, except the MWCNT doped samples, where it showed a significant decrease. Nanoparticles were also observed to bring a change in spectral behavior of doped samples. Transmission studies indicated enhancement of optical hysteresis in almost all the doped samples. The observations indicate a promising future for the investigated composites to be used as functional materials with electro-optical memory.

Chapter wise Summary of the Findings

Chapter 1: A general overview of the liquid crystals and their phases with a special emphasis on the chiral phase has been given in this chapter. The influence of external stimuli on the pitch related properties of the chiral phase has been discussed. A brief introduction of nanoparticles used as dopants in the present study and their role in changing the properties of liquid crystals has been summarized. A brief review of their applications and the research work being done in this field has been added.

Chapter 2: The selection of liquid crystals and nanoparticles (used as dopants), their properties, preparation of doped samples with desired concentration of dopant and the procedure followed to ensure a homogeneous mixing of nanoparticles into liquid crystals have been included in this chapter. The experimental setup and methodology used for

fabricating liquid crystal cells and filling of doped liquid crystal samples in them were thoroughly explained. Details of the procedure adopted for functionalization of nanoparticles have also been given. An appraisal of the role of polarizing optical microscope in deciphering the phase changes after induction of nanoparticles was discussed. Other characterization techniques employed for the analysis of nanoparticles and doped samples, like Transmission electron microscopy (TEM), Fourier transform infrared (FTIR) Spectroscopy, Fluorescence Spectrophotometry (PL), dielectric spectroscopy, and Abbe's refractometer were reviewed.

Chapter 3: Induction of chirality in a nematic liquid crystal mixture and optimization of chiral dopant concentration into it, to form a suitable matrix for nanoparticle dispersal has been discussed. Our objective was to look for the enhancement of optical and electro-optical properties like morphology, contrast, photoluminescence, threshold voltage for switching, dielectric constant, and optical hysteresis in the doped samples. We investigated the change brought about in these properties of the NLC after doping with five different concentrations of chiral molecules. We found the **2.5 wt% sample (CLC III) to be most appropriate for nanoparticles doping.** The main features of this concentration (CLC III) are as follows

1. Morphology: Till this concentration, the microtextures do not show any defects or discontinuities in the uniform texture, however after this, the defects start appearing (CLC IV and CLC V)
2. Optical hysteresis: At this concentration, the optical hysteresis just starts coming in the sample, so there is a scope for its increase/decrease/disappearance of memory on nanoparticle doping.
3. PL intensity: The emission peak intensity and electro-optical response of PL emission peak for this sample are maximum for CLC III, which increases prospects of its use as a potential optical material.

Our observations illustrated that the induction of memory as a result of manipulation of the helix director remains an active field of study and leads to new qualitative effects which can be useful for the development of memory based bistable low power devices.

***Chapter 4*:** Octadecylamine functionalized Single-Walled Carbon Nanotubes (SWCNT) dispersion in induced CLC influenced the collective orientation of nematic liquid crystal molecules in helical layers. Varying dopant concentration manipulated the properties of the doped matrix. The functional group has restricted the CNTs from the aggregate formation. As confirmed by polarized fluorescence spectroscopy, highly anisotropic nature of single wall CNTs enhanced the anisotropy of the liquid crystal and influenced the switching behavior by significantly bringing down the threshold voltage. The $\pi-\pi$ interaction of SWCNTs present in the planar alignment layers and chiral nematic liquid crystal molecules affects the molecular relaxation process. We also observed and quantified an electro-optical hysteresis of permanent nature. The results indicated the stabilization of the sample which is indicated in the enhancement of electro-optic memory (significantly at 0.3wt% CNTs doping). These properties favour potential practical utility of the material in optical memory devices and display technology.

The dispersal of COOH functionalized Multi-walled carbon nanotubes (MWCNT) into the induced chiral nematic liquid crystals confined in a planar aligned cell led to an improved electro-optic response regarding an increase in refractive index, and dielectric constant of the CLC. We investigated the physical, optical and electro-optical behavior of the doped samples with different dopant concentrations and confined in similar boundary conditions. Polarized fluorescence spectroscopy established the anisotropic changes brought in by CNT doping with a significant increase in absorbance of the doped samples. The early onset of Freedericksz transition also endorses the change in switching behavior of the CLC after doping. The reorientation of the liquid crystal director and CNTs with applied electric field was observed until the homeotropic state was achieved. We also noted the emanation of memory in the doped samples after the withdrawal of the electric field.

Chapter 5: The addition of different concentrations of Dodecanethiol functionalized silver nanoparticles in to a CLC, have successfully modulated the photoluminescence behaviour of a chiral liquid crystal. The 0.005-0.020wt% of Agnp doped composites show a quintessential organisation of the silver nanoparticles in the liquid crystal matrix, thus making the tuning of the luminescence properties of the chiral liquid crystal possible.

Homogeneous dispersal of silver nanoparticles into CLC also brings memory in the doped sample cells. The enhanced intrinsic field created by silver NPs in the doped sample contributed to the improved electro-optical response and a strong memory effect. The interaction of the collective electron cloud oscillations in the silver NPs with the electromagnetic wave of incident light traversing through the doped CLC medium probably brings about extraordinary results. Electrically induced Optical hysteresis and enhanced photoluminescence were observed in the doped samples, which virtually vamooses at 0.020wt% dopant concentration. We have recorded an uptrend of enhancement in emission peak intensity till 0.015wt% dopant concentration above which, we noticed a fall in the peak intensity. We also detected a significant shift in the peak position with chiral dopant concentration. The enhanced electro-optical response of this nanocomposite CLC, like reduced threshold voltage and better optical contrast, pave the way for its plausible use as a tunable optical functional material with electro-optical memory.

Another study based on the Impact of chirality on nematic liquid crystal matrix doped with Dodecanethiol-capped silver nanoparticles (Agnps). The temperature dependent morphological behaviour was investigated by polarized optical microscopy. We recorded a lowering of the threshold of Freedericksz transition and about a tenfold rise in dielectric constant with rising temperature in the chiral samples. We also observed a pronounced surge in photoluminescence in addition to an irreversible memory in the chiral medium.

The second part of the chapter deals with the emergence of optical hysteresis and enhanced photoluminescence in chiral medium dispersed with functionalized Aluminum-doped ZnO nanoparticles. We recorded a lowering of the threshold of Freedericksz transition and a nearly tenfold rise in dielectric constant with temperature. Irreversible memory was recorded in doped samples and measured with transmission studies. The improved blue emission ensures the enhancement of optical properties of CLC samples. The overall enhancement of peak intensity is also remarkable in doped samples. More than three-fold enhancement in the peak intensity was recorded for 0.01wt% doping of AZO nanoparticles. These properties ensure its use as a promising optical material.